WARSAW UNIVERSITY OF TECHNOLOGY

DISCIPLINE OF SCIENCE – CHEMICAL SCIENCES
FIELD OF SCIENCE – NATURAL SCIENCES

# PH. D. Thesis

Yu-Sheng Chen, M.Sc.

**Comparative analysis of synthesis routes and aluminum doping effects on NMC type cathode material**

Supervisors:

Prof. Władysław Wieczorek
Prof. Dr. Robert Dominko

WARSAW 2025

# COMPARATIVE ANALYSIS OF SYNTHESIS ROUTES AND ALUMINUM DOPING EFFECTS ON NMC TYPE CATHODE MATERIAL

Yu-Sheng Chen





The doctoral thesis has been carried out in a collaboration between Warsaw University of Technology and Slovenian National Institute of Chemistry within Destiny – European Research Institute.

This project has received funding from the European Union's Horizon 2020 research and innovation programme under the Marie Skłodowska-Curie grant Agreement N°945357

# ACKNOWLEDGMENTS

As a part of the DESTINY PhD programme acknowledges funding from the European Union's Horizon2020 research and innovation programme under the Marie Skłodowska-Curie Actions COFUND – Grant Agreement No: 945357

This thesis is the result of three years of work, which I have carried out at Warsaw University of Technology (WUT) and the Slovenian National Institute of Chemistry (NIC). This period was pivotal in my life, both scientifically and personally. I would like to express my gratitude to the amazing individuals I had the pleasure of meeting and working with.

First and foremost, I would like to express my sincere gratitude to my two supervisors, Prof. Władysław Wieczorek and Prof. Robert Dominko. Prof. Wieczorek introduced me to the remarkable international battery community and acted as a scientific mentor who facilitated countless opportunities. Prof. Dominko's belief in my abilities pushed me to undertake new challenges and fostered new collaborations. Both mentors have contributed significantly to my growth as a young scientist.

It was an honor to be a Destiny PhD Student, and I am immensely grateful to the entire Destiny community for their support during my studies. My journey began in Amiens and concluded in Warsaw, marked by numerous fruitful discussions during Destiny meetings, which were instrumental in my progress.

I extend my appreciation to all members of the Research Group at WUT and at NIC. They made my PhD studies extraordinary, providing both intellectually stimulating discussions and enjoyable social gatherings.

# ABSTRACT OF THE THESIS

This study thoroughly analyzes the fabrication processes and the impact of aluminum doping on NMC 811 cathode materials. We compare two distinct synthesis approaches: hydroxide co-precipitation and solid-stage calcination for polycrystalline (PC) cathodes and molten salt calcination for single-crystalline (SC) cathodes. Furthermore, we systematically introduce aluminum dopants at different stages of these processes. The aim is to understand the effect of doping on the structural, morphological, and electrochemical properties of NMC cathodes. Our results, obtained through extensive characterizations using techniques such as X-ray diffraction (XRD), scanning electron microscopy (SEM), transmission electron microscopy (TEM), and galvanostatic cycling tests, emphasize the potential of aluminum doping in improving the performance of polycrystalline NMC cathodes.

Keywords: NMC, high voltage cathodes, aluminum doping , synthesis and characterization.

# STRESZCZENIE PRACY DOKTORSKIEJ

Celem pracy doktorskiej było zbadanie wpływu sposobu syntezy oraz domieszkowania aluminium na właściwości materiałów katodowych z grupy NMC 811. W tym celu porównano materiały uzyskane dwoma różnymi metodami : współstrącanie wodorotlenków i kalcynację w fazie stałej w przypadku katod polikrystalicznych oraz kalcynację stopionych soli ą w przypadku katod monokrystalicznych. Do otrzymanych materiałów katodowych na różnych etapach procesu otrzymywania systematycznie wprowadzano my domieszki aluminium. Istotnym celem pracy było zbadanie wpływu domieszkowania na właściwości strukturalne, morfologiczne i elektrochemiczne katod NMC. Wyniki, uzyskane przy zastosowaniu takich technik, jak dyfrakcja promieni rentgenowskich (XRD), skaningowa mikroskopia elektronowa (SEM), transmisyjna mikroskopia elektronowa (TEM) i testy cykli galwanostatycznych, pozwaalają na sywierdzenie, że dodatek domieszki aluminium poprawia wydajności pracy półogniw zawierających polikrystaliczne katody NMC.

Słowa kluczowe: materiały katodowe z grupy NMC, wysokonapięciowe materiały katodowe, domieszkowanie glinem, synteza , badania struktury, cyklowanie półogniw.

# LIST OF PUBLICATIONS

This thesis is based on the results published in the following papers:

## Paper I

Optimizing High-Energy Lithium-Ion Batteries: A Review of Single Crystalline and Polycrystalline Nickel-Rich Layered Cathode Materials: Performance, Synthesis and Modification

*Yu-Sheng Chen[1,2], Robert Dominko[1,3,4], Maciej Marczewski[2], Władysław Wieczorek[2]

*Journal of Applied Physics A*

## Paper II

Comparative Analysis of Synthesis Routes and Aluminum Doping Effects on NMC Type Cathode Material

*Yu-Sheng Chen[1,2], Elena Tchernychova[1], Anton Meden[3], Samo Hočevar[1], Władysław Wieczorek[2], Robert Dominko[1,3,4]

(under process of publishing)

# TABLE OF CONTENT

## Contents

# LIST OF ABBREVIATIONS

| Abbreviation | Definition |
|---|---|
| NMC | Nickel Manganese Cobalt |
| LCO | Lithium Cobalt Oxide |
| NCA | Nickel Cobalt Aluminum |
| LFP | Lithium Iron Phosphate |
| LTO | Lithium Titanate Oxide |
| LiOH | Lithium Hydroxide |
| XRD | X-ray Diffraction |
| SEM | Scanning Electron Microscopy |
| TEM | Transmission Electron Microscopy |
| XPS | X-ray Photoelectron Spectroscopy |
| EIS | Electrochemical Impedance Spectroscopy |
| CV | Cyclic Voltammetry |
| EDX | Energy Dispersive X-ray Spectroscopy |
| ICP-MS | Inductively Coupled Plasma Mass Spectrometry |
| TGA | Thermogravimetric Analysis |
| DSC | Differential Scanning Calorimetry |
| NMR | Nuclear Magnetic Resonance |
| HR-TEM | High-Resolution Transmission Electron Microscopy |

# Chapter 1
# INTRODUCTION

## 1. Background

This thesis explores advancements in rechargeable lithium-ion batteries (LIBs), a critical technology in the contemporary energy landscape. Introduced commercially in the early 1990s, LIBs have revolutionized portable electronics and are now integral to electric vehicles (EVs) and large-scale energy storage systems. Their high energy density, long cycle life, and declining manufacturing costs have positioned them as essential components in the transition to sustainable energy solutions. [1,2]

The global shift towards renewable energy sources (RES) such as solar and wind power is driven by the urgent need to reduce greenhouse gas emissions and combat climate change. These renewable sources, however, are intermittent and require efficient energy storage systems to balance supply and demand and ensure a stable energy grid. LIBs are particularly well-suited for this role due to their efficiency, scalability, and fast response times. [3]

In addition to grid energy storage, LIBs are central to the electrification of the transportation sector. The replacement of internal combustion engines with electric motors in vehicles offers numerous advantages: reduced emissions, lower noise pollution, decreased reliance on fossil fuels, and lower operating costs. Electric vehicles (EVs) equipped with LIBs benefit from high energy efficiency and the ability to recapture energy during braking. However, challenges such as lower energy density compared to liquid fuels, long charging times, capacity degradation over time, and safety concerns related to thermal runaway remain significant.

The demand for high-capacity, reliable batteries is increasing rapidly. For instance, in Europe, the demand for such batteries is projected to grow by up to 70% from 2018 to 2025. This surge is driven by both the increasing adoption of RES and the rising popularity of EVs. In 2023, global demand for EV batteries reached over 750 GWh, a 40% increase from 2022. Electric cars account for 95% of this growth, with the fastest increases seen in China, followed closely by Europe and the United States.

China has been a leader in EV battery demand, with plug-in hybrid electric vehicles (PHEVs) making up about one-third of total electric car sales in 2023 and 18% of battery

demand. Chinese manufacturers are also marketing more extended-range EVs (EREVs), which use an electric motor as their primary powertrain but include a combustion engine for battery recharging when needed. EREVs have larger batteries than traditional PHEVs, enabling longer electric ranges and total ranges up to 1,000 km when the internal combustion engine is used.

The growth in EV battery demand has driven significant increases in the extraction and refining of critical raw materials like lithium, cobalt, and nickel. In 2023, battery demand for lithium reached around 140 kt, accounting for 85% of total lithium demand. Cobalt demand for batteries increased by 15% to 150 kt, making up 70% of total cobalt demand. Nickel demand from batteries was up nearly 30%, accounting for over 10% of total nickel demand. Despite high levels of investment in mining and refining, ongoing growth in battery demand requires continuous expansion of supply chains to avoid bottlenecks and ensure resilience against potential disruptions.

Battery production is increasingly localized near demand centers, with China, Europe, and the United States leading in manufacturing capacity. In 2023, Europe produced 110 GWh and the United States 70 GWh of EV batteries. [4] China remains the largest producer with 950 GWh, [5] with a highly integrated supply chain and a substantial share of global manufacturing capacity. International cooperation and trade are essential for the expansion of EV markets, with significant investments in battery manufacturing announced across various regions.

Battery prices have seen fluctuations due to the volatility of critical mineral markets. In 2022, the cost of LIB packs increased for the first time in years, but by 2023, prices had fallen by nearly 14% due to stabilizing mineral costs. Innovations in battery chemistries, such as lithium iron phosphate (LFP) and emerging technologies like sodium-ion batteries, are expected to further reduce costs and reliance on critical minerals.

Continued research and development in LIB technology are crucial for overcoming existing challenges and enhancing performance, longevity, and safety. As the world transitions towards a sustainable energy future, LIBs will play a pivotal role in enabling the widespread adoption of renewable energy and the electrification of transportation, contributing to a cleaner, more energy-efficient world.

## 2. Battery history

The 1970s energy crisis spurred scientists to search for alternatives to fossil fuels. Exxon, one of the largest oil giants, created a research group dedicated to replacing petroleum. At the time, the only rechargeable batteries on the market were lead and nickel-cadmium batteries. A high-energy-density, high-voltage, low-environmental-impact battery was desperately needed.

Stanley Whittingham, while working at Exxon after completing his studies at Stanford University, discovered that potassium ions could increase the energy density of titanium disulfide ($TiS_2$) during research on superconducting materials. To further enhance energy density, lithium ions were substituted for potassium, leading to the development of the $Li/TiS_2$ system. [6] This system not only marked the first demonstration of a working rechargeable lithium battery but also laid the foundation for lithium-ion battery technology by introducing the key components: lithium, transition metals, and intercalation compounds. The $Li/TiS_2$ system delivered a voltage of approximately 2.5 V. However, cycling the battery caused the formation of metallic lithium dendrites, which posed significant safety hazards.

The cell voltage is determined by the energy difference between the redox energies of the anode and the cathode. In other words, the cathode energy should be as low as possible and the anode energy should be as high as possible, which means that the cathode would require the stabilization of higher oxidation states with a lower-lying energy band, while the anode would require the stabilization of lower oxidation states with a higher-lying energy band. Switching from metal sulfides to metal oxides leads to a greater energy band difference and a higher voltage of the cell because the $O^{2-}$:2p band lies lower than the $S^{2-}$:3p band. (Fig. 1) [7]

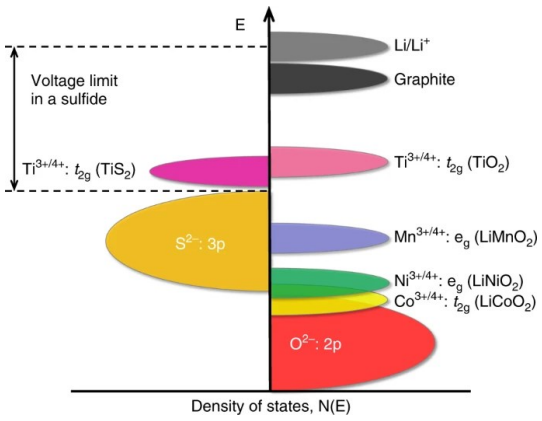


Figure 1 The energy band gap for cathode materials [7] Copyright 2023, Nature communications

Based on energy band theory, John Goodenough worked with several researchers around the world to systematically experiment with various transition metal oxides. In the 1980s, three promising cathode types were proposed: layered $LiCoO_2$, spinel $LiMn_2O_4$, and polyanion $LixFe_2(XO_4)$. These became the foundation of the huge battery market we have today. With help from Akira Yoshino, the layered $LiCoO_2$ (LCO) was the first cathode to be commercialized. The chemical reactions inside this battery during discharging are as follows:

$$LiCoO_2 \rightarrow Li_{1-x}CoO_2 + xLi^+ + xe^- \; C_6 + xLi^+ + xe^- \rightarrow Li_x C_6$$

$$LiCoO_2 + C_6 \rightarrow Li_{1-x}CoO_2 + Li_x C_6$$

Even today, it dominates the majority of the market share in consumer electronics. Moreover, the majority of the market share for electrical mobility lies in the layered and polyanion cathode types, such as $LiNi_xCo_yAl_zO_2$(NCA), $LiNi_xCo_yMn_zO_2$(NCM), and $LiFePO_4$ (LFP).

With historical opportunity and the efforts of several great scientists, the lithium-ion battery has been a game-changing technology. The LCO-based cathode, for example, has an energy density of 278 Wh $kg^{-1}$ (700 Wh $L^{-1}$), making it the most popular choice for mobile devices. Despite its great success, the high cost of cobalt and its limited capacity (~140 mAh $g^{-1}$) make it unsuitable for use in electric vehicles. Recent breakthroughs in ternary cathode technology, however, have made lithium-ion batteries more cost-effective and increased their energy density, leading to a boom in the electric vehicle industry.

## 3. Cathodes for EVs

Lithium-ion batteries (LIBs) have profoundly impacted the fields of mobile devices and electric vehicles (EVs), revolutionizing modern life. Lithium, the lightest solid element on Earth, has evolved from being part of explosive and hazardous metallic batteries to the foundation of the safe and lightweight lithium-ion batteries we use today. This evolution is a testament to the relentless efforts of researchers, recognized by the awarding of the Nobel Prize in Chemistry in 2019 to John B. Goodenough, M. Stanley Whittingham, and Akira Yoshino. Their pioneering contributions underscore the significance of LIBs in contemporary energy storage.

Since Sony Corporation first commercialized LIBs in 1991, there have been substantial advancements at the material, cell, and production levels. Although silicon-based anodes hold great promise, several challenges remain unresolved, resulting in graphite anodes still being the

predominant choice. Conversely, cathode technology has experienced continuous improvement. Initially, Mizushima et al. developed $LixCoO_2$ (LCO), which has an unstable structure when $x < 0.5$ [1,2] and is hindered by the high cost of cobalt, limiting its application in EVs.

$LiNiO_2$ (LNO) emerged as a potential alternative to LCO cathodes due to its similar layered structure, which allows for high theoretical energy density and ionic conductivity. LNO offers a higher capacity since nickel serves as the redox-active element throughout the charge/discharge cycle. Additionally, nickel is more abundant and less expensive than cobalt. However, recent geopolitical developments, such as the Russia-Ukraine conflict, have caused significant fluctuations in nickel prices. Consequently, the nickel market is likely to become more volatile, emphasizing the importance of recycling and developing new supply chains. Despite its advantages, LNO's commercialization was hindered by safety concerns. Researchers have explored various elemental substitutions to balance energy density, stability, and cost. This led to the successful commercialization of two NMC cathode materials: NCM ($LiNi_xCo_yMn_zO_2$) and NCA ($LiNi_xCo_yAl_zO_2$).

Another popular cathode material is olivine structured LiFePO4 (LFP). Compared to NCM/NCA, LFP is significantly cheaper (80-135USD $kWh^{-1}$ vs. 100-175 USD $kWh^{-1}$ for NCA/NMC) [8], has a longer cycle life, and is safer, but has a lower energy density. For the large-scale implementation of EVs, LFP is expected to dominate the short- and medium-range EV market and gradually increase its share in global battery production. Despite the tremendous price fluctuation of nickel in 2022 due to the Russia-Ukraine conflict and strong competition from LFP cathodes, NMC cathodes remain the only choice for long-range EVs, making them the focus of this review.

## 4. Property overview of Ni-rich Cathodes

### 4.1.Structure

Lithium transition-metal (TM) oxides $LiMO_2$ (M = Co, Ni, Mn, Al, etc.), have a layered structure with the close-packed oxygen anions in a cubic arrangement and crystallize in the α-$NaFeO_2$ structure belonging to *R*3-*m* ($D_{3d}^5$) space group. In NMC cathodes such as NMC and NCA, $Ni^{2+}$, $Co^{3+}$, $Mn^{+,}$ and $Al^{3+}$ occupy the TM sites in the layered *R*-3*m* crystal structure. [9,10] This layered structure can transform into a rock-salt cation mixing phase with an Fm-3m structure after cycling, as shown in Fig. 2.

Most layer cathodes have a theoretical capacity of around 280 mAh $g^{-1}$ [11]. For high Ni cathode (nickel>50%), nickel ions are in the form of $Ni^{2+/3+}$. During charging, $Ni^{2+/3+}$ is oxidized to $Ni^{4+}$, providing high capacity. However, it has been suggested that the reduction of $Ni^{3+}$ to $Ni^{2+}$ can lead to the formation of $O^{2-}$ on the surface of the high-nickel cathode. This can react with $H_2O$ and $CO_2$ from the atmosphere and $Li^+$ to form lithium residuals. [12]

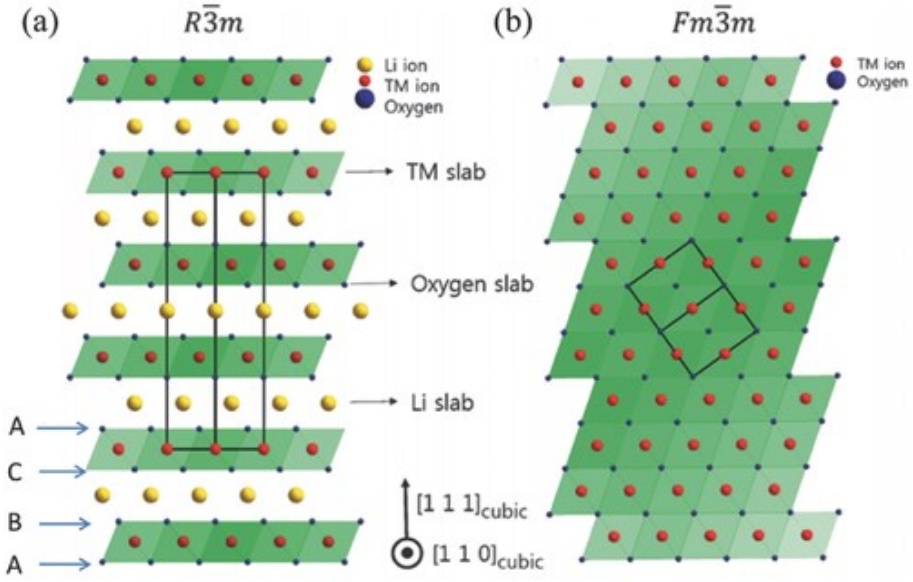


Figure 2 Schematic illustrations of the ordered and disordered phase in layered nickel-rich lithium transition-metal oxides and their structural transition. a) Well-ordered R-3m phase called "O3-type" structure; b) The cation disorder or cation mixing phase with Fm-3m structure transformed from R-3m layered phase. [13] Copyright 2015, Wiley-VCH.

### 4.2.General Comparison between Single Crystalline and Polycrystalline Cathode

Single-crystalline (SC) Ni-rich NMC cathodes are characterized by their unique particle morphology, typically consisting of micron-sized particles with low porosity and a robust structure. This design provides several advantages over polycrystalline (PC) NMC cathodes, particularly in cycling and thermal stability, as illustrated in Figure 3.[14]

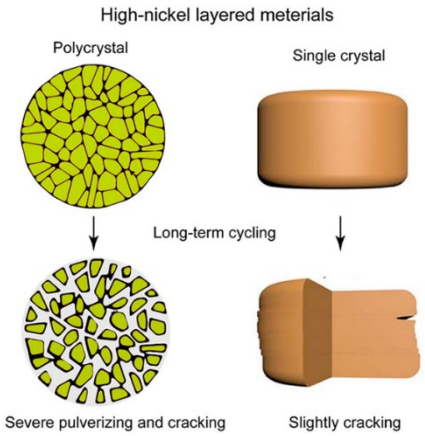


Figure 3 Schematic illustration of polycrystal and single-crystal [14] Copyright 2021, Energy Storage Materials

Single-crystal (SC) NMC cathodes, while demonstrating promising performance in conventional lithium-ion batteries, exhibit even more pronounced advantages in solid-state batteries (SSBs). The solid-solid interfaces inherent to SSBs present unique challenges, including maintaining structural integrity, minimizing interfacial resistance, and preserving lithium diffusivity. SC cathodes, characterized by continuous lithium-transport channels and a reduced number of grain boundaries, offer significant potential for enhancing the reliability and performance of SSB systems. For example, the enhanced mechanical strength of SC materials contributes to preserving cathode structure and integrity during high-pressure cell assembly processes. [15,16] Moreover, SC cathodes show promise in addressing one of the primary limitations of SSBs: low ionic diffusivity. The absence of grain boundaries in SC cathodes significantly reduces the occurrence of severe intergranular cracking, a phenomenon with divergent implications in liquid and solid electrolyte systems. While in liquid electrolytes, such cracking can lead to increased surface area and apparent Li-diffusion, in SSBs, cracked polycrystalline (PC) cathodes suffer from loss of contact with solid electrolytes, resulting in performance degradation. (Fig. 4 A and b) In contrast, SC cathodes maintain superior contact with solid electrolytes and provide uninterrupted Li-transport pathways. Experimental studies have demonstrated higher lithium diffusion coefficients in SC cathodes compared to their PC counterparts, particularly at elevated voltages. [17] This synergistic combination of structural stability and enhanced ionic diffusivity positions SC cathodes as a promising avenue for advancing SSB technology, potentially overcoming critical barriers in the development of high-performance solid-state energy storage systems.

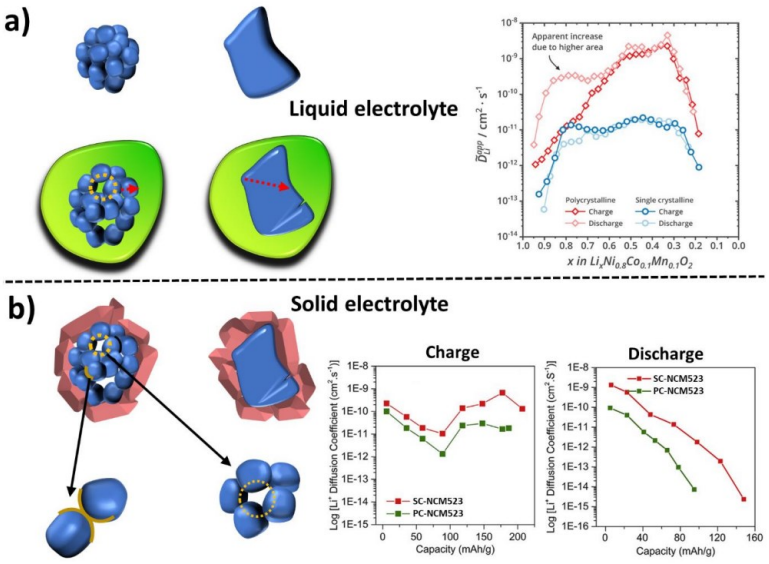


Figure 4 Schematic depiction of polycrystalline (PC) and single-crystal (SC) cathodes, illustrating the impact of particle fracture and grain boundaries. The figure also shows the apparent lithium-diffusion coefficient ($\tilde{D}_{Li}^{app}$) during the initial charge/discharge cycle for NMC cathodes. a) represents data for NMC 811 with a liquid electrolyte, and b) shows data for NMC 523 with a solid electrolyte. [17] Copyright 2021, Wiley-VCH and 2020 Elsevier

Nevertheless, single-crystalline technology faces several challenges that need to be addressed, including low-rate ability, low high-voltage stability, and higher production costs. [18] The key differences between PC and SC NMC cathodes using a hexagonal radar chart in Fig. 5, and details of these properties are summarized in Table 1. This visualization highlights the trade-offs between the two cathode types, aiding in the selection of the appropriate material based on specific application requirements. The following part of the chapter provides an in-depth exploration of SC Ni cathode, encompassing its mechanism, strengths, weaknesses, synthesis methods, and strategies for enhancement.

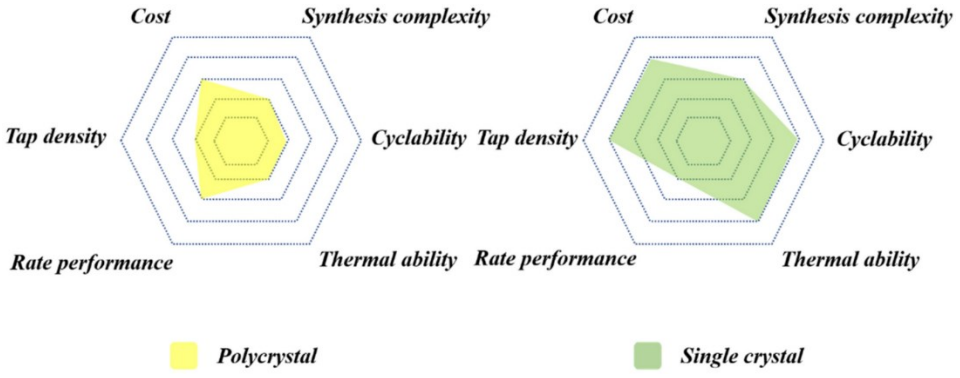


Figure 5 Comparative Performance of Polycrystalline and Single-Crystal NMC Cathodes in Lithium-Ion Batteries. SC NMC demonstrates superior cycle life and thermal stability, while PC NMC offers advantages in energy density, rate capability, and cost-effectiveness. [19] Copyright 2022, Electrochemical Energy Reviews

Table 1 Analytic Comparison of Polycrystalline and Single-Crystal NMC Cathodes

| Characteristic | PC NMC | SC NMC |
|---|---|---|
| Cycle Life/Stability | Lower. Prone to microcracks and degradation, leading to capacity fade over many cycles. | Higher. Resistant to microcracks, resulting in improved stability and longer cycle life. |
| Thermal Stability | Lower. More susceptible to thermal runaway and safety concerns. | Higher. Less prone to thermal runaway, enhancing safety. |
| Energy Density | Slightly higher due to higher tap density (packing efficiency). | Slightly lower due to lower tap density. |
| Rate Capability | Higher. Can deliver energy at higher rates (fast charging/discharging). | Lower. Slower energy delivery at high rates. |
| Cost | Lower. The manufacturing process is simpler and more established. | Higher. The manufacturing process is more complex and requires specialized precursors. |
| Production Complexity | Lower. Easier to synthesize with existing methods. | Higher. Synthesis requires precise control and specialized techniques. |

### 4.3.Morphology of NMC: Comparison of SC and PC Cathodes

The typical NMC cathode particles are polycrystalline, which are secondary particles with diameters ranging from 10 micrometers. Each secondary particle is composed of many primary particles, each with a diameter of a few hundred nanometers to a few micrometers. The particle size can range from a few micrometers to tens of micrometers. SC-NMC cathode particles frequently exhibit well-defined, geometric forms, resembling octahedrons or truncated octahedrons. The morphology difference between SC and PC-NMC is shown in Fig. 6.

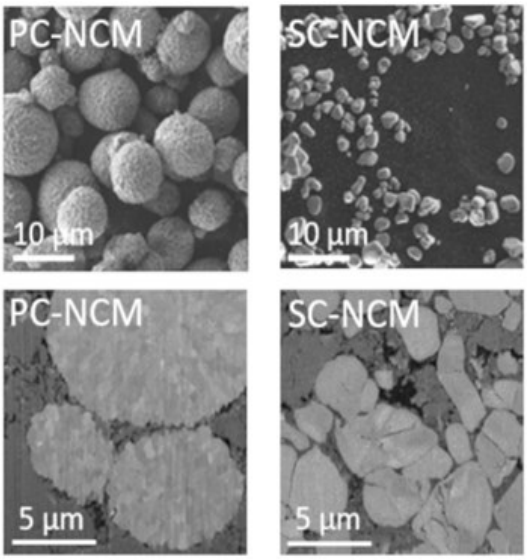


Figure 6 SEM images of PC-NCM and SC-NCM powders are shown in the top row. The middle row displays cross-sectional SEM images of pristine PC-NCM and SC-NCM cathodes, while the bottom row features those of cycled cathodes. [20] Copyright 2021, Journal of The Electrochemical Society

Due to their unique particle structure and morphology, single-crystal NMC cathodes are widely believed to exhibit superior performance in several key aspects when used in practical lithium-ion batteries (LIBs) compared to polycrystalline NMCs. These aspects include cycling stability, outgassing behavior, and thermal stability. This can be further illustrated as follows: (1) In SC primary particles, the mechanical integrity of NMC materials is improved by effectively suppressing the formation of intergranular microcracks. This improvement is achieved by the absence of grain boundaries in these particles. [21,22] (2) The unique structure of SC-NMC materials, characterized by a low specific surface area, can alleviate issues commonly encountered in PC-NMC materials with high specific surface areas.

However, these enhancements are only found at low Ni content (Ni<60%). For example, Dahn's group systematically studied single-crystal NMC532. They observed that it could maintain thousands of cycles without undergoing structural degradation. [23–26]. As for high nickel cathode (Ni>80%), the conclusion regarding the electrochemical performance of NMC-based cathodes, particularly single-crystal NMCs, remains questionable due to discrepancies in previously published literature. Notably, the disruptive variation in electrochemical performance observed at different Ni contents necessitates a comprehensive comparison between polycrystalline and single-crystal NMC cathodes. Such a comparison is crucial to

evaluate the potential of these materials for future high-energy-density lithium-ion batteries, allowing for an accurate assessment of their value in the industry.

### 4.4.Electrochemical Comparison between SC and PC Cathode

The comparison between single-crystal and polycrystalline NMCs with varying Ni contents in terms of cycling stability is provided in Fig. 7, indicating that the performance difference heavily relies on the amount of Ni present, with the dividing line occurring Ni~0.7 (Line 1). For single-crystal NMCs, the cycling stability surpasses that of polycrystalline NMCs when the Ni content is below 0.6. This conclusion is supported by Dahn's research, which demonstrated that single-crystal NMC523 could endure numerous cycles with minimal capacity loss, a feat unattainable for polycrystalline NMCs [23,25].

Conversely, when the Ni content exceeded 0.76 (Ni-rich), the trend reversed. Overall, polycrystalline NMCs demonstrated superior cycling stability compared to unmodified single-crystal NMCs. Notably, the performance of single-crystal NMCs can significantly improve with various modification strategies. (Line 2 in Fig. 7). Under Ni-rich component conditions, the final cycle capability of single-crystal NMCs can sometimes even exceed that of polycrystalline NMCs. For instance, after 100 cycles at 0.2 C, Ni-rich single-crystal NMC cathodes show remarkable capacity retention of 100.09%, which is achieved through optimization of the synthesis process. [27] and 96.2% after 150 cycles at 1 C [28]. Material coating, doping, and electrolyte additive application have been effective in improving the stability of single-crystal NMC cathodes.

As the Ni content increases to 0.95–1.0 (Ni-ultrahigh), polycrystalline NMCs become the dominant performers, with few single-crystal NMC cathodes reported in the literature and even fewer surpassing the performance of the polycrystalline particles. There is significant room for enhancing the electrochemical performance of single-crystal NMCs. Notably, under Ni-rich conditions, the electrochemical performance of single-crystal NMCs can be optimized to match or surpass that of polycrystalline NMCs. Furthermore, if other properties, such as thermal stability after long-term cycling and overcharge resistance, are superior to those of polycrystalline NMCs, then single-crystal NMCs would be a promising choice for industrial applications.

In summary, SC NMC cathodes demonstrate superior cycle life and thermal stability compared to PC NMC cathodes, making them promising for high-performance lithium-ion batteries.

However, SC NMCs face challenges in terms of higher cost, more complex production processes, and lower rate capability.

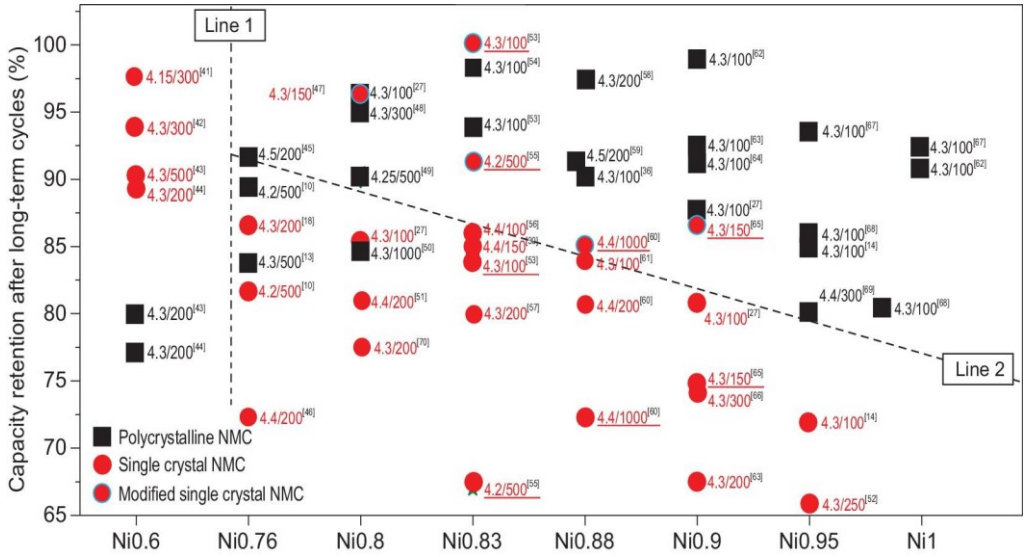


Figure 7 Performance comparison between PC and SC NMC cathodes. Note such as 4.15/300 means the cathodes have undergone 300 charge/discharge cycles with an upper voltage limit of 4.15 V. [29] Copyright 2023, National Science Review

## 5. Degradation Mechanism of PC Ni-rich Cathodes

The use of high-nickel content layered oxides in both PC and SC cathode materials can hinder their cycle and thermal stability, leading to a decrease in electrochemical performance over time. This degradation is caused by several mechanisms, including phase distortion [30], irreversible release of oxygen (electrolyte oxidation) [31] , transition-metal dissolution [32] and anisotropic lattice distortion (particle cracking), as shown in Fig. 8. [33] The use of high-nickel content layered oxides in cathode materials can hinder their cycle and thermal stability, leading to a decrease in electrochemical performance over time. This degradation is caused by several mechanisms, including phase distortion.

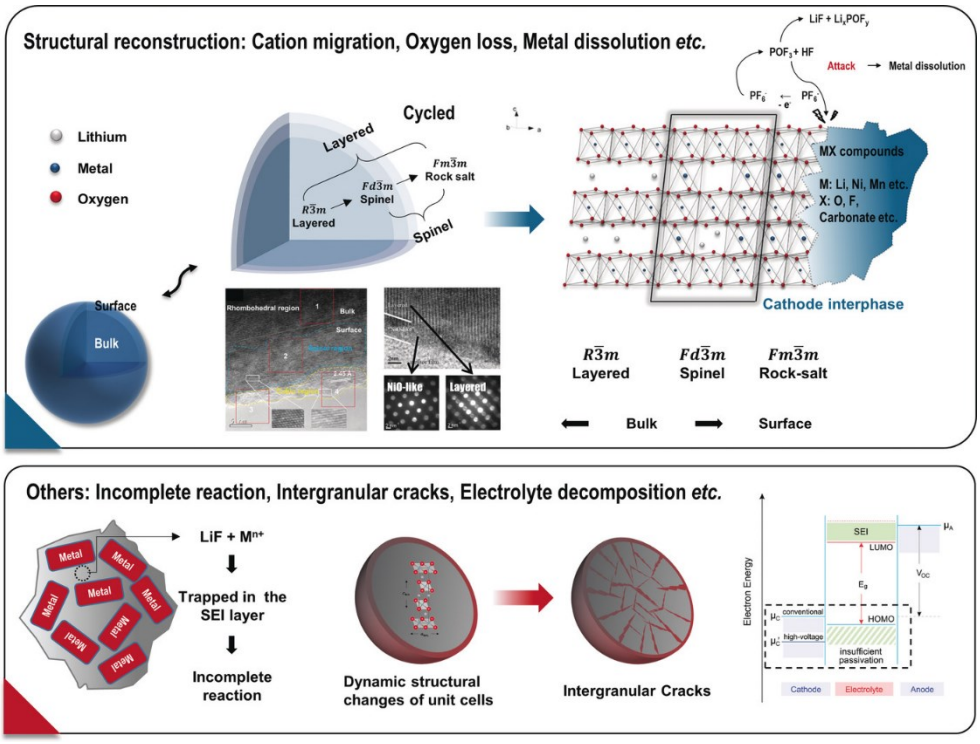


Figure 8 schematic diagrams for degradation mechanisms and factors, including crystal phase transformation, transit metal dissolution, oxygen loss, etc. [34] Copyright 2023, Angewandte Chemie

### 5.1.Cationic Mixing, Cation Migration

Before the cycling, due to various synthetic parameters, challenges can also arise from cation mixing at the atomic level, where the comparable ionic radii of Ni (0.69 Å) and Li (0.72 Å) can result in anti-site mixing across the layers. [35] A similar off-stoichiometry is also observed during the synthesis of $Li_{1-z}Ni_{1+z}O_2$(LNO). The excess $Ni^{2+}$ ions occupy sites in the lithium layer, blocking $Li^+$ ion diffusion pathways and causing local layer collapse during charge through cation shrinkage, which is manifested in a largely irreversible capacity loss during the first cycle. This phenomenon is called cation mixing.[36]

Similar to cation mixing, the first step of structural degradation during the cycle is through the migration of transition metals from their octahedral sites into the Li octahedral sites. Such cationic migration takes place at high Li vacancies (excessive Li-deintercalation) and/or high temperature, which give rise to the phase transition of the layered (R-3m) structure to the $LiMn_2O_4$-type spinel phase (Fd3m). [30] Based on in situ heating STEM/EELS [37], it was shown that structural degradation is more severe and occurs at lower temperatures as the nickel content increases.

The quantitative measure of cation mixing can be quantified by the ratio of $I_{(003)}/I_{(104)}$. A higher value of this ratio indicates lower cation mixing. H.-J. Noh et al. have shown that an excess of nickel ions in NMC can lead to increased cation mixing, as described in Table 2, hindering Li+ diffusion and reducing the material's electrochemical ability. [38]

Table 2 Intensity ratio $I(003)/I(004)$ of the $Li[Ni_xCo_yMn_z]O_2$ ($x$ = 1/3, 0.5, 0.6, 0.7, 0.8 and 0.85). [38] Copyright 2013, Journal of Power Sources

| Layer cathode | $I_{(003)}/I_{(104)}$ |
|---|---|
| $Li[Ni_{1/3}Co_{1/3}Mn_{1/3}]O_2$ | 1.35 |
| $Li[Ni_{0.5}Co_{0.2}Mn_{0.3}]O_2$ | 1.32 |
| $Li[Ni_{0.6}Co_{0.2}Mn_{0.2}]O_2$ | 1.26 |
| $Li[Ni_{0.7}Co_{0.15}Mn_{0.15}]O_2$ | 1.2 |
| $Li[Ni_{0.8}Co_{0.1}Mn_{0.1}]O_2$ | 1.19 |
| $Li[Ni_{0.85}Co_{0.075}Mn_{0.075}]O_2$ | 1.18 |

### 5.2.Phase Transformation

The layered cathode is thermodynamically favorable to transform from layered → spinel → rock-salt structure as shown in Fig. 9. Certain conditions such as a high cutoff voltage, high temperature, or a degrading electrochemical environment accelerate the transformation process. The rock-salt phase has very low ionic conductivity, blocks the $Li^+$ diffusion channel, and obstructs the de/intercalation process. The capacity retention decreases as the rock-salt phase forms with cycling. From XANES and XPS studies, [39,40] the surface of Ni-rich layered material (e.g., $Li_{1-x}Ni_{0.73}Co_{0.17}Al_{0.10}O_2$) can be observed covered with unwanted Li compounds, such as $Li_2CO_3$, $ROCO_2Li$, LiF, etc. The lithium compounds of rock-salt crystal structure increase with the number of cycles.

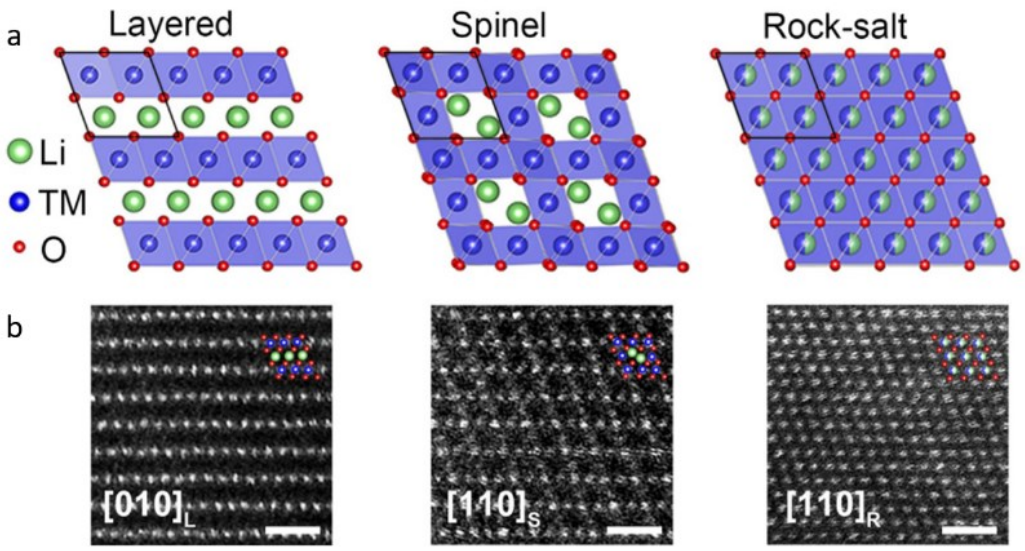


Figure 9 (a) The atomic structural models and (b) corresponding high-resolution HAADF-STEM images [41] Copyright 2020, Angewandte Chemie

### 5.3.Side reactions with electrolytes

The side reactions with electrolytes are suggested to be the initial trigger to the chain reaction of phase transformation in Ni-rich cathodes. The presence of $H_2O$ in the electrolyte can hydrolyze $LiPF_6$ to generate hydrofluoric acid (HF), which can attack the surface of the layered cathode, leading to TM cation dissolution. Furthermore, electrolyte penetration into the bulk of cathode particles can severely damage the structure and cause cracking. The generation of HF through the reactions of $H_2O$ (1) and at high temperatures (2)(3) can accelerate this process, as shown in the chemical reactions below:

$$LiPF_6 + H_2O \rightarrow LiF\downarrow + POF_3 + 2HF \quad (1)$$

$$LiPF_6 \rightarrow LiF\downarrow + PF_5 \quad (2)$$

$$PF_5 + H_2O \rightarrow POF_3 + 2HF \quad (3)$$

### 5.4.Micro-cracking

Another side effect of phase distortion in Ni-rich cathodes is anisotropic stress caused by the change in the c-axis during charge/discharge, which can result in micro-cracking on the surface of the cathode. The "fresh surface" created by these cracks reacts severely with the electrolyte, leading to transition-metal dissolution and oxygen loss.

These crack networks along the grain boundaries can be infiltrated by the electrolyte, resulting in the formation of an insulating NiO-type cathode-electrolyte interface. [9,42,43] The surface changes that occur during the use of Ni-rich cathodes can lead to a loss of active cathode material and increased charge transfer resistance, resulting in rapid capacity fade and drastically reduced lifetime. The anisotropic expansion and shrinkage of the primary particles in polycrystalline NMCs drive the formation of microcracks. These microcracks increase the contact between the electrode material and the electrolyte, exacerbating side parasitic reactions. [44]

Hu *et al.* [45] observed and quantified lattice and morphological changes in primary particles of polycrystalline NMCs, as shown in Fig. 10 correlating these changes with the formation, evolution, and eventual micro-cracking of microcracks/macrocracks within the polycrystalline NMC particles.

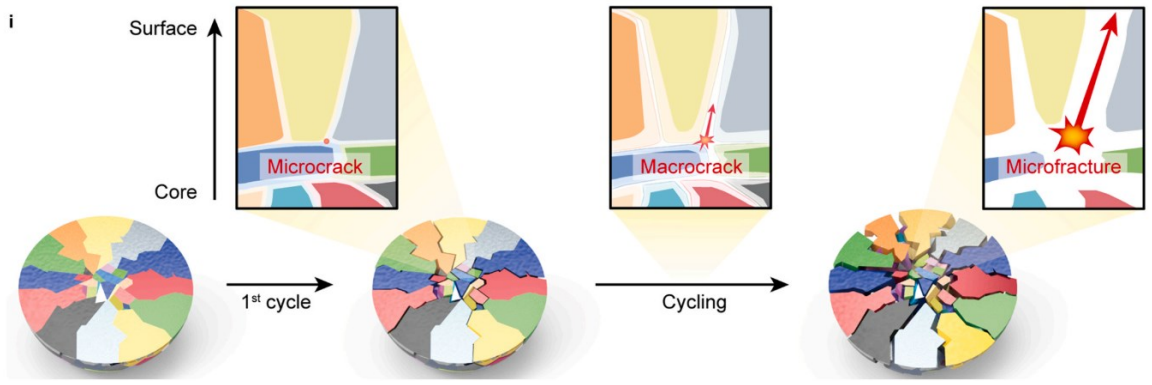


Figure 10 Schematic illustration of the cracking process during cycling. [45] Copyright 2021, Nano Energy

### 5.5.Gas Evolution

The residual lithium compounds, such as $C_3H_6O_3$ (ethyl hydrogen carbonate), $Li_2CO_3$, and LiOH on the surface of the high-nickel cathode generate gas through electrochemical oxidation reactions and chemical reactions, as shown below. This can lead to a series of safety issues, such as thermal runaway and the formation of flammable gases.

The degradation mechanisms of high-nickel cathodes become more severe as the nickel content increases. The c-axis lattice change, gas evolution, and anisotropic lattice distortion of high-Ni cathodes are shown in Figure 11.

$$2Li_2CO_3 \rightarrow 4Li^+ + 4e^- + 2CO_2 \uparrow + O_2 \uparrow \quad (4)$$

$$Li_2CO_3 + 2HF \rightarrow 2CO_2 \uparrow + H_2O + 2LiF \quad (5)$$

$$C_3H_6O_3 + Li_2CO_3 + 2HF \rightarrow C_3H_5O_3Li + CO_2 \uparrow + H_2O + LiF \quad (6)$$

$$4LiOH \rightarrow 4Li^+ + 4e^- + 2H_2O + O_2 \uparrow \quad (7)$$

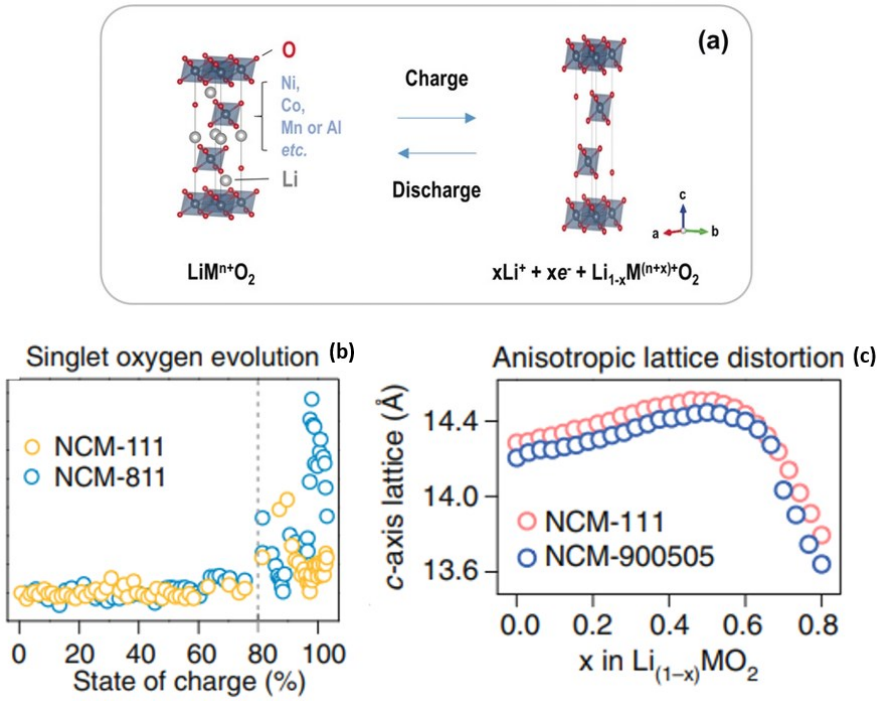


Figure 11 Schematic diagram of a) c-axis lattice change, reaction mechanism for b) oxygen evolution and c) anisotropic lattice distortion for low- and high-Ni NCM cathode [34] Copyright 2023, Angewandte Chemie

### 5.6.Thermal Runaway

Thermal runaway is a dangerous safety issue in lithium-ion batteries (LIBs). It can occur under extreme conditions, such as thermal abuse, short circuits, overcharging, nail penetration, and crushing. [46] Thermal runaway includes several stages: cell failure and drastic heat release → separator melting → short circuit of the cell → more heat and oxygen release. When an electric vehicle is involved in an accident, this thermal runaway can lead to an explosion or extreme fire. To avoid thermal runaway, the thermal stability of materials, the protection of battery packs, and the thermal management of batteries are all important, with the thermal stability of materials being the most fundamental.

Increasing the nickel content in cathode materials can lead to thermal lattice decomposition in the highly delithiated state (high charge state), singlet oxygen evolution, and reduced thermal

stability. [44] Ni-low NCM materials are more thermally stable than their Ni-rich NCM counterparts.

Common techniques for thermal stability characterization are differential scanning calorimetry (DSC) and thermogravimetric analysis (TGA). Materials with high thermal stability have higher temperatures and lower heat emission exothermic peaks. As shown in Figure 12, the heat flows and the DSC peak temperature of the charged high-Ni cathode are significantly higher than those of the low-nickel cathode, indicating a severe safety issue with high-nickel cathodes. It is important to address this issue to improve the safety of LIBs.

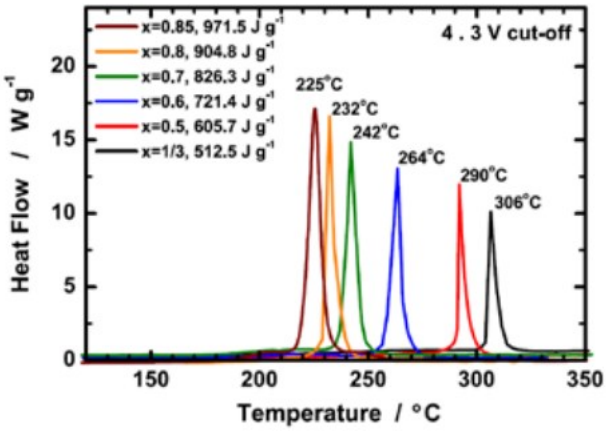


Figure 12 DSC of charged NCM materials [47] Copyright 2019, Journal of Physics

## 6. Degradation Mechanism of SC Ni-rich Cathodes

The SC NMC cathode exhibits a similar degradation mechanism to the PC cathode. However, due to its unique morphology, the SC NMC cathode, especially at low Ni content (≤60%), shows promise in enhancing safety and cycle life, primarily by avoiding micro-cracking, as discussed in the previous chapter. However, Ni-rich single-crystal NMC cathodes experience even faster capacity decay than polycrystalline NMC cathodes, rendering them unsuitable for practical applications. Therefore, this chapter aims to systematically review the attenuation mechanisms of single-crystal NMCs and generate fresh insights into valuable research pathways.

Although single-crystal NMC cathodes were developed to address the significant problems caused by intergranular cracks in polycrystalline NMC cathodes, these single-crystal cathodes

can experience slice gliding, the formation of cracks within the grains, and the breakdown of particles into smaller pieces, as shown in Fig. 13. These issues are particularly prevalent under high voltage, high temperature, and high nickel content conditions. [48–51] While a formation mechanism has been proposed and discussed to explain the observed issues, a comprehensive understanding remains elusive. It is hypothesized that planar gliding could lead to crack formation, which in turn allows electrolyte penetration and subsequent detrimental reactions. [52]

Regarding the significant intragranular cracks, one potential cause is the internal stress that arises between different phases within the cathode material [53], oxygen vacancies [54], and a dislocation-based crack incubation mechanism [55]. Additionally, the surface of single-crystal NMC cathodes has been observed to pulverize after prolonged cycling. This is likely due to a mismatch between the crystal structure at the surface and the rest of the particle, combined with the significant volume changes that occur during charging and discharging. [49,53]

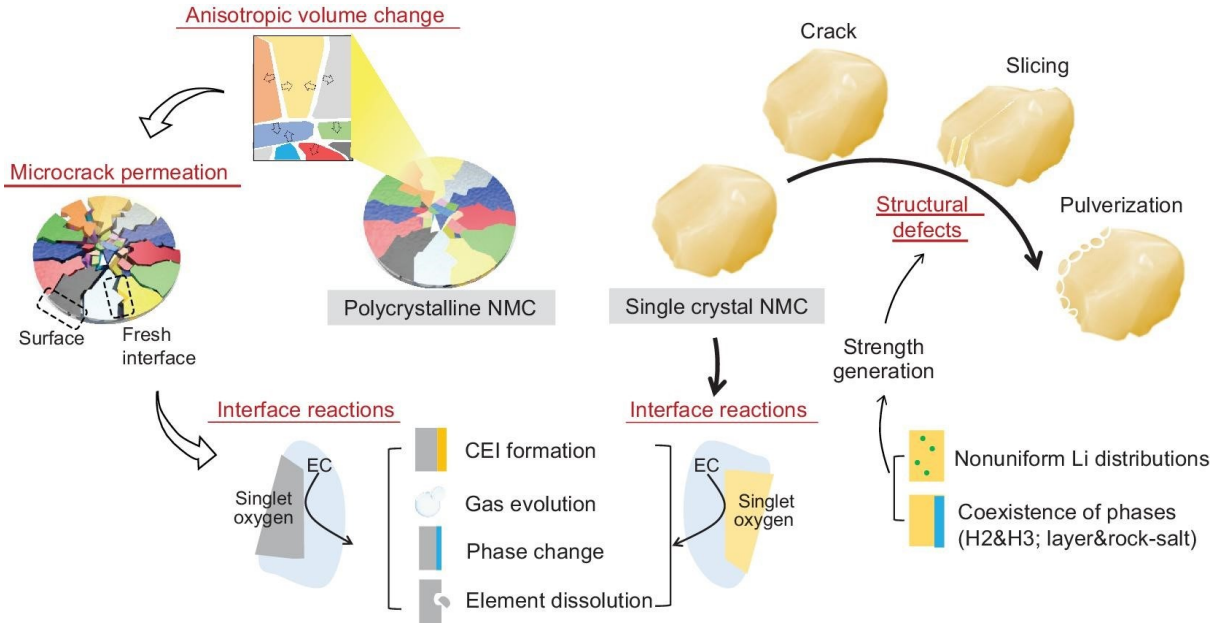


Figure 13 Comparing the Degradation Mechanisms of Single-Crystal and Polycrystalline NMCs. [29] Copyright 2023, NSR National Science Review

## 7. Synthesis of PC Ni-rich Cathodes

The primary objective in synthesizing Hi-Ni NMC layered oxide cathodes is to maximize energy density while maintaining cycle life and safety. This necessitates optimizing the Ni content for high capacity, along with Mn and Co for stability and structural integrity.

Several synthesis methods are available, each with distinct advantages and challenges, including solid-state, co-precipitation, spray pyrolysis, sol-gel, and hydrothermal methods. Co-precipitation is the most commonly used method, followed by solid-state reaction and spray pyrolysis. [56] Each method has its advantages and disadvantages, which can be seen in Table 3 and Fig. 14.

Co-precipitation is widely used due to its ability to produce homogenous materials with controlled particle size and morphology, but it can be complex and generate wastewater. Solid-state reactions offer simplicity and accurate stoichiometry but may result in less homogenous products. Spray pyrolysis enables rapid and scalable production, yet the resulting particles can be smaller and less durable. Understanding these trade-offs is crucial in selecting the appropriate method to achieve the desired cathode performance for specific applications.

Table 3. NMC cathode synthesis method summary [57] Copyright 2018, Materials Research Express

| Methods | Highlights |
|---|---|
| Solid State [58] | [+] Most simple process, correct stoichiometry |
| | [−] Time and energy consuming, low homogeneity |
| Co-precipitation [59] | [+] High morphology and homogeneity, tap density, well atomic-level mixing |
| | [−] Complex parameter control, long residence time, large wastewater, |
| Spray pyrolysis [60] | [+] Faster synthesis, scalable, spherical morphology |
| | [−] Smaller and fragile particles resulting lowering cyclability |

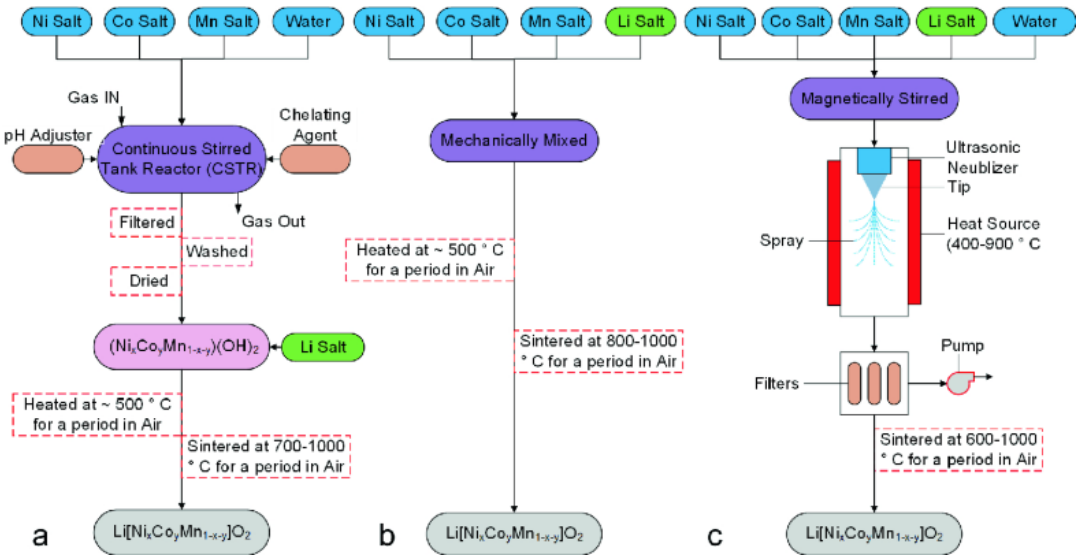

Figure 14 Schematic of NMC battery synthesis methods: a Co-precipitation, b Solid state, c Spray pyrolysis. [61] Copyright 2021, Springer International Publishing

### 7.1.Co-precipitation

Co-precipitation is a widely employed technique for the synthesis of uniform particles at the atomic level through the dissolution of multiple metal salts. The process can be broadly categorized into three stages: (1) nucleation of hydroxide precursor particles, (2) agglomeration of these primary particles, and (3) growth of secondary particles with a defined morphology.

The resulting morphology of the particles has significant implications for the material's rate capability, structural properties, and thermal stability. The manipulation of several key parameters allows for fine-tuning of particle morphology: pH, temperature, stirring speed, reaction time, atmosphere, and the concentration of chelating agents. The most common morphology of particles produced using the co-precipitation method is polycrystalline spherical particles with a size range of 3-12 μm, composed of nano-sized primary particles (50-100 nm). [62] However, by adjusting the co-precipitation conditions, it is possible to produce special morphologies such as single-crystalline.

#### 7.1.1. Co-precipitation Type

The three main types of metal ion sources for the synthesis of NMC precursors are hydroxide, carbonate, and oxalate metal salts. Among these, hydroxide co-precipitation is the most inexpensive method for producing high tap density particles, followed by carbonate and then oxalate. However, to prevent the formation of impurities such as MnOOH and $MnO_2$, which can result from the oxidation of $Mn^{2+}$ to $Mn^{3+/4+}$ when the reaction is exposed to oxygen, hydroxide co-precipitation of NCM must take place in an inert atmosphere such as nitrogen or argon.

Carbonate co-precipitation does not require an inert atmosphere because the Mn stays in the $2^+$ oxidation state during the reaction. However, the disadvantages of this method include the formation of oversized secondary particles and a large surface area, which makes the precursor vulnerable to water in the air and prone to fracturing during calendaring.

Oxalate co-precipitation is cheaper and less harmful to the environment compared to the other two methods, but its slower reaction rate and tendency to deviate from the desired composition of the feed remain challenges.[63]

### 7.1.2. Parameters of Synthesis

The hydroxide precursor process is the main process for layered cathode synthesis for the following reasons. During calcination, the valences of the transition metals usually rise to balance the change of anion groups (i.e., from $-(OH)_2/-CO_3$ to $-O_2$). The change of anion groups during calcination is accompanied by the release of $H_2O$ for hydroxide precursors or $CO_2$ for carbonate precursors, as well as the formation of pores. As the mass fraction of anion groups in hydroxide precursors is lower than that in carbonate counterparts, hydroxides release less gas and can form denser cathodes. [64]

The hydroxide precursors process originated from the early studies of Samsung SDI Co. [65] Lee et al. optimized the synthesis condition ranging from 0.12–0.36 M ammonia, pH 11–12, and stir rate of 400–1000 rpm. [66] As the chelating agent increased from 0.12 to 0.36M, tap density increased from 2.04 to 2.23. The results also showed that the increased stir rate also resulted in more spherical and homogenous secondary particles.

The influence of pH is the most important factor because the hydroxide ion is the target precipitation agent. The higher pH values mean a greater driving force for nucleation and growth, leading to smaller secondary particles due to higher supersaturation and faster precipitation speed. [67,68] Barai et al. [69]calculated the impact of pH on the size of secondary particles. The experimental results in Fig. 15 a-c matched the calculated results and demonstrated the relation between pH and particle size.

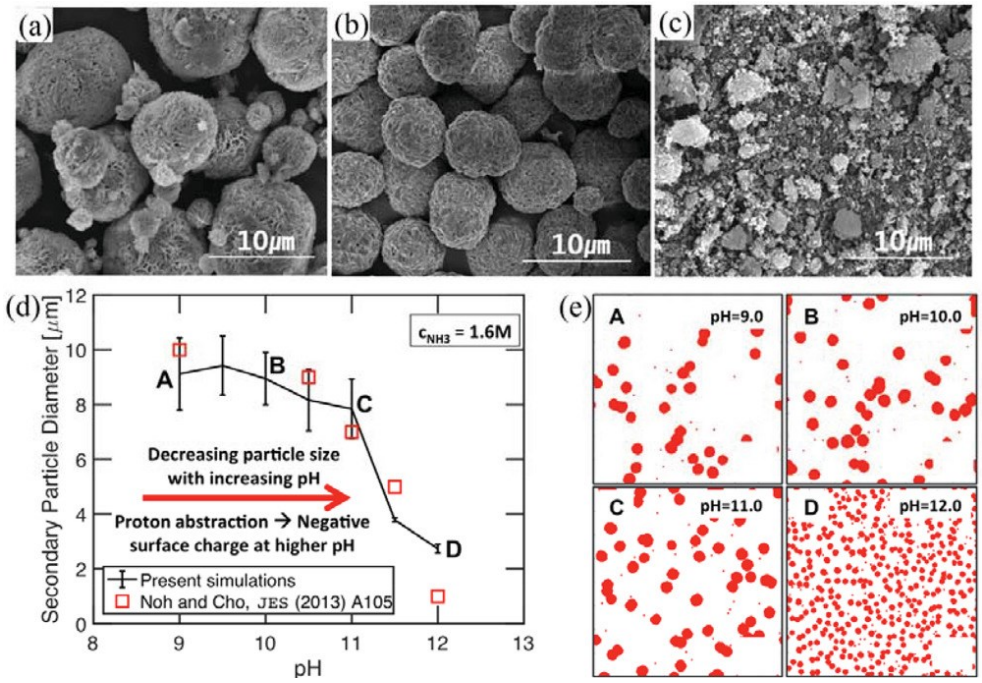


Figure 15 a–c) SEM images of $Ni_{0.5}Co_{0.2}Mn_{0.3}(OH)_2$ precursors synthesized at pH values of 9.0, 11.0, and 12.0, respectively. [70] d) Experimental result (red squares) and calculated result (black line with error bars) of variations in secondary particle size at various pH values, together with e) the predicted particle size distribution at the corresponding pH values. [69] Copyright 2019, The journal of physical chemistry

After the co-precipitation reaction, the precursor is dried and mixed with lithium salt then calcinating at a temperature range from 700-1000 ºC. The synthesis condition must be optimized for the high-Ni cathode in which nickel atomic content is more than 60%. The production processes for hi-Ni cathode are shown in Fig. 16, including modified co-precipitation, LiOH (instead of $Li_2CO_3$) as the Li source, longer, multistep calcination using flowing $O_2$, necessary post calcination surface treatments and vacuum/$N_2$ packaging; most equipment necessitates high corrosion resistance (LiOH and $O_2$) and strict humidity control. [71]

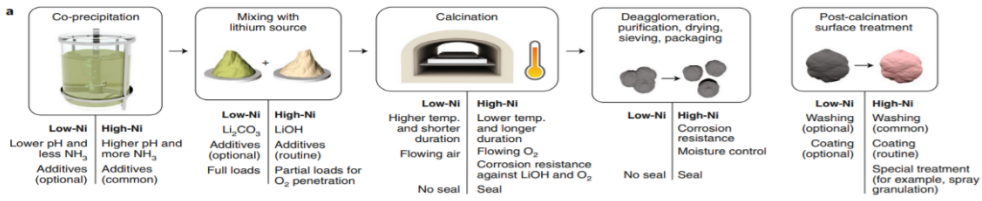


Figure 16 Schematic illustration of the industrial synthesis of Low-Ni | Hi-Ni layered oxides cathode. [71] [72] Copyright 2020, American Chemical Society

Moreover, post-calcination surface treatments are mandatory as the chemical reactivity of the surface layer is increased due to the more oxidizing $Ni^{3+}/Ni^{4+}$ redox potential. [35] The use of excess Li precursors during the manufacturing process likely leads to Li residual on the surface of the Hi-Ni cathode, usually in the form of unreacted $Li_2O$, which quickly reacts with moisture and $CO_2$ to form LiOH or $Li_2CO_3$. [44] The presence of $Li_2CO_3$ on the surface of the Hi-Ni cathode appears to be unavoidable. Washing these cathode materials to remove such residues is often crucial for electrochemical performance. [73,74] However, excess water was proposed to lead to severe extraction of Li from the layered structure, while ethanol was suggested to be a promising (but more costly) alternative. [75]

In conclusion, co-precipitation is by far the most popular synthesis method of NMC/NCA. Good mixing at the atomic level, high tap density, and low cost are the key factors of its popularity. On the other hand, complex synthesis parameters and a large amount of waste ammonia water remain challenging for industrial applications, but it is by far the most suitable method for batch production.

### 7.2.Solid-state synthesis

The solid-state reaction method is the simplest and the oldest method to synthesize NMC/NCA. The mainstream two-step synthesis includes mechanical mixing (with mortar, pestle, or mechanic milling), a low-temperature heat treatment at about 500 ºC, and a high-temperature sintering at 800~1000 ºC.

The advantages of the solid-state reaction include easy processes and correct stoichiometry of lithium and transit metal, yet it requires strong mechanical mixing and a long, high-temperature sintering process. Transit metal atoms must move relatively long distances to form a layered structure, so the high temperature can accelerate the diffusion process and a long calcination time can stabilize the structure. It inevitably leads to high energy consumption. Nonetheless, low homogeneity and poor morphology significantly hinder the electrochemical performance.

## 8. Synthesis of SC Ni-rich Cathodes

The production of single-crystal NMCs in large quantities is similar to that of polycrystalline NMCs. Methods for various synthetic steps can be modified and combined. The combination of high-temperature solid reaction and co-precipitation has gained more attention compared to other techniques like sol-gel [76] and spray pyrolysis [77]. Given that this combination presents

promising prospects for practical applications, our focus will be on the various changes in parameters within this combination.

### 8.1.Co-precipitation Method for Synthesizing Precursors of SC Ni-rich Cathodes

Co-precipitation-based synthesis can be divided into three types based on calcination conditions: high-temperature synthesis [78], multi-step synthesis [79], and molten-salt synthesis [48]. As described in the previous chapter, the co-precipitation approach is frequently used to create precursors for both single-crystal and polycrystalline NMCs [80]. As shown in Fig. 17, the salt solution concentration, pH, reaction temperature, reaction time, stirring speed, and other factors significantly impact the morphology, particle size, and agglomeration degree of the hydroxide precipitates. [81] Usually, SC precursors are smaller than precursors for PC NMC synthesis. [78] Radii of hydroxide precursors for PC NMCs are about 10 μm, while those for SC NMCs range from 2 to 5 μm [78]. Precursors with medium-sized and dense-fibriform morphology can help prevent primary particle agglomeration during high-temperature sintering, facilitating the formation of well-dispersed monocrystalline grains. Therefore, precise control over both the primary and secondary particle sizes of hydroxide precursors is crucial. There are generally two ways to obtain such hydroxide precursors: crushing larger precursors used for polycrystalline NMCs into smaller ones (I and III in Fig. 17) or synthesizing precursors of a suitable size directly. (II and IV in Fig. 17)

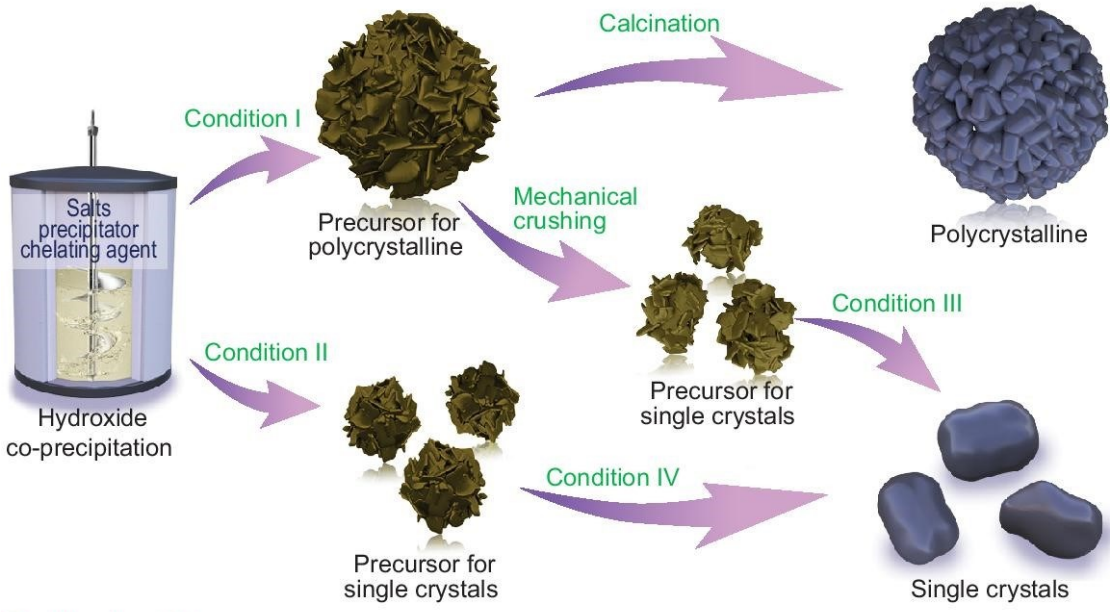


Figure 17 Synthesis Methods for SC and PC NMC cathodes [29] Copyright 2023, NSR National Science Review

### 8.2.High-temperature solid-state Method for synthesizing SC Ni-rich Cathodes

High-temperature synthesis is the simplest and most commonly used method for the commercial mass production of single-crystal NMCs. This process typically involves three steps: mixing precursors with lithium sources, producing $(NixMnyCoz)(OH)_2$ precursors—which are now readily available due to advancements in synthesis techniques—and heat treating the primary particles at approximately 900°C. This high-temperature treatment is essential for the particles to grow sufficiently into single crystals instead of polycrystals. [50]

However, maintaining the temperature above 900°C can result in excessive lithium volatilization, leading to agglomerated, irregular particles, increased lithium evaporation, and higher energy consumption. [82,83] Additionally, high temperatures aggravate cationic disordering in single crystals, potentially forming a rock-salt phase on the particle surface, which increases impedances and lowers performance. (Fig. 18) Key factors in high-temperature synthesis, such as sintering temperature and duration, and Li/TM (transition metal) ratios, significantly influence the crystal structures and particle morphologies of single-crystal NMCs. To remove excess lithium and stabilize the surface of single crystals, post-treatments like washing or secondary sintering are generally necessary. Although washed single-crystal NMC622 shows higher capacities, it cycles poorly after the washing-heating treatment due to surface structure damage.

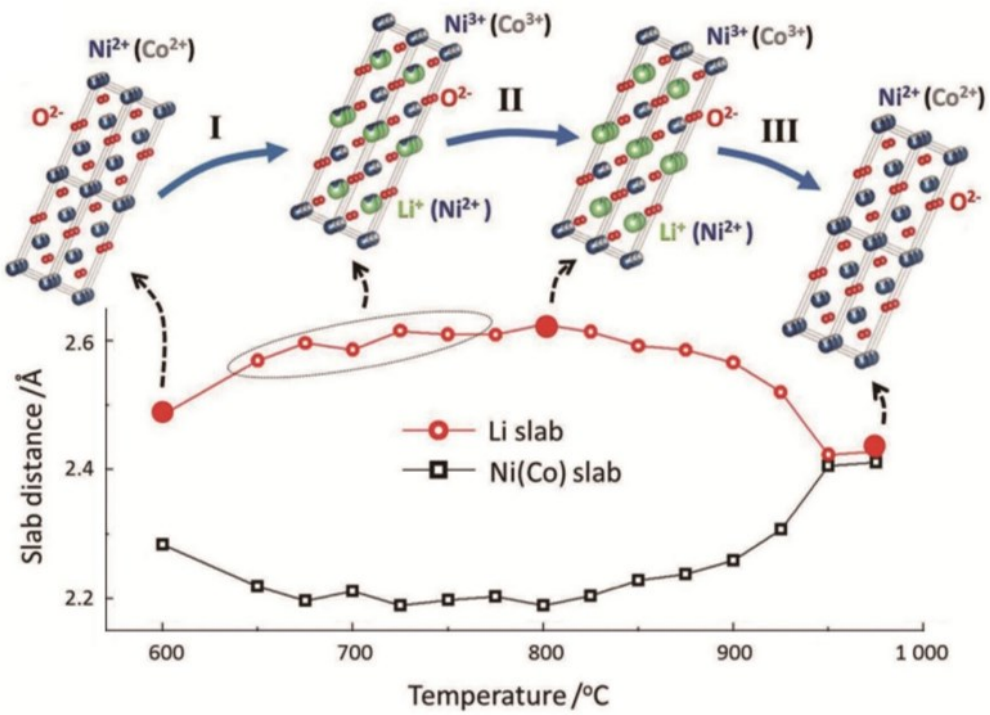


Figure 18 A schematic illustration depicting the phase evolution of intermediates and the variation in slab distance between Li and Ni (Co) as a function of temperature. [84] Copyright 2022, Electrochemical Energy Reviews

### 8.3.Flux Method for Synthesizing SC Ni-rich Cathodes

Given the morphological and structural defects induced by high temperatures, synthesizing single-crystal nickel-rich cathodes at temperatures below 950 °C is essential. This can be achieved using the low mutual melting eutectic of molten salt or flux growth methods. Unlike high-temperature solid-state reactions, flux growth is a liquid-phase method that yields high-quality, well-developed oxide crystals at low temperatures. During sintering, fluxes become molten, allowing lithium sources and transition metal (TM) sources to react and form single crystals. Active elements dissolve and diffuse in the molten-salt flux, facilitating rapid crystal growth. This process requires only a low sintering temperature, which helps minimize cationic mixing and particle agglomeration. The schematic diagrams of the synthesis method of SC cathodes are shown in Fig. 19.

The crystal formation mechanism involves three sequential processes: dissolution, nucleation, and crystal growth. The growth rate of particles is closely related to the degree of supersaturation. Excessively high supersaturation results in numerous crystalline sites and dendrite growth, rather than well-faceted new crystal growth, while excessively low supersaturation prevents nucleation. Therefore, identifying the optimal supersaturation point is

crucial for producing high-quality single-crystal materials. Additionally, achieving uniform single-crystal size depends on the relative rates of nucleation and growth, which necessitates precise temperature control. [84]

Among flux methods, using salt as the flux is known as the molten salt method. Based on their chemical components, molten salts are divided into two categories: those containing lithium elements (e.g., LiCl, $LiNO_3$, and $Li_2SO_4$) and those without lithium elements (e.g., NaCl and KCl). The amounts of molten salts used are typically several times higher than the amounts of lithium and transition metal (TM) sources, leading to significant residual fluxes on particle surfaces after sintering. These residual fluxes are electrochemically insulating and must be removed by dissolution in common solvents, preferably water. However, high-nickel layer oxides are susceptible to damage from atmospheres containing $H_2O$ and $CO_2$ [85,86]. Research indicates that washing can effectively remove residual surface salts and that superficial properties are modified through $Li^+/H^+$ exchange behavior [87,88].

In conclusion, molten-salt synthesis faces several challenges, including high costs associated with materials, technologies, and equipment, a tedious procedure, and poor product consistency and production capacity.

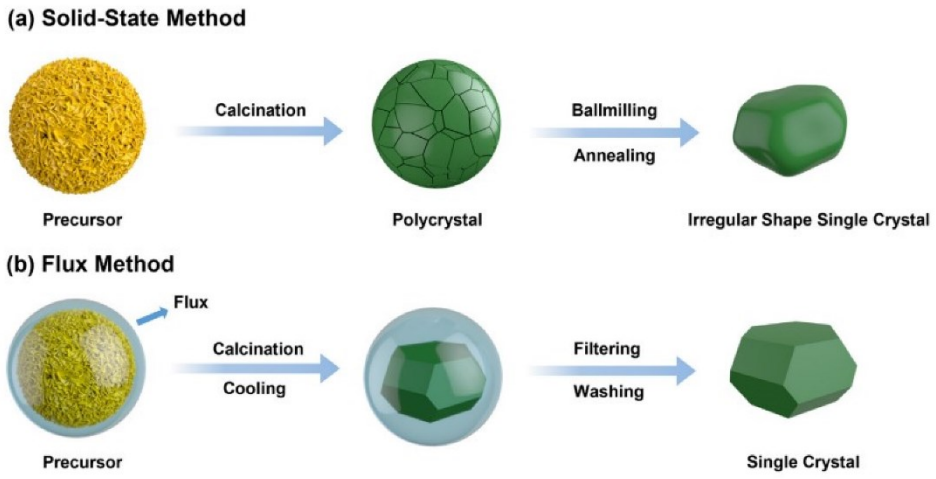


Figure 19 Schematic diagrams of the main synthesis strategies for single-crystal nickel-rich NCM materials [19] Copyright 2021, Elsiver

## 9. Modification for PC Ni-rich Cathodes

Unremitting efforts have been made on the modification of NMC cathodes. Approaches consist of coatings to protect irreversible reactions to electrolytes; modification of internal structures

through doping or gradient concentrations; or more dramatic structural strategies, such as single crystals, heterostructures, and microstructures. Several modification methods will be introduced in this chapter, including their theoretical mechanisms, methods, and practical examples.

### 9.1.Doping for PC Ni-rich Cathodes

Doping is a modification method by introducing selected molecules into the layered structure of the cathode to strengthen the NMC cathode in terms of capacity, stability, and rate ability, etc. Based on the site that can be substituted in the crystal structure, doping can be classified into three types: lithium sites at 3a, transition metal sites at 3b, and oxygen sites at 6c. Theoretically, doping does not alter the structure of the cathode material, nor does it form impurities. In reality, optimal amounts of dopant ought to be very small, as disadvantages often coincide with benefits. Large usage can severely worsen electrochemical properties. [89]

Although the mainstream synthesis method is through co-precipitation, doping is often done during the lithium impregnation step. Dopants are coated onto cathode materials and incorporated into final products during heat treatment, and a large amount can result in notable compositional non-uniformity and performance inconsistency at industrial production scales. [71]

The doping mechanism was proposed as shown in Fig. 20. Doping can restrain $Ni^{2+}$ from occupying $Li^{+}$ vacancies, which decreases the phenomenon of cation mixing, increases the unit cell parameter, and improves the electrochemical performance of the material by lowering the irreversible capacity loss during cycling.

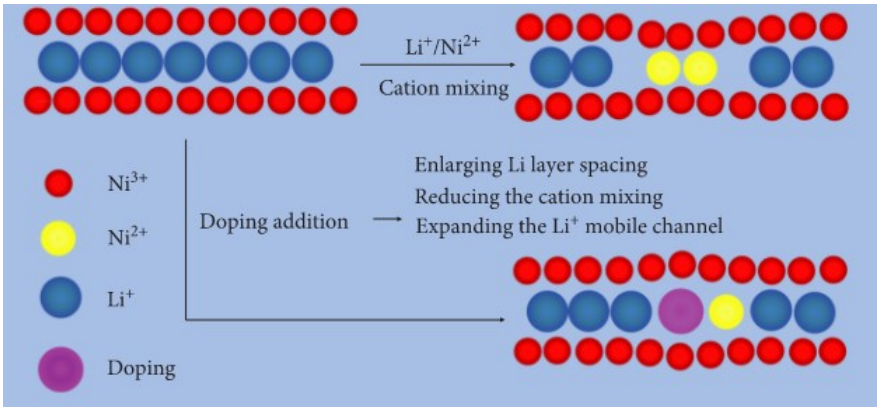


Figure 20 Doping mechanism theory [90] Copyright 2019, International Journal of Photoenergy

### 9.1.1. Doping on different sites (Li, TM, and O2)

Doping on the transition metal site is the most used method. Fundamental properties such as stoichiometry, site occupancy, and long-range ordering are crucial to a strategic compositional design. For instance, dopant cations with an ionic radius smaller than $Ni^{3+}$ (0.56 Å) tend to cluster (for example, $Al^{3+}$, 0.535 Å), whereas larger cations promote the formation of rock-salt structures (for example, $Ti^{4+}$, 0.605 Å; $Zr^{4+}$, 0.72 Å; $Nb^{5+}$, 0.64 Å; $W^{6+}$, 0.60 Å) or substitute $Li^{+}$ in the lithium slabs (for example, $Ni^{2+}$, 0.69 Å; $Mg^{2+}$, 0.72 Å) depending on their valence states. Metal–oxygen bonds are strengthened by certain dopants (for example, Al, Ti, Nb, Zr, Ta, W, Cr) and weakened by others (for example, Zn). The comparison of doping on different sites is shown in Fig. 21. [71]

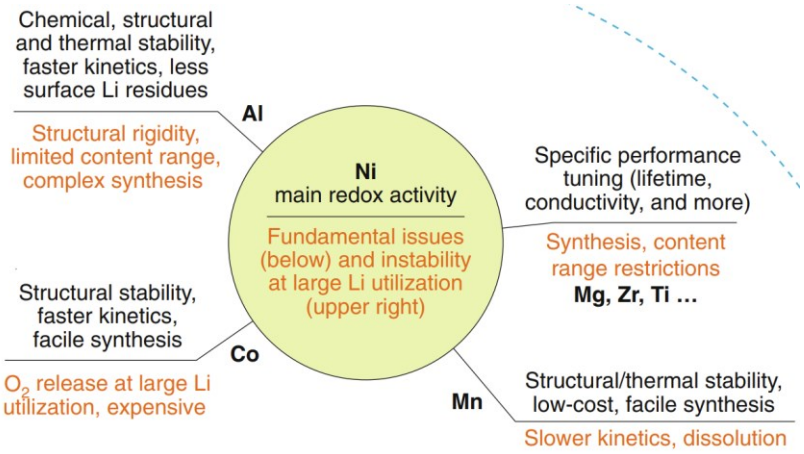


Figure 21: A comparison among a variety of dopants established at industrial production (that is, Co, Mn, Al, Mg, Zr, Ti, and more) in property tuning, costs, and ease of synthesis [35,71,91] Copyright 2020, Nature Energy

Cations can also be doped on lithium sites to enforce structure stability. Na-doped samples have structure stability, resulting in better rate performance, good oxidation resistance, lower potential polarization, etc. On the other hand, K has a similar chemistry to Na and a larger ionic radius (1.38 vs. 1.02 Å), and lower electronegativity [92,93]. Dopant $K^{+}$ replaces lithium with a larger ionic radius steadily, which can restrain the irreversible phase transition between H2 and H3 and the formation of spinel and rock salt phases.

### 9.2.Coating for PC Ni-rich Cathodes

As described in the previous chapter, several intrinsic drawbacks make NMC cathode unable to fully fulfill the needs of EV applications. Degradation mechanisms that reduce voltage and retention include instability of the delithiated state of layered TM oxides, side reactions with electrolytes, phase transitions, structural degradation, TM cation dissolution, oxygen evolution,

and cracking.[94] Surface coating is an effective solution to extend the cycle retention.[95] An effective coating material should prevent reaction with the electrolyte and process high electronic transmission ability. It is recognized that the thin, uniform, and highly conductive coating layer is the most crucial element since the coated material is electrochemical inactive and decreases the energy density.

Despite several positive electrochemical results that have been proposed on surface coating, the mechanism and the features of surface coating are yet well understood. Generally, the coating mechanism can be categorized into (1) Prevent direct contact between electrolyte and bare cathode. Subsequently, it can suppress metal dissolution and avoid the problem of excess lithium on the surface. (2) Coating, which is a type of "HF scavenger", can react and eliminate the HF in the electrolyte near the cathode surface, protecting the cathode from HF attack. (3) Coating can slow down the John-Teller effect, leading to suppression of phase transition and the improvement of structural stability. (4) Coating with high conductivity can reduce the polarization and the interfacial resistance of the cell, as well as increase the lithium transportation between cathodes and electrolytes.

Coating methods range from industry-feasible wet and dry processes to highly uniform but costly chemical vapor deposition (CVD) [96] and atomic layer deposition (ALD) [97,98]. The wet process washes off surface Li residues directly with water or organic solvent while coating precursors are precipitated onto the cathode and form a more uniform coating upon solvent evaporation during the dry process. [71,99] Water-based washing promotes surface rock-salt phase formation (Li leaching) and decreases specific capacity and cyclability. On the other hand, wet coating in organic solvent avoids such issues but increases the cost and the risk of fire. [71,99]. CVD and ALD provide uniformity. Even though the recent advances in continuous ALD systems drastically decrease the cost, these methods need to decrease further in the price for large-scale implementation.

## 10. Modification for SC Ni-rich Cathodes

To modify single-crystal (S.C.) NMC cathodes, the primary and traditional strategies are atom doping and surface coating. Atom doping involves substituting atoms in the crystal lattice (nickel, cobalt, manganese sites) with stable dopants such as calcium, magnesium, aluminum, titanium, zirconium, molybdenum, tungsten, niobium, and tellurium. This process strengthens

the structural integrity and mitigates tension during phase transitions in lithiation and delithiation. [100–109]

Surface coating, on the other hand, applies protective layers to prevent the cathode materials from reacting with the electrolyte, thus reducing parasitic side reactions. Oxide coatings, for instance, react with HF to prevent cathode corrosion, while fluoride and phosphate coatings form thermodynamically stable layers after initial cycles. [110–119] Although these strategies delay cathode degradation, mechanical stress continues to build at the grain boundaries, eventually causing structural failure and capacity loss.

### 10.1. Doping for SC Ni-rich Cathodes

To address the problem of slower Li+ diffusion rates and persistent Li diffusion imbalance in SC cathodes, doping strategies are being extensively researched. These strategies focus on forming strong bonds between the doping elements and oxygen, which suppresses the cation mixing effect, effectively stabilizing the crystal structure and mitigating internal structural deformation. [120]

For instance, Liu et al. significantly enhanced the rate capability and lifespan of single crystals by doping 0.6 mol% B into $LiNi_{0.83}Co_{0.05}Mn_{0.12}O_2$ SC cathode. They formed pouch-type full cells that showed a remarkable capacity retention rate of 91.35% after 500 charge-discharge cycles, a significant improvement compared to the undoped sample, which had a retention rate of 66.95%. [121]

Similarly, Sim et al. demonstrated that a 0.05 mol% Va-doped single crystal with 84% Ni content achieved an excellent initial discharge capacity of 204.4 mAh g-1 and a capacity retention rate of 88.1% over 80 cycles. This improvement was attributed to the enhancement of Li-ion kinetics through Va-ion doping. [121]

Also, Ou et al. co-doped Al and Zr into $LiNi_{0.88}Co_{0.09}Mn_{0.03}O_2$ single crystals. This co-doping strategy improved rate performance and lifespan at both low and high voltages up to 4.6 V. The cells maintained a high capacity of 121.2 mAh g−1 even after 350 cycles at a high discharge rate of 5.0 C. The success was attributed to the synergy of Al and Zr co-doping: Al ions were effectively incorporated into the single-crystal NCM lattice, while the less soluble Zr ions aggregated on the external particle surface. This synergy improved Li-ion mobility, alleviated

internal deformation, and effectively suppressed Li/Ni cation mixing, even under high-voltage conditions and complete Li depletion. [122]

Efforts to address the Li diffusion imbalance in Ni-rich single crystals through doping are ongoing. These strategies fundamentally enhance Li-ion mobility and stabilize the crystal structure, ultimately extending the lifespan of the materials.

### 10.2. Coating for SC Ni-rich Cathodes

Despite their modified morphology, Ni-rich single-crystal cathodes experience surface degradation, leading to relatively low first-cycle charge/discharge efficiency. The irreversible capacity loss during the initial cycle cannot be restored, posing a significant challenge when transitioning from half-cell evaluations with unlimited Li supply to full-cell applications with limited cathode material. Therefore, enhancing the initial Coulombic efficiency is crucial.

One major cause of low initial Coulombic efficiency is surface degradation, which includes side reactions and cation mixing during the initial charge. Surface Ni becomes unstable, undergoing cation mixing and reacting with the electrolyte to form byproducts like NiO. To mitigate these issues, surface modifications using additives and coatings are essential, similar to approaches used for polycrystalline counterparts. These modifications aim to either prevent direct contact with the electrolyte or stabilize surface Ni ions, thereby increasing the activation energy for severe cation mixing and improving efficiency.

Zeng et al. proposed a surface coating strategy to form multifunctional $LiBO_2$/$LiAlO_2$ layers on NMC532 [123]. The $LiAlO_2$ layer maintains intimate contact with the cathode, while $LiBO_2$ serves as an external isolation layer to prevent interfacial instability between the cathode and the electrolyte. This coating strategy potentially enhances the electrochemical performance of the cathode.

Zeng et al. synthesized surface aluminum-doped single-crystal NMC532 through a combination of coprecipitation and calcination. [124] The aluminum content on the surface and in the bulk of the product is approximately 1.05% and 0.02%, respectively. This surface aluminum doping results in NMC532 with improved capacity retention at high temperatures and higher cutoff voltages due to a more stable interfacial structure.

Additionally, Zhao et al. demonstrated that fluorine-doped single-crystal nickel-based cathode materials facilitate the expansion of the unit cell along the c-axis, which enhances the kinetics of $Li^+$ transport. [125] The calculated lithium-ion diffusion coefficient ($DLi^+$) suggests smoother lithium-ion migration, thereby improving the electrochemical performance of the cathode materials.

However, surface modifications alone, such as addressing Li diffusion imbalance and bulk structure degradation, have limitations in fundamentally solving issues in Ni-rich single-crystal cathodes. Therefore, improvements through surface modification are typically limited to a few percentage points. Further research and a deeper understanding of these mechanisms are required to fully explore the potential of this area.

## 11. Characterization Technique

This section introduces the techniques, methods, and procedures used to evaluate properties of NMC cathode materials, study synthesis processes, and analyze the compositions and morphologies of the modified cathodes. For a fundamental understanding of the relationship between the synthesis methods applied and the resulting cathode properties, and further battery performance, a manifold of techniques has been applied, both computational and experimental. Below, a brief introduction to the techniques and methods used is presented, preceded by a summary of the applied techniques, along with their scientific targets.

### 11.1. XRD

X-ray diffraction (XRD) is a powerful analytical technique complementary to conventional imaging methods, providing detailed information about the crystallographic structure, chemical composition, and physical properties of materials. Unlike optical microscopy, which is limited by the Abbé diffraction limit (approximately $\lambda/2$, where $\lambda$ is the wavelength of light), XRD overcomes these limitations by utilizing X-rays. These X-rays, generated by an X-ray tube, are directed at the sample where they interact with the atomic planes in the material, producing a diffraction pattern. The positions and intensities of these diffracted beams are recorded, revealing the sample's crystallographic structure with high precision.

XRD is particularly well-suited for identifying phases in polycrystalline materials and measuring the size and strain of crystalline regions. For instance, in the analysis of battery electrodes, XRD can determine the crystalline phases present in both the anode and cathode

materials. Samples prepared for XRD analysis are typically ground into fine powders to ensure a uniform diffraction signal. During the analysis, the sample is exposed to X-rays typically at a fixed angle, and the diffracted X-rays are detected by a goniometer, which measures their intensity and angle of deviation. This data is then processed to produce a diffraction pattern, which can be matched to known standards for phase identification.

For example, in the study of NMC cathodes, XRD can detect changes in the crystalline structure as lithium ions intercalate during battery operation. An XRD analysis was performed using a Cu Kα radiation source with a wavelength of 1.54 Å. The sample was scanned over a 2θ range from 10° to 80°, with a step size of 0.02° and a counting time of 1 second per step. This high-resolution data allows for the precise determination of the NMC's interlayer spacing and the identification of any new phases that form during the charge and discharge cycles.

### 11.2. ICP

Inductively Coupled Plasma (ICP) is a highly sensitive and versatile analytical technique used for elemental analysis, often employed alongside traditional spectroscopic methods to determine the composition of various samples. Unlike techniques that rely on the diffraction or absorption of light, ICP utilizes a high-temperature plasma source to excite atoms and ions in the sample, causing them to emit characteristic wavelengths of light. This emitted light is then analyzed to quantify the elemental composition with exceptional precision

ICP is particularly well-suited for detecting trace elements in a wide range of matrices, from environmental samples to biological tissues. For example, in the analysis of trace metals in water, the sample is first nebulized into a fine aerosol and introduced into the plasma, which is typically sustained by a radio frequency (RF) generator. The high temperature of the plasma (approximately 10,000 K) efficiently atomizes and ionizes the sample. The emitted light from these excited species is collected and analyzed by a spectrometer, allowing for the detection and quantification of elements at concentrations as low as parts per billion (ppb).

For instance, in the study of environmental pollutants, ICP can identify and measure heavy metals such as lead, mercury, and arsenic in soil or water samples. A typical ICP analysis might involve an ICP-OES (Optical Emission Spectroscopy) system with a radial or axial viewing configuration. Samples are often prepared by acid digestion to ensure complete dissolution of the elements of interest. During analysis, the sample aerosol is introduced into the plasma torch, and the emitted light is collected by a monochromator, which separates the light into its

component wavelengths. The intensities of these wavelengths are measured and compared to calibration standards to determine the concentrations of the elements in the sample.

ICP's ability to provide rapid, accurate, and multi-element analysis makes it an invaluable tool in fields ranging from environmental monitoring to industrial quality control and biomedical research.

### 11.3. SEM

Scanning electron microscopy (SEM) is a complementary technique to conventional optical microscopy with a greater resolution power. The Abbé diffraction limit sets the resolution limitation to approximately equal to λ/2, where λ is the wavelength of the light, but is here overcome by the substitution of visible light with an electron beam. The beam of electrons from an electron gun is directed to magnetic lenses which collimate and focus the beam to a small spot (Figure 22). The beam spot is used to scan the sample, and its size determines the resolution of the SEM – it can be even below 10 nm. The interaction of the electron beam with the sample yields several different radiations, including secondary electrons as a result of a series of excitations and emissions of electrons close to the surface. Thus, the emission of secondary electrons is a surface phenomenon, which can be used to provide a surface image by correlating the intensity of the secondary electrons with the position of the beam on the surface.

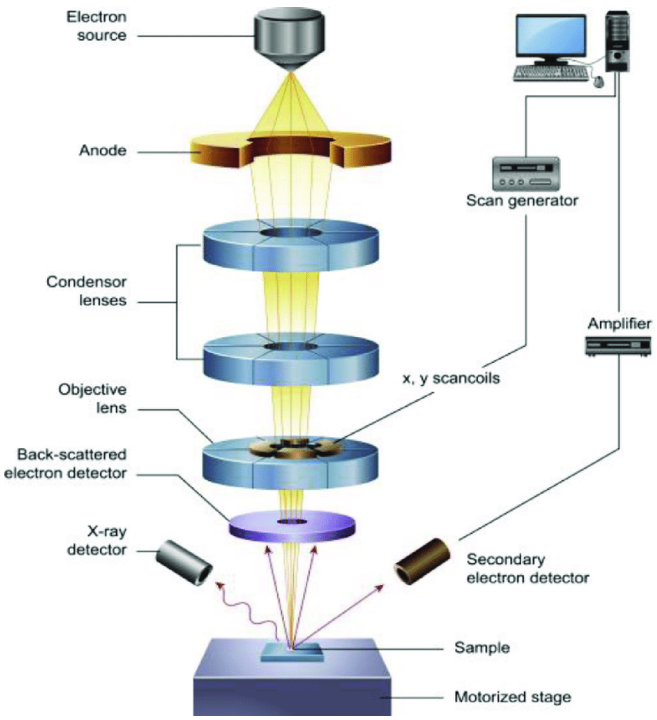

Figure 22: Scheme of SEM. Copyright 2020, Nanotechnology and the Environment

SEM imaging is well suited for morphology studies of different types of electrodes. Imaging was carried out with 5 kV acceleration voltage with secondary electrons. A 60 µm objective aperture was used and the working distance was set to 5 mm.

### 11.4. TEM

TEM overcomes this limitation by using a beam of electrons, which have much shorter wavelengths than visible light. In TEM, electrons are transmitted through an ultra-thin sample, interacting with its internal structure to form an image (Figure 23). The resolution of TEM can be as fine as 0.1 nm, allowing for the visualization of individual atoms.

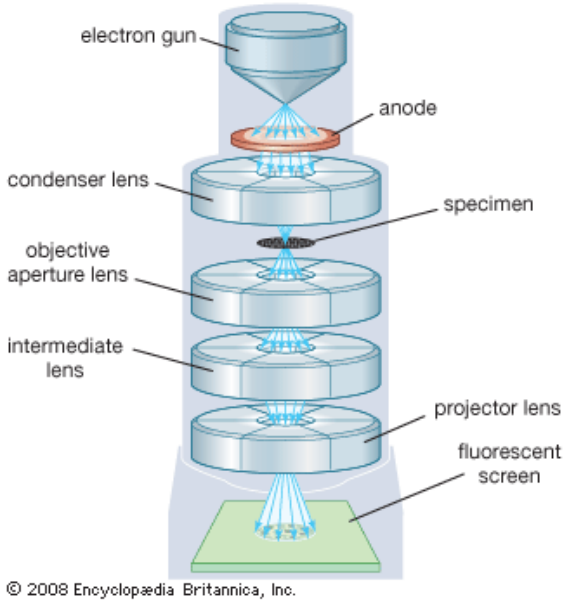


Figure 23: Scheme of TEM setup. Copyright © 2008 Encyclopaedia Britannica, Inc.

TEM is particularly well-suited for examining the internal structure and morphology of materials at the nanoscale. For example, in the study of nanoparticles, TEM can reveal the size, shape, and crystallographic orientation of individual particles. Samples for TEM analysis must be carefully prepared to be extremely thin, often less than 100 nm thick, to allow electrons to pass through. The electron beam, generated by an electron gun and focused by electromagnetic lenses, interacts with the sample, and the transmitted electrons are collected to form an image on a fluorescent screen or a digital detector.

For instance, in the characterization of semiconductor materials, TEM can provide insights into the arrangement of atoms at defects, interfaces, and grain boundaries. A typical TEM analysis

might involve the use of a high-voltage electron microscope operating at 200 kV to 300 kV. The sample is mounted on a specialized grid and placed into the vacuum chamber of the TEM. As the electron beam passes through the sample, interactions such as elastic scattering produce contrast in the image, which is then magnified by additional lenses to provide a highly detailed view of the material's internal structure.

TEM's ability to deliver atomic-scale images and its versatility in analyzing a wide range of materials make it an indispensable tool in materials science.

### 11.5. TEM-EELS

Electron Energy Loss Spectroscopy (EELS) is a powerful technique used in electron microscopy to investigate the electronic structure and chemical composition of materials at the nanoscale. By directing a focused beam of electrons with a narrow energy range through an ultra-thin sample, EELS measures the energy lost by electrons due to inelastic scattering. This energy loss provides information about interactions such as inner-shell ionizations, plasmon excitations, and electronic transitions. In the high-loss spectrum, the ionization edges are characteristic of the elements in the sample, enabling precise identification of elemental composition and chemical bonding states. When combined with a Cs-corrected Scanning Transmission Electron Microscope (STEM), EELS achieves high spatial and energy resolution, allowing detailed studies of material properties, such as oxidation states, band structure, and local thickness variations, at resolutions as fine as ~0.1 nm. This makes EELS an indispensable tool for advanced materials characterization, particularly in energy and nanotechnology research.

### 11.6. Galvanostatic cycling

Galvanostatic cycling is a fundamental electrochemical technique used to evaluate the performance of battery electrodes by measuring their capacity retention, rate capability, and cycling stability. In this method, a constant current is applied to the electrode during both charge and discharge cycles, while the voltage is monitored over time. This provides a direct assessment of how the electrode material behaves under typical operating conditions, making it essential for characterizing lithium-ion batteries.

Galvanostatic cycling measures the amount of lithium that can be reversibly intercalated and de-intercalated into the cathode material, which translates to the specific capacity of the electrode. The technique also reveals critical properties such as the voltage profile, Coulombic

efficiency, and capacity fade over extended cycles. These factors are key indicators of the material's long-term stability and suitability for commercial applications.

For example, in the study of NMC811 cathodes, galvanostatic cycling can demonstrate the material's high initial discharge capacity and its ability to retain this capacity over hundreds of cycles. Cycling tests are typically carried out at different current densities to assess the rate capability of the electrode material, showing how well it performs under both slow and fast charge/discharge conditions. A typical test might involve cycling the cell at a current rate of C/10 (where C is the current required to fully charge or discharge the battery in one hour) for initial capacity measurements, followed by faster rates like 1C to evaluate rate performance.

# Chapter 2
# SYNTHESIS & PREPARATION

## 1. Scope of the study

This thesis investigates the synthesis methods and effects of aluminum doping on nickel-manganese-cobalt (NMC) 811 cathode materials, with a focus on improving their structural and electrochemical stability. The study centers on comparing two synthesis techniques: (1) hydroxide co-precipitation followed by solid-state calcination for creating polycrystalline (PC) cathodes, and (2) molten salt calcination for single-crystalline (SC) cathodes. Additionally, the research explores the introduction of aluminum dopants at various stages of these processes to understand how they affect the structural, morphological, and electrochemical characteristics of NMC cathodes.

A key focus of this study is the stabilization of cathode material interfaces and interphases, particularly in relation to the interactions between aluminum dopants and the NMC host structure. By incorporating aluminum, this research aims to enhance the cathode's structural integrity, improve performance, and extend the material's lifecycle.

The study employs various advanced characterization techniques—including X-ray diffraction (XRD), microscopy, and galvanostatic cycling tests—to systematically assess how synthesis methods and aluminum doping influence NMC cathode properties. These techniques help clarify how different synthesis parameters impact capacity retention and performance, underlining the importance of precise control over these variables.

Lastly, this research aims to contribute to the broader goal of improving the stability and longevity of lithium-ion batteries by refining the composition and structure of NMC811 electrode materials through targeted synthesis methods and doping strategies. By comparing these techniques, this study aims to determine the optimal approach for incorporating aluminum doping to enhance structural and electrochemical stability.

## 2. Initial experimental Setup for precursor synthesis

Building on the foundational work outlined in the timeline, the synthesis of NMC cathode materials involved several critical steps and improvements to ensure reproducibility and precision. The synthesis of NMC cathode materials began with the co-precipitation method to

produce the precursor, then calcinated with solid-state method, as detailed in Chapter 1, Section 7: Synthesis of PC Ni-rich Cathodes. This method served as the foundation for developing the cathode materials and allowed for iterative improvements in experimental design.

### 2.1 Initial Setup for Co-precipitation

The synthesis of NMC precursors using the co-precipitation method began with a fundamental experimental setup that served as the basis for subsequent refinements. Initially, a 2000 mL beaker was used as the reaction vessel, placed on a magnetic stirrer to ensure continuous mixing of the reaction solution. Two separatory funnels were positioned above the beaker, one containing a solution of metal salts and the other a precipitating agent and sodium hydroxide. The reactants were added gradually to the beaker, and the pH of the solution was monitored manually using a pH meter.

Although this initial setup allowed the reaction to proceed, it quickly revealed limitations that needed addressing to achieve consistent and high-quality precursors. The flow rates of the reactants could not be precisely controlled, resulting in inconsistencies in particle size and morphology. Additionally, maintaining a stable pH throughout the reaction proved challenging due to the reliance on manual adjustment. (Fig. 24) These issues were further compounded by suboptimal mixing, particularly as reaction volumes increased, leading to variations in precursor properties. suboptimal mixing, particularly as reaction volumes increased, leading to variations in precursor properties.

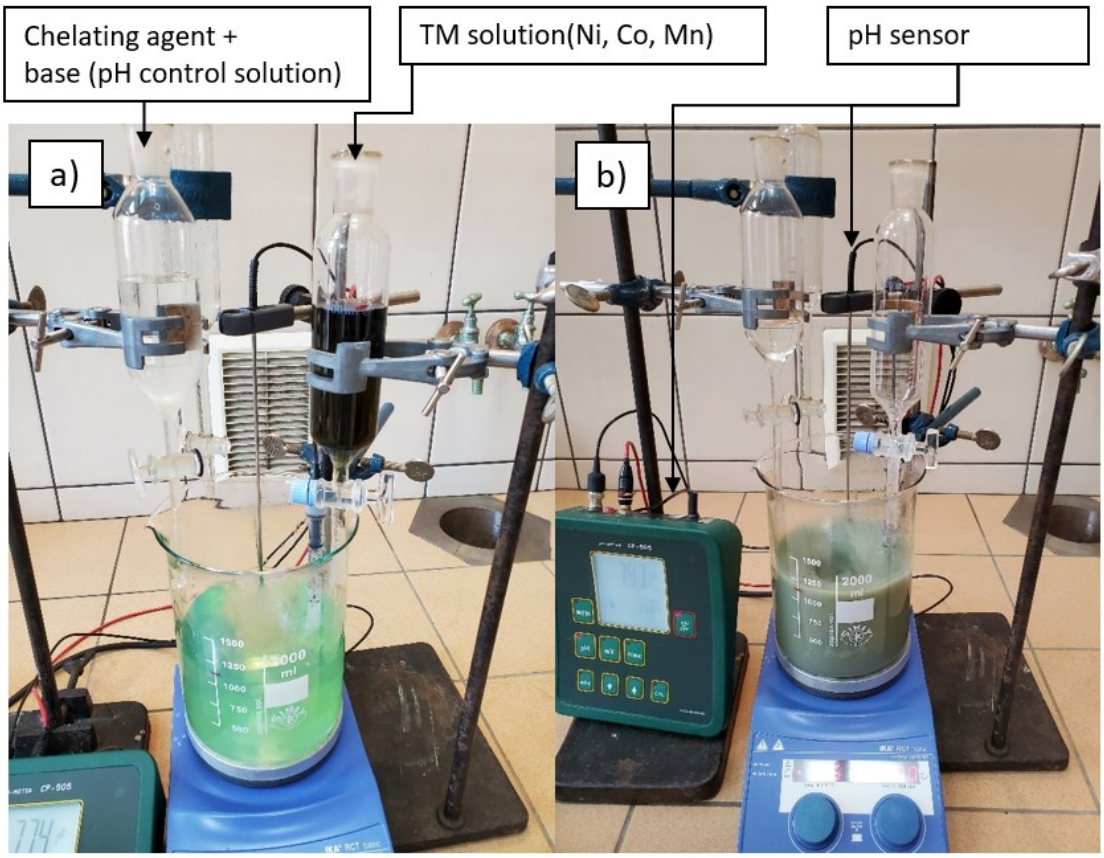


Figure 24 a) The initial experimental setup for NMC precursor synthesis via the co-precipitation method. A 2000 mL beaker serves as the reaction vessel, positioned on a magnetic stirrer to ensure continuous mixing. Two separatory funnels are used: one containing the chelating agent combined with a base (pH control solution) and the other containing the transition metal (TM) solution (Ni, Co, Mn). b) Co-precipitation solution after chelating agent combined with a base and TM solution were added.

### 2.2. Temperature and Evaporation Challenges

To address additional challenges observed during the early experiments, efforts were made to manage temperature inconsistencies within the beaker and mitigate water evaporation during the reaction. A simple yet practical approach was attempted by covering the beaker with tape and a rag (Fig. 25). This modification aimed to reduce heat loss and minimize the evaporation of water, which could affect the concentration of the reaction solution. However, despite these adjustments, the solution's temperature still fluctuated due to the limited insulation provided by the cover, and water evaporation remained a concern during extended synthesis periods. These shortcomings highlighted the need for further improvements to ensure better thermal stability and reaction consistency.

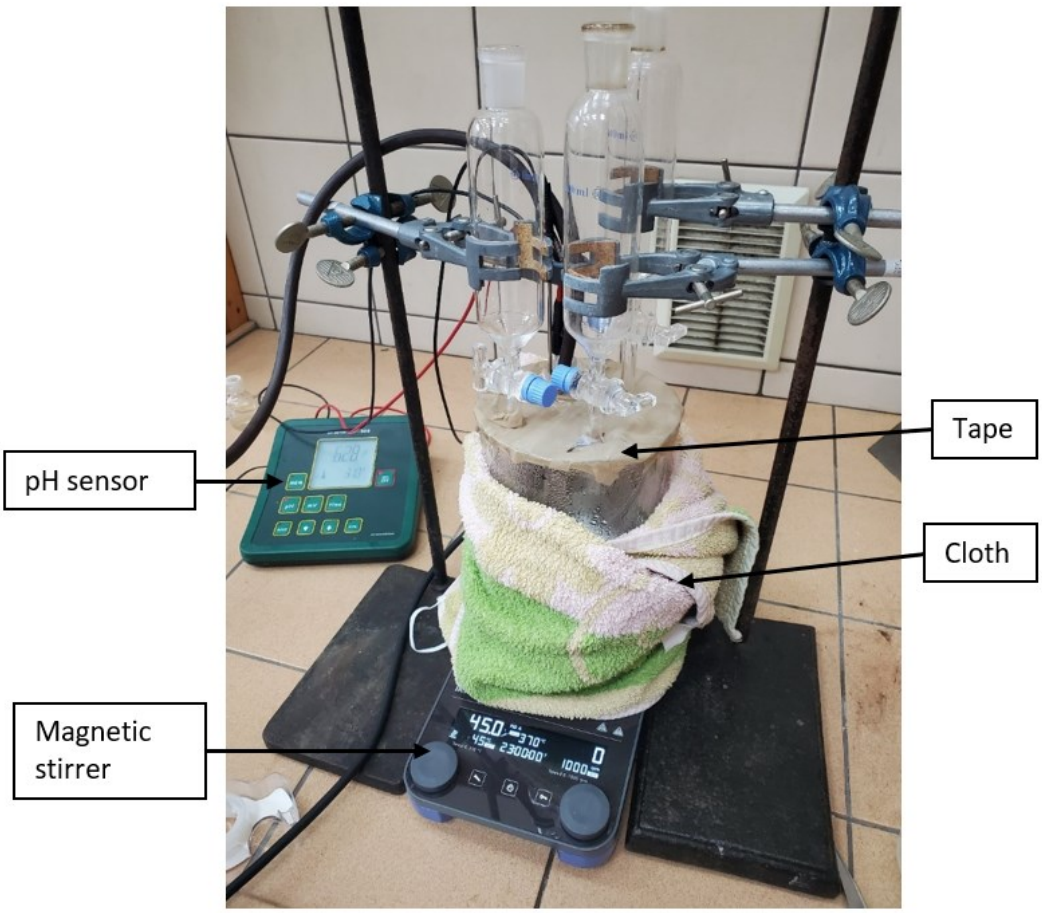


Figure 25 A modified experimental setup for NMC precursor synthesis, designed to address temperature inconsistencies and mitigate water evaporation. The beaker is covered with tape and a cloth to reduce heat loss and minimize evaporation during the co-precipitation process.

### 2.3. Jacket reactor and atmosphere control

The next improvement was the addition of a temperature-controlled reactor using a heated oil circulation system. This system maintained consistent and uniform thermal conditions around the reaction vessel, eliminating temperature fluctuations that could affect reaction kinetics and precursor uniformity. This advancement was especially critical for synthesizing precursors sensitive to temperature variations.

To improve the homogeneity of the reaction mixture, the magnetic stirrer was replaced with a custom-designed impeller. (Fig. 26) This modification ensured more effective mixing, particularly for larger reaction volumes, leading to a more uniform distribution of reactants within the solution. Furthermore, the integration of automated titration pumps allowed for a precise and continuous feed-in flow rate of the reactants. This innovation significantly reduced

inconsistencies in the addition of the metal salt and precipitating agent solutions, leading to improved control over particle size and morphology.

Additionally, the setup was upgraded with the inclusion of a nitrogen atmosphere to minimize exposure to ambient air. This modification prevented unwanted side reactions, particularly the oxidation of transition metals, and ensured a controlled reaction environment, further improving the quality and reproducibility of the NMC precursors.

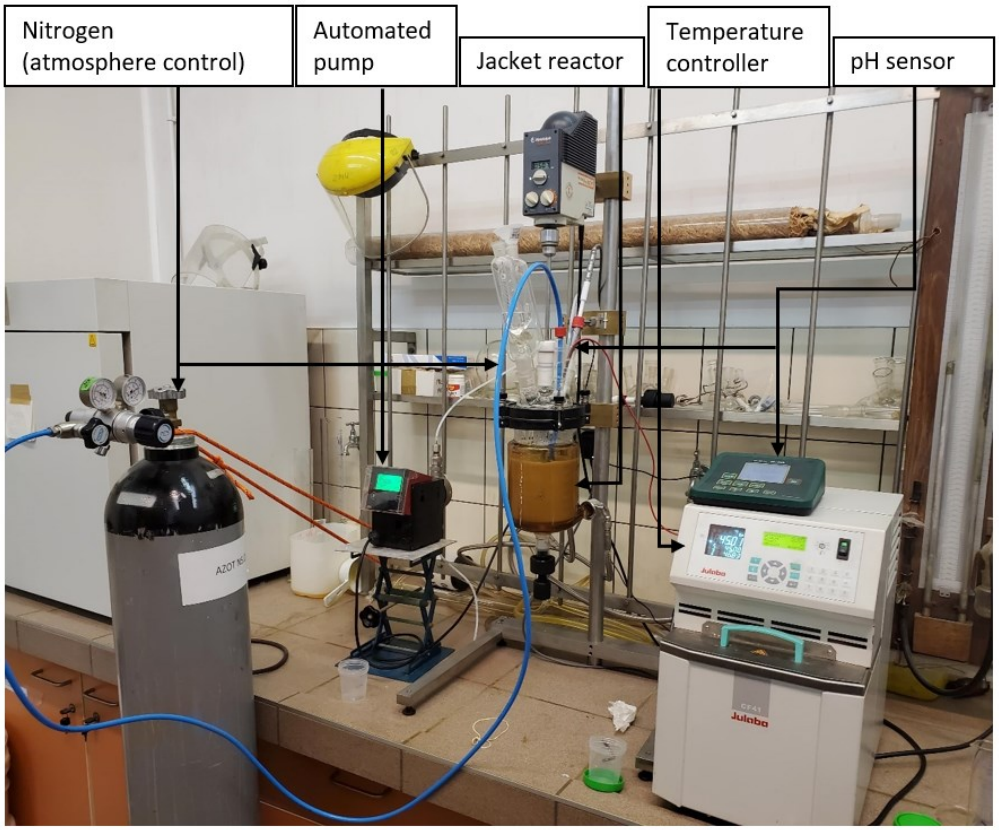


Figure 26 The upgraded experimental setup for NMC precursor synthesis, featuring a jacketed reactor with a temperature-controlled oil circulation system, pH sensor, and a nitrogen atmosphere control system.

### 2.4. Real-Time pH Monitoring with Feedback Control

While the initial experiments laid the groundwork, more advanced optimization was essential to meet stringent electrochemical performance benchmarks. Maintaining the target pH during the reaction relied on manual adjustments, which introduced variability during longer synthesis runs. Additionally, while the controlled temperature and enhanced mixing addressed many issues, the need to further automate the pH control process became apparent. Inconsistent pH

levels, even with improved flow rate control, highlighted the importance of developing a feedback system to dynamically link pH monitoring with reactant addition.

Recognizing these challenges, the final setup incorporated additional advancements to address these limitations, integrating real-time pH monitoring with automated flow rate control and enhancing the inert atmosphere to optimize the reaction environment further.

This next phase was done in the setup where pH sensor is linked directly to the feed-in flow rate, creating an automated feedback loop that dynamically adjusted the addition of the precipitating agent to maintain a steady pH. This automation significantly improved control over the reaction kinetics, ensuring uniform particle size and morphology. Also, an inert nitrogen atmosphere was incorporated into the setup, as depicted in Figure 27. This addition reduced contamination from atmospheric $CO_2$ and oxygen, preserving the chemical stability of the reaction components and preventing unwanted side reactions. Together, these modifications transformed the initial rudimentary system into a sophisticated and reliable setup tailored for producing high-quality NMC precursors.

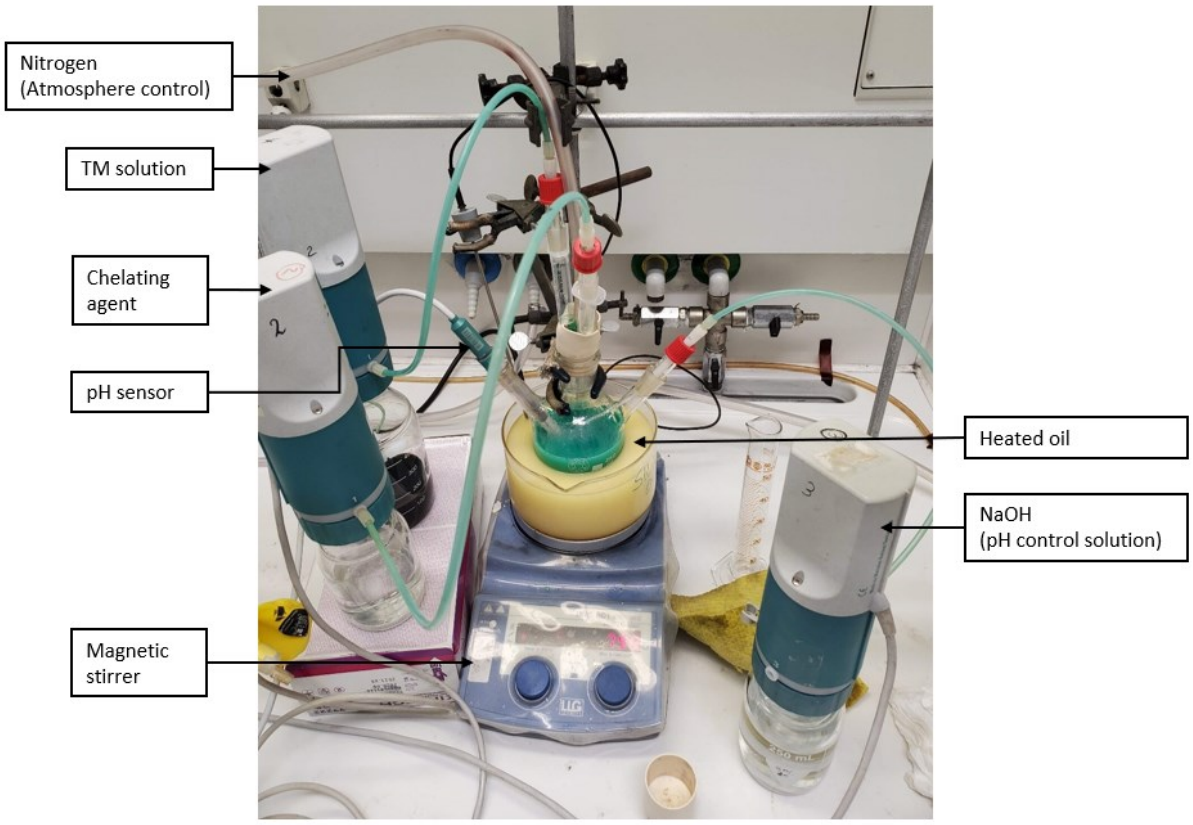


Figure 27 The upgraded experimental setup for NMC precursor synthesis, featuring pH sensor linked directly to the feed-in flow rate.

### 2.5. Conclusion and Future Improvements

After several improvements done, the current setup represents an initial configuration that achieved an acceptable level of precision and reproducibility for the co-precipitation process. However, there remains significant room for further improvement. For instance, the size of the reactor could be scaled up to accommodate larger reaction volumes while maintaining uniform mixing and temperature control. Additionally, the nitrogen atmosphere system requires enhancements, particularly a more advanced detection mechanism to prevent nitrogen leakage and ensure a consistently inert environment. Furthermore, the reactor design could be modified to include an outlet for continuous reaction processes, which would enable more efficient synthesis and improve scalability. These improvements will be essential for advancing the system towards industrial-level applications and achieving even greater consistency in precursor quality.

With the foundational setup in place, the next stage of development focused on fine-tuning key reaction parameters to optimize the co-precipitation process. Among the parameters investigated, pH and reaction time were identified as critical factors that directly influenced the morphology, particle size distribution, and compositional uniformity of the synthesized precursors. These parameters were systematically varied to determine their impact on precursor quality and electrochemical performance.

The flow rate of the reactants, reaction temperature, and mixing speed were initially adopted from established values in the literature, serving as baseline conditions. These values provided a reliable starting point, minimizing variability while allowing for controlled evaluation of the selected parameters. The fine-tuning process involved incremental adjustments to pH and reaction time, guided by a combination of theoretical insights and experimental observations. This approach not only ensured a deeper understanding of the reaction dynamics but also laid the groundwork for achieving reproducible results across different batches of NMC precursors.

## 3. Synthesis Parameter Optimization

After the initial experimental setup, the next step is to achieve the desired electrochemical performance for the NMC811 cathode materials, which requires a rigorous optimization of synthesis parameters. This involved a structured approach that included defining benchmarks from literature, designing experiments, and refining the parameters through comprehensive characterization. The process ultimately focused on improving three key aspects of

performance: initial discharge capacity, rate capability, and particle morphology.

### 3.1.Establishing Performance Benchmarks

To establish a foundation for optimization, key performance indicators were derived from a review of contemporary literature on NMC811 cathode materials. These benchmarks were crucial in aligning the research with industry standards, ensuring that the synthesized materials could compete with existing NMC811 cathode performances.

The first target was the initial discharge capacity, with an aim to exceed 200 mAh/g at 0.1C. This value reflects the high energy density expected from nickel-rich NMC cathodes, ensuring that the synthesized materials align with the state-of-the-art in terms of capacity. Simultaneously, maintaining high capacity during subsequent cycles was essential for verifying the structural integrity and lithium-ion mobility within the cathode.

The second metric, rate capability, was evaluated by subjecting the material to a sequence of progressively increasing charge/discharge rates, followed by a return to the initial low rate. The goal was to achieve stable capacity retention without sudden drops, indicative of stable lithium-ion diffusion and good structural resilience across a range of current densities. This characteristic is vital for the material's applicability in high-power lithium-ion batteries.

Lastly, particle morphology was optimized to promote mechanical stability and efficient electrochemical performance. Based on SEM analysis from the literature, particle sizes were targeted at 3–6 μm for single-crystalline NMC811, and 10–15 μm for polycrystalline secondary particle. Uniform particle size distribution and smooth surfaces were sought to reduce internal strain during cycling and to support uniform lithium-ion diffusion pathways.

### 3.2.Experimental Setup and Refinement of Precursor Synthesis

In line with the benchmarks, a co-precipitation method was employed for precursor synthesis, as it allows for precise control over particle formation and composition. A series of optimization steps were undertaken to refine the process parameters. The concentration of the metal sulfate feedstock and the alkaline solutions (NaOH and $NH_4OH$) were carefully calibrated to achieve consistent precipitation, ensuring that the stoichiometry and morphology of the resulting hydroxide precursor would be ideal for subsequent calcination.

Fine-tuning the feed rate played a critical role in controlling particle size and homogeneity. A slower feed allowed for more gradual nucleation and growth of particles, resulting in well-defined spherical structures, while preventing agglomeration. Maintaining uniform particle formation was essential to ensure consistent performance during the electrochemical testing phases.

The control of reaction conditions, particularly temperature and pH, was paramount. A reaction temperature of 60°C facilitated the desired reaction kinetics, while a carefully maintained pH in the range of 10–11 ensured proper co-precipitation and structural integrity of the particles. Subtle variations in these parameters had a significant impact on the precursor morphology, particularly the uniformity and size distribution of the secondary particles, which ultimately influence the electrochemical properties.

### 3.3.Optimization of Sintering Conditions

Following precursor synthesis, the sintering process played a crucial role in determining the crystalline structure and electrochemical behavior of the final NMC811 cathode. For polycrystalline materials, a two-step solid-state calcination process was employed, which included a preliminary low-temperature stage to facilitate phase formation, followed by a high-temperature treatment to enhance crystallinity and phase purity. The calcination was carried out in an oxygen-rich environment to prevent oxygen loss, ensuring structural stability.

In contrast, for the single-crystalline NMC811, a molten salt method was adopted. By optimizing the ratio of lithium salts (LiOH and $LiNO_3$) in the flux and adjusting the calcination temperature, larger, uniform single crystals were produced.

The heating and cooling rates were carefully controlled throughout the sintering process to minimize thermal stress and prevent particle cracking. The optimization of these parameters was vital in achieving the desired particle size distribution and maintaining structural integrity, both of which are key to sustaining high performance during charge-discharge cycling.

### 3.4.Conclusion for Synthesis Parameter Fine-tuning

This iterative optimization process involved fine-tuning critical synthesis parameters. For instance, adjustments to the co-precipitation pH or calcination temperature significantly

influenced the final material properties. The introduction of aluminum doping at specific stages, such as during co-precipitation or sintering, was also systematically optimized to enhance performance metrics.

By correlating results from characterization techniques like XRD, SEM, inductively coupled plasma (ICP) analysis, and transmission electron microscopy (TEM), a final optimized set of synthesis conditions was established. These optimized parameters yielded NMC811 cathodes with enhanced capacity retention, rate capability, and morphological stability, meeting or surpassing literature benchmarks.

In conclusion, the optimization of synthesis parameters described in Chapter 4.4 provided a robust foundation for producing high-performance NMC811 cathode materials. The final synthesis steps were illustrated in the next paragraph: 5. Optimized Synthesis of NMC811 Cathodes: Co-Precipitation, Molten Salt, and Aluminum Doping Techniques.

## 4. Optimized Synthesis steps of NMC811 Cathodes: Co-Precipitation, Molten Salt, and Aluminum Doping Techniques

Two distinct synthetic routes were employed in this study to produce NMC cathode materials: Hydroxide co-precipitation followed by solid-state calcination for polycrystalline (PC) NMC811 and a molten salt calcination approach for single crystalline (SC) NMC811 materials. In addition, aluminum doping is systematically introduced at different stages of these processes.

For the co-precipitation synthesis, we used an aqueous solution containing $NiSO_4$, $CoSO_4$ and $MnSO_4$ with a cationic ratio of Ni:Co:Mn=8:1:1 and a concentration of 2.0 mol $dm^{-3}$. The precursors were placed in a customized continuous stirred tank reactor (CSTR) with a volume of 250 ml. The synthesis was carried out under an $N_2$ atmosphere.

At the same time, an aqueous 2.0 mol $dm^{-3}$ NaOH solution and the prescribed amount of an aqueous 2.0 mol $dm^{-3}$ $NH_4OH$ solution were added to the reactor, the latter serving as a chelating agent. First, all solutions introduced were boiled for 15 minutes to ensure degassing. Subsequently, 100 ml of deionized water (DI) was added before the co-precipitation process was initiated.

The pH values of the composite solutions were strictly monitored and regulated to maintain a pH range between 10 and 11, depending on the different requirements of the process. The secondary particles, a result of the agglomeration of the primary acicular structure, turned into

spherical particles, which was promoted by vigorous stirring with a magnetic stirrer at a constant temperature of 60°C and 800 rpm (revolutions per minute). The feeding step is set for one hour, after which the solution is stirred continuously for 12 hours. Subsequently, the solution containing the NMC precursor with a ratio between Ni:Mn:Co (8:1:1) was filtered, washed and dried overnight in a vacuum dryer at 80°C. The precursor was stored at low oxygen and moisture content.

In the post-calcination phase, the precursor was first mixed with various lithium salts and spun for 15 minutes at a speed of 200 rpm using three 10 mm diameter balls. For the PC material, the NMC precursor is mixed with LiOH in a molar ratio of 1:1.05. In the case of the SC material, the NMC precursor is mixed with LiOH and $LiNO_3$ in different ratios.

The calcination process consists of two steps that are specifically tailored to the respective cathode type. For the PC material, the first step is carried out at 500°C for 5 hours at a heating rate of 5°C/min, which is supported by an $O_2$ gas flow in a tube furnace. The subsequent step is carried out at 750°C for 12 hours at a heating rate of 3°C/min. and a cooling rate of 5°C/min. down to 200°C. There is no break between the calcination steps.

In the case of the SC material, two different methods of molten salt are used. In the first method, a mixture of an NMC precursor obtained by the co-precipitation method at pH=10, LiOH and $LiNO_3$ in a molar ratio of 1:0.42:0.63 is used, which is referred to as SC1. After mixing, the mixture is calcined at 500°C for 5 hours at a rate of 5°C/min, followed by a further calcination at 750°C for 12 hours at a rate of 3°C/min. It is then cooled to 200°C at a rate of 5°C/min in an $O_2$-rich atmosphere. The second method for the SC materials utilizes a mixture of NMC precursor with an excess of LiOH and $LiNO_3$ in a ratio of 1:3.42:5.58, referred to as SC9. After mixing, this composition is calcined at 500°C for 5 hours at a rate of 5°C/min, then the temperature is raised to 850°C for 15 hours at the same rate before cooling to 200°C at a rate of 5°C/min.

It is important to note that both LiOH and $LiNO_3$ are hygroscopic and quickly absorb moisture from the air. Therefore, these components must be handled and weighed in a glove box to minimize contact with ambient moisture.

Doping during the co-precipitation phase was achieved by integrating aluminum sulfate ($Al_2(SO_4)_3$) in stoichiometric proportions of 1-2 mol% with other transition metal salts. The process was carried out under controlled conditions with all other parameters kept constant to

ensure consistency and reproducibility of the results.

For doping during the calcination phase, aluminum hydroxide ($Al(OH)_3$) was added in stoichiometric amounts of 1-2 mol% to the mixture of the NMC precursor and the lithium salts. Similar to co-precipitation, care was taken to keep all other parameters constant throughout the process.

# Chapter 3
# RESULTS & DISCUSSIONS

## 1. Characterization Method

The following sections provide detailed descriptions of the instruments used for each characterization method. These include X-ray diffraction (XRD) for phase identification and crystallographic analysis, scanning electron microscopy (SEM) for morphological evaluation, and inductively coupled plasma-mass spectrometry (ICP-MS) for elemental composition analysis. By specifying the equipment and procedures, this section highlights the precise analytical techniques employed to assess the structural, chemical, and electrochemical properties of the synthesized cathode materials.

Table 4: Summary of the applied techniques

| **Technique** | **Scientific target** |
|---|---|
| Solid-state synthesis | Phase formation<br>Crystallinity |
| X-ray diffraction (XRD) | Phase identification<br>Crystallographic structure |
| ICP (Inductively Coupled Plasma) | Elemental composition, Purity |
| Scanning electron microscopy (SEM) | Morphology of cathode materials<br>Particle size and distribution |
| Transmission electron microscopy (TEM) | Atomic-scale structure<br>Interface analysis |
| Galvanostatic cycling | Capacity retention<br>Cycling stability |

### 1.1.SEM

Scanning electron microscopy (SEM) was carried out using a Zeiss Supra 35 VP (Carl Zeiss, Oberkochen, Germany) microscope equipped with an energy-dispersive X-ray (EDX) spectrometer (Oxford Instruments, model Inca 400). The microscope was operated at a voltage of 5 kV for SEM procedures and 20 kV for EDX analyses.

### 1.2.XRD

X-ray powder diffraction patterns (XRD) of the samples were collected on PANanalytical X`pert 5 PRO MPD diffractometer with Cu Kα1 radiation (1.54056 Å) in the range of 5 - 80° in steps of 0.034°.

### 1.3.Rietveld refinement

Rietveld refinement, performed using HighScore Plus, is to determine the crystallographic structure of materials. The process begins with importing and preparing the diffraction data, including background subtraction to isolate diffraction peaks. Phase identification follows, where experimental patterns are matched against reference databases to determine the phases present in the sample. Initial structural models, including atomic positions and unit cell parameters, are input for each identified phase, alongside instrument parameters. The refinement process iteratively adjusts model parameters to minimize the difference between observed and calculated patterns, employing a strategic approach to refine significant parameters progressively. The final validated model is then exported, with results documented through detailed reports and visualizations.

### 1.4.ICP-MS

Inductively coupled plasma-mass spectrometry (ICP-MS) was used for the determination of the ratio between Ni:Mn:Co and Al for the selected samples. Samples were dissolved in diluted nitric acid. After that, the samples were analyzed by ICP-MS. The measurements were carried out using an inductively coupled plasma elemental mass spectrometer (Agilent 7500ce Series) equipped with an octopole collision cell. The samples were diluted ten times in a glass flask containing 1.0 mL sample + 0.1 mL of $HNO_3$ (65%, Merck, Darmstadt) + 0.05 mL of 10 mg $L^{-1}$ IS (Y, Sc, Ge, Gd, Merck, Darmstadt), and filled with Milli-Q ultrapure water (Millipore, Bedford, MA, USA) to 10.0 mL.

### 1.5.HR-TEM

The changes in the distribution and morphology of NMC811 nanocrystals were investigated using a Cs-corrected scanning transmission electron microscope (STEM) JEM-ARM200CF equipped with a cold field emission gun (FEG) source at 80 kV, a JEOL Centurio 100 $mm^2$ EDXS detector and JEOL STEM detectors (JEOL, Tokyo, Japan). High-resolution, high-angle,

annular dark-field/bright-field modes (STEM-HAADF, STEM-BF) were used for material imaging.

### 1.6.STEM-EELS

For EELS analysis, a Cs-corrected scanning transmission electron microscope (STEM) JEM-ARM200CF equipped with a cold FEG source operating at 80 kV (JEOL, Tokyo, Japan) and a Gatan GIF Quantum energy filter was employed. By analyzing the fine structures of the O K and Mn, Co, and Ni L2,3 edges, distinctions in electronic transitions and bonding environments were revealed.

### 1.7.Electrochemical test

The electrochemical properties of the synthesized NMC materials were investigated using pouch cells at ambient temperature in an argon-filled glovebox with less than 1 ppm $H_2O$ and $O_2$. For this study, the cathode was prepared by mixing the active material, polyvinylidene fluoride (PVDF), and carbon black in a ratio of 8:1:1. For this purpose, 250 mg of the cathode powder was mixed with 31.25 mg of carbon black (Sigma-Aldrich) and PVDF solution (Mw ~ 534,000, Sigma-Aldrich) in 781 µL 4 wt% NMP (1-methyl-2-pyrrolidinone, anhydrous, 99.5%, Sigma-Aldrich). This mixture was homogenized with three 10 mm diameter balls in a ball mill at 200 rpm for 15 minutes, and then the slurry was poured onto carbon-coated aluminum foil and dried overnight at 80 °C in a vacuum dryer. The dried electrodes were cut into 12 mm diameter discs and pressed with 1 tonne of pressure. Metallic lithium foil (99.9%, Sigma-Aldrich) served as a counter electrode.

The half cells were filled with an electrolyte consisting of 1.0 M $LiPF_6$ in an EC:DEC=1:1 (99.9%, max. 20 ppm $H_2O$, Solvionic). The charge/discharge tests were carried out at room temperature in a voltage range of 3.0–4.3 V against $Li^+/Li$ using a VMP3 potentiostat. The study was conducted at a C-rate of 0.1C for 3 cycles, followed by 0.2C, 0.5C, 1C, 2C, 5C, and then 0.1C for 5 cycles. This procedure was developed to evaluate both the capacity and rate performance of the materials under different loading conditions.

## 2. Results and discussion

### 2.1.List of samples

The full list of samples used in the chapter “Results and discussion” is shown in Table 5. These samples were selected to evaluate how various doping levels and synthesis methods influence

performance. Most samples were prepared using an NMC precursor synthesized at a pH of 10. Two additional precursors, precipitated at higher pH levels, are labeled as PC10.5 and PC11, indicating precipitation occurred at pH 10.5 and 11, respectively.

Table 5 Selected samples of NMC 811 used in this chapter

| Sample name | pH of co-precipitation | sintering method | Comment |
|---|---|---|---|
| PC-air | 10 | sintering 500/750°C with 1.05 mol Li | Co-precipitation in the air atmosphere |
| PC-air solid Al 1% | | | Co-precipitation in the air atmosphere 1% Al doping during calcination |
| PC | | | / |
| PC10.5 | 10.5 | | / |
| PC11 | 11 | | / |
| PC solid 1% | 10 | | 1% Al doping during calcination |
| PC solid 2% | | | 2% Al doping during calcination |
| PC co-p 1% | | | 1% Al doping during coprecipitation |
| PC co-p 2% | | | 2% Al doping during coprecipitation |
| SC1 | | Molten salt 500/750°C with 1.05 mol Li | / |
| SC1 solid 1% | | | 1% Al doping during calcination |
| SC1 co-p 1% | | | 1% Al doping during coprecipitation |
| SC1 co-p 2% | | | 2% Al doping during coprecipitation |
| SC9 | | Molten salt 500/850°C with 9 mol Li | / |
| SC9 co-p 1% | | | 1% Al doping during coprecipitation |

### 2.2.SEM

The SEM analysis highlights the morphology of NMC precursors synthesized under varying pH conditions and different conditions/mixing regimes. Fig 28 a), prepared at pH 10 in a blade mixer, exhibits a fairly uniform particle morphology with well-defined granularity, reflecting a controlled and homogeneous precursor formation process. This result underscores the effectiveness of the blade mixer in promoting consistent particle distribution. Conversely, the sample in Fig 28 b), synthesized at pH 11 in a blade mixer, shows larger agglomerations and a less uniform structure.

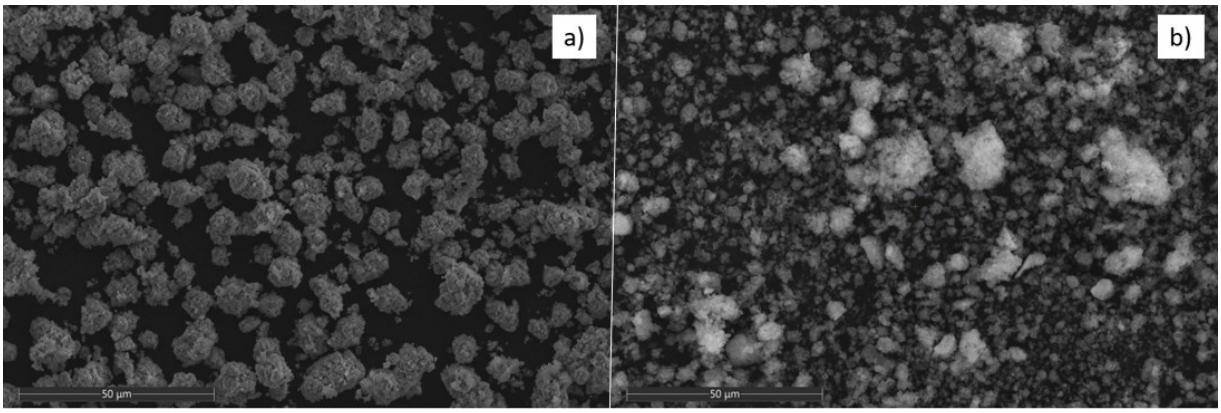


Figure 28 SEM images of NMC precursors synthesized at different pH values using a blade mixer, labeled as (a) pH 10 and (b) pH 11, at 1000× magnification.

Building on the preliminary experiments, further optimization was conducted during secondment, where co-precipitation experiments systematically varied pH (9.5–10.2) and reaction time (1–12 hours) under controlled nitrogen atmospheres and automated pH control (Fig. 29). At lower pH values (9.5 and 9.7), precursors exhibited elongated and irregular morphologies indicative of incomplete growth and increased agglomeration. As the pH increased to 10, the particles evolved into more compact, spherical secondary structures with a homogeneous distribution, significantly improving precursor uniformity. However, excessively high pH values (>10.2) led to rapid precipitation, resulting in uneven particle sizes and agglomeration.

Although the precursors synthesized during secondment lacked the uniformity achieved in preliminary experiments, the introduction of better atmospheric and pH control substantially enhanced the electrochemical performance in half-cell testing, as shown in “2.5 Electrochemical Test “ Fig. 36. These results emphasize the critical influence of synthesis parameters, including pH, reaction time, and atmospheric conditions, on precursor morphology and the properties of the final cathode material.

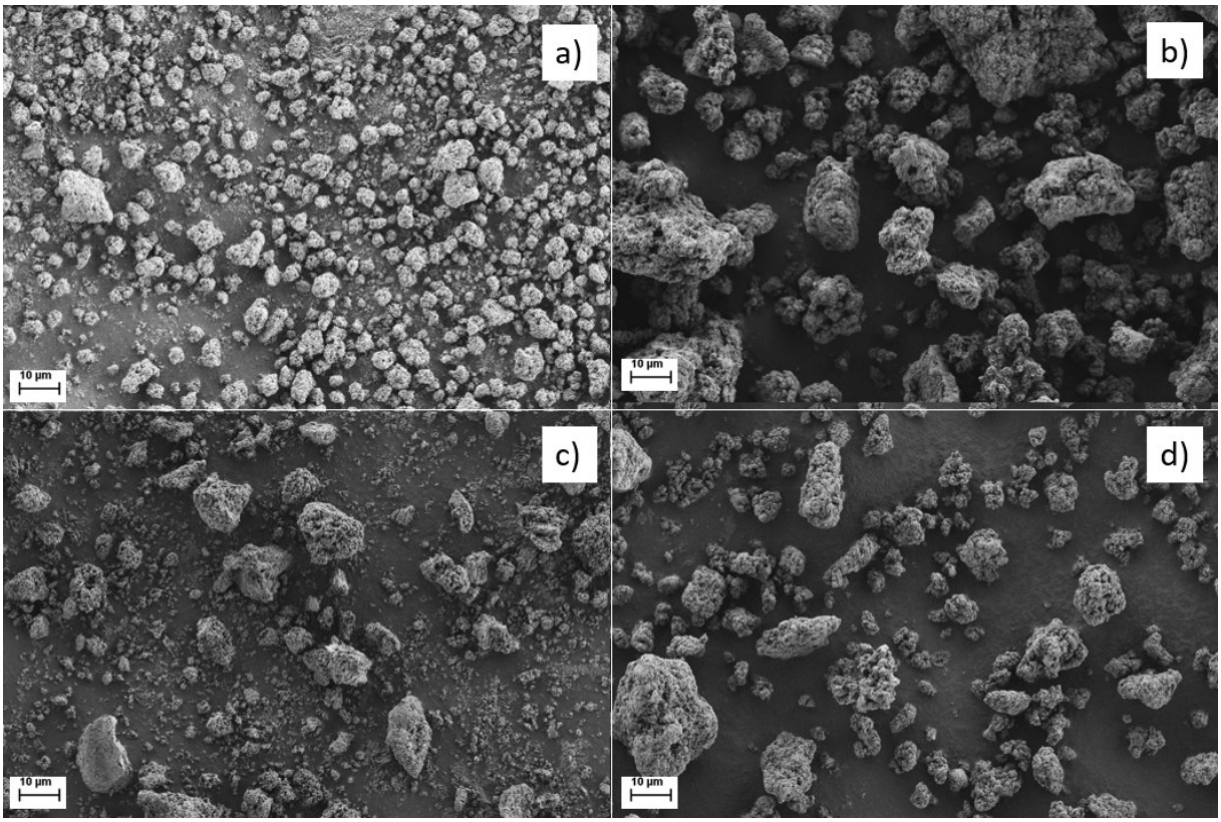


Figure 29 SEM images of NMC precursors synthesized at varying pH values, labeled as (a) pH 9.5, (b) pH 9.7, (c) pH 10, and (d) pH 10.2, after 12 hours of co-precipitation at 2000× magnification. The images illustrate the evolution of precursor morphology with changing pH.

Reaction time also played a pivotal role in precursor morphology. SEM images demonstrated that shorter co-precipitation durations (1–3 hours) produced irregular and loosely agglomerated particles, characteristic of incomplete growth. Extending the reaction time to 5 hours resulted in the emergence of more spherical particles, and by 12 hours, the particles achieved a highly uniform, well-distributed spherical morphology. This progression highlights the necessity of adequate reaction time to enable the coalescence and growth of primary and secondary particles, which are critical for downstream processing.

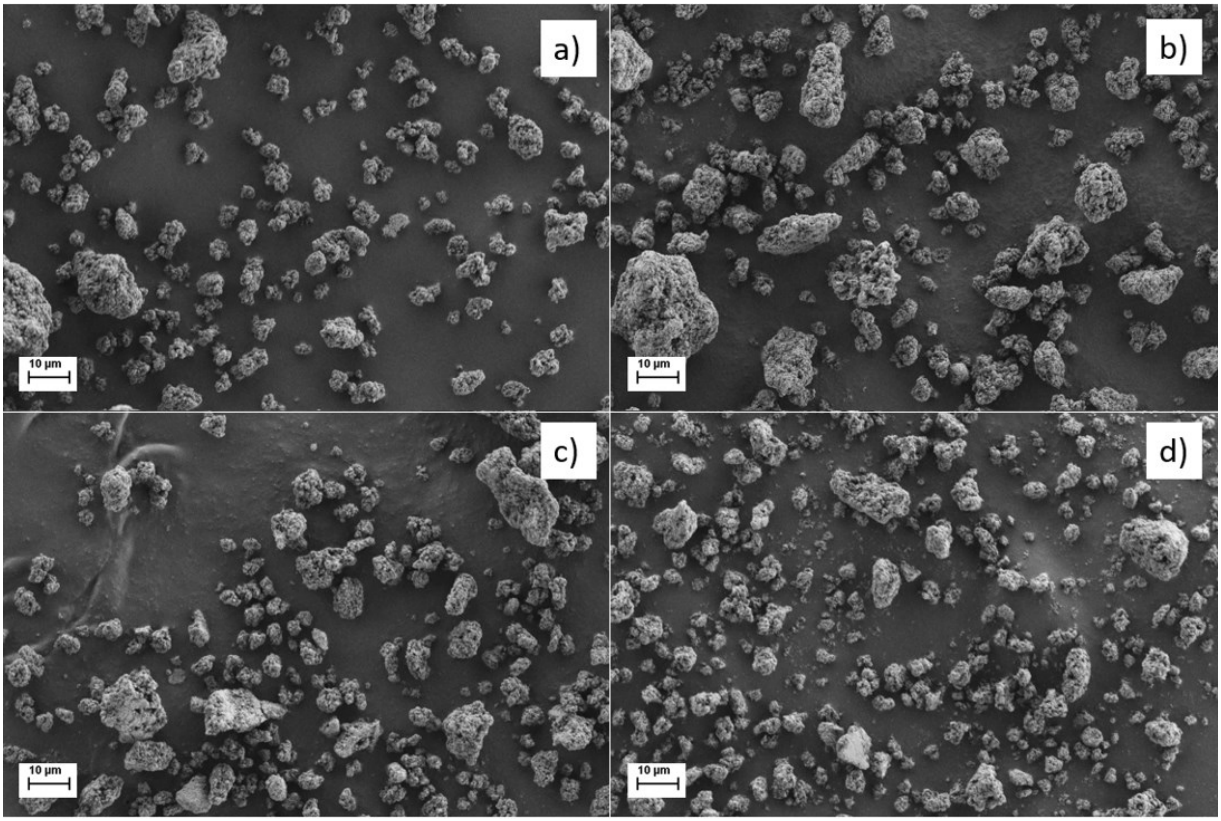


Figure 30 SEM images of NMC precursors extracted at different co-precipitation times, labeled as (a) 1 hour, (b) 3 hours, (c) 5 hours, and (d) 12 hours, at a pH of 10.2, with 2000× magnification. The images depict the evolution of particle morphology with increasing reaction time.

As for the synthesis of polycrystalline (PC) and single-crystalline (SC) NMC811 cathode, the PC synthesis method employed a two-step calcination process, producing smaller primary particles with sizes between 0.1 and 0.5 µm. (Fig. 31 a) This resulted in larger, more agglomerated secondary particles, typically measuring 10–15 µm. (sample PC in Table 5) SEM imaging highlighted the porous and irregular structure of PC samples, which contrasts sharply with the dense and well-defined morphology of SC materials. These differences in particle size and morphology directly correlate with the calcination techniques, as described in "Material Preparation"

In contrast, the SC process (sample SC1 in Table 5), characterized by higher calcination temperatures and the use of molten salt, resulted in larger primary particles ranging from 0.5 to 3 µm, contributing to the formation of dense and compact secondary particles. These SC secondary particles' sizes were predominantly in the 3–6 µm range, as observed in SEM analysis. (Fig. 31 b)

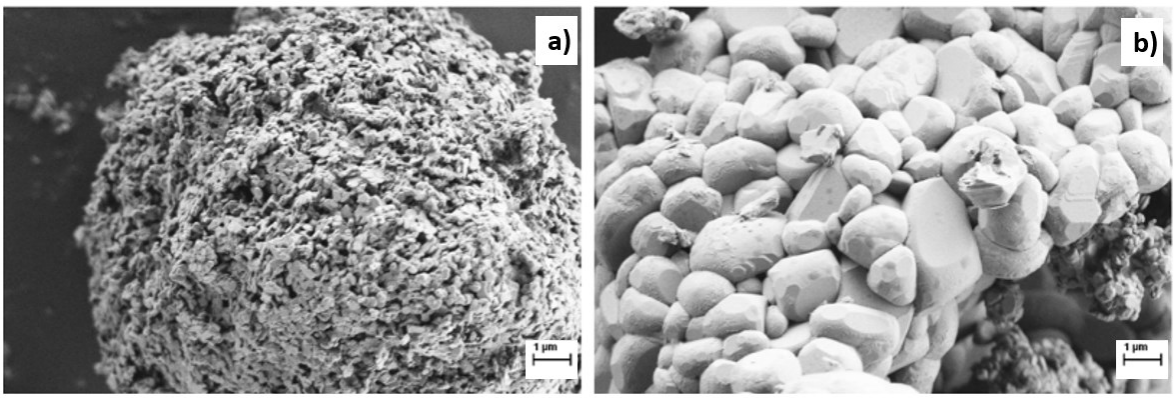


Figure 31: SEM images of NMC811 cathode materials at 20,000x magnification, comparing the polycrystalline and single-crystalline structures. a) sample “PC” displays a highly porous, sponge-like morphology. b) Sample: ”SC1” material exhibits well-defined, dense polyhedral particles ranging from 1-3 µm in size.

Despite the effort of parameter fine-tuning for NMC precursor, both PC and SC cathodes deviate from the idealized homogeneous spherical morphology commonly reported in the literature. The particles exhibit irregular and porous structures, suggesting variations in the synthesis conditions, particularly in terms of the applied mechanical forces. For instance, the use of a magnetic stirrer may have provided insufficient shear force during the co-precipitation process, leading to the formation of non-uniform aggregates rather than uniformly spherical particles. The non-uniform aggregates observed in these samples suggest that post-treatment techniques, such as mechanical milling or wind-sieving, may be required to achieve a more homogeneous particle morphology.

PC samples, as shown in (a) and (b), feature large, irregularly shaped agglomerates with a rough surface texture. The co-precipitated PC sample in (c) shows a slightly smaller and more fragmented particle morphology compared to the non-doped PC material. This fragmentation may indicate the impact of dopant incorporation on particle growth or the agglomeration mechanism during synthesis.

In contrast, SC samples in (d) and (e) demonstrate a distinctly different morphology, characterized by denser and more compact structures with smaller crystallites visible on the particle surface. The co-precipitated SC1 sample in (f) appears more refined, with smaller subunits forming a relatively uniform surface. However, the morphology still lacks the smooth spherical characteristics ideal for cathode materials, further emphasizing the role of synthesis parameters in determining the particle structure.

These morphological differences underscore the sensitivity of particle formation to synthesis conditions, including stirring intensity, precursor concentration, and dopant addition. The observed variations in particle structure are expected to influence the electrochemical performance of the cathode materials, particularly in terms of lithium-ion diffusion and cycling stability.

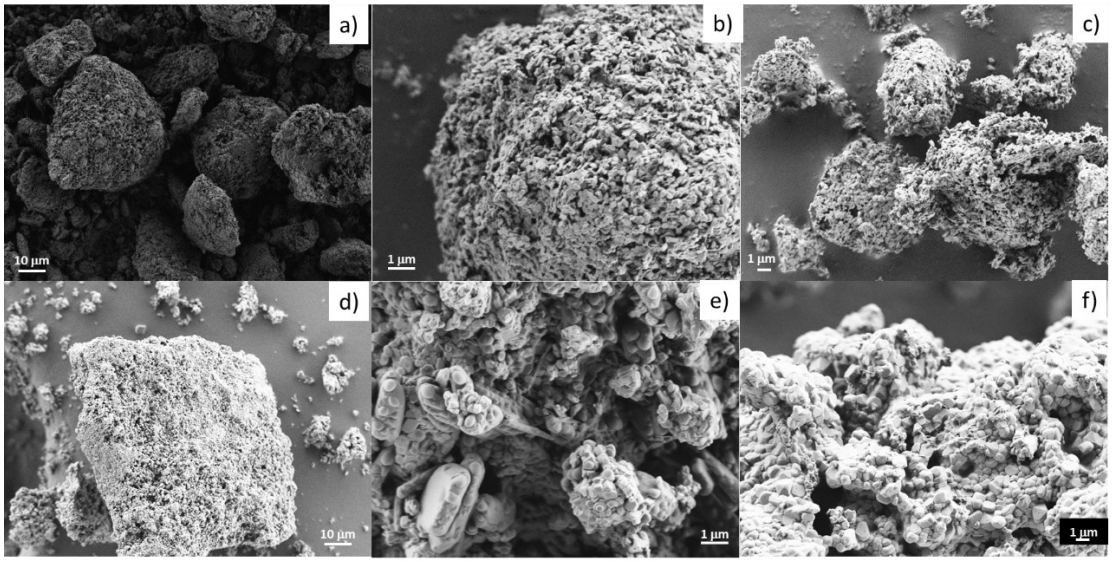


Figure 32: SEM micrographs of a), b) PC, c) PC co-p 1%, d), e) SC1, and f) SC1 co-p 1% samples.

### 2.3.XRD

In the early stages of synthesis, samples prepared using an air atmosphere during the co-precipitation step exhibited pronounced structural deficiencies. (PC-air1~3 in Fig. 37 a and b) The XRD patterns of these materials revealed broad and poorly defined diffraction peaks, particularly at the (006/102), and (108/110) planes. (PC in Fig.37 b) These deficiencies were traced to oxygen infiltration during the precursor synthesis, resulting from inadequate de-gassing and insufficient control over the reaction environment. The presence of oxygen led to the unwanted oxidation of transition metal salts, resulting in a precursor of compromised quality. The implementation of a nitrogen ($N_2$) atmosphere during the co-precipitation step addressed many of these issues. XRD patterns of samples synthesized under a nitrogen atmosphere displayed sharp and well-defined diffraction peaks, particularly at the (006/102), and (108/110) planes. These structural deficiencies, as evidenced by the XRD patterns, correlate with the reduced electrochemical performance observed, particularly in terms of capacity retention and rate capability.

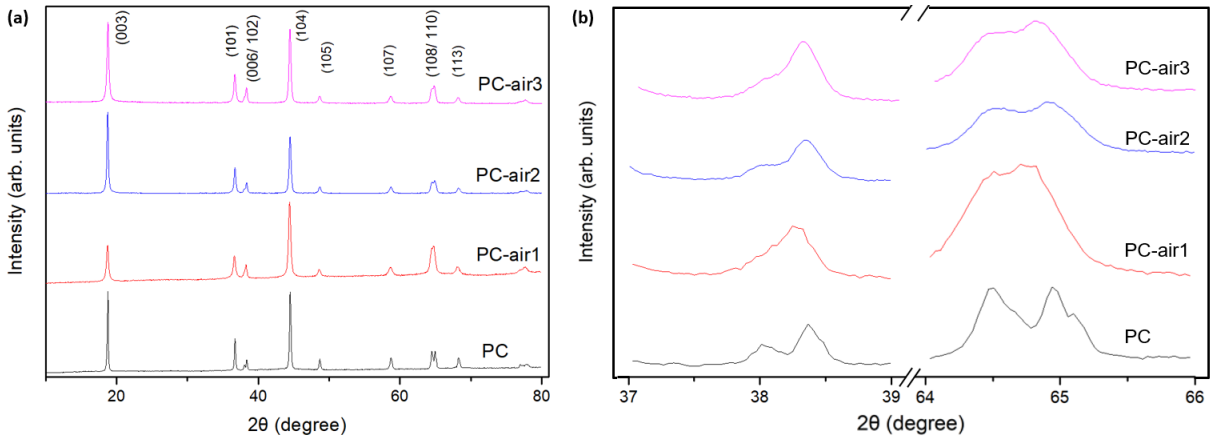


Figure 33 The XRD patterns of two NMC811 samples synthesized using different atmospheres during the co-precipitation process are presented. (a) NMC811 samples synthesized under varying atmospheric conditions during the co-precipitation process, labeled as PC, PC-air1, PC-air2, and PC-air3. (b) Magnified view of the (006/102), and (108/110) planes in (a).

After resolving the atmospheric issues during the co-precipitation process, which improved the structural integrity and crystallinity of the NMC811 samples, the focus shifted to systematically exploring various doping methods to further enhance the material's properties. These doping experiments were conducted in a controlled and methodical manner, evaluating different dopant elements, concentrations, and incorporation techniques. Both co-precipitation and solid-state doping methods were employed, allowing for a comprehensive comparison of their effects on the structural, morphological, and electrochemical characteristics of the NMC811 cathodes. As shown in Figure 38, the diffraction patterns of the samples prepared in this study show clear signals that can be attributed to the structure crystallized in the R-3m space group. The diffraction patterns exhibit sharp, well-defined peaks, indicative of high crystallinity. The characteristic peaks corresponding to the (006)/(102) and (108)/(110) planes are distinctly split, reflecting the layered hexagonal α-$NaFeO_2$ structure. (Fig. 38 b) [126,127]

The incorporation of aluminum into the NMC811 using the solid-state method results in variations in peak sharpening and intensity, particularly around the (108) and (110) planes. Importantly, no impurity phases are detected in the diffraction patterns, confirming the effective substitution of Al within the NMC811 lattice.

However, the PC co-p 1% and PC co-p 2% samples demonstrated weaker structural integrity at the (006)/(102) and (108)/(110) planes compared to other samples. This is evidenced by broader and less intense peaks in these regions, suggesting a degree of structural distortion or increased cation mixing. These observations may be attributed to incomplete incorporation or uneven distribution of Al dopants during the co-precipitation process, leading to localized structural inhomogeneities.

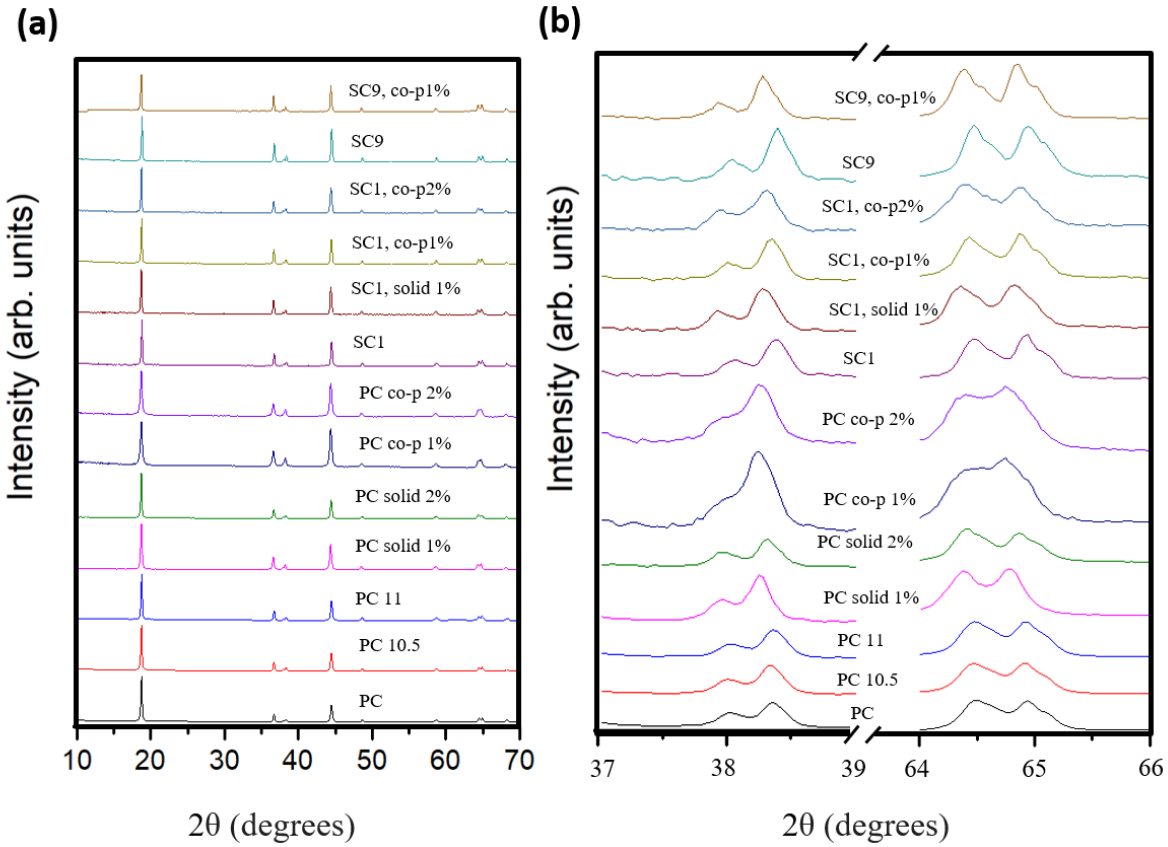


Figure 34: Normalized XRD patterns for all selected Al-doped NMC811 samples analyzed in this chapter. (a) Full XRD scan (10–70°) and (b) focused scan highlighting the (006)/(102) and (108)/(110) planes (37–39° and 64–66°). The complete list of samples is provided in Table 5.

### 2.4.Rietveld refinement

Besides the XRD results presented in the previous section, our focus was also on the crystallographic parameters that are summarized for all samples within this study in Table 8, which summarizes the key structural parameters obtained through Rietveld refinement. In this method, an observed XRD pattern is compared to a calculated one, which is generated based on an initial structural model. The differences between the observed and calculated patterns are minimized by adjusting various parameters, such as unit cell dimensions and atomic positions until the best fit is achieved. This fitting process allows for the accurate determination of key structural parameters, including lattice constants, atomic site occupancy, and the degree of crystallographic disorder.

Table 6 Rietveld refinement with structural parameters and initial discharge capacity

| Sample name | a [Å] | c [Å] | Volume [Å$^3$] | c/a | $I_{003}/I_{104}$ | 0.1C cap. [mAh/g] |
|---|---|---|---|---|---|---|
| PC | 2.870 | 14.193 | 101.270 | 4.945 | 1.091 | 200.11 |
| PC10.5 | 2.871 | 14.196 | 101.328 | 4.945 | 1.073 | 197.85 |
| PC11 | 2.871 | 14.199 | 101.390 | 4.945 | 1.012 | 205.15 |

| | | | | | | |
|---|---|---|---|---|---|---|
| PC solid 1% | 2.877 | 14.213 | 101.871 | 4.940 | 1.035 | 167.59 |
| PC solid 2% | 2.873 | 14.210 | 101.593 | 4.946 | 1.040 | 208.61 |
| PC co-p 1% | 2.879 | 14.217 | 102.049 | 4.938 | 1.008 | 168.10 |
| PC co-p 2% | 2.878 | 14.215 | 101.966 | 4.939 | 1.073 | 151.93 |
| SC1 | 2.873 | 14.208 | 101.572 | 4.945 | 1.107 | 203.99 |
| SC1 solid 1% | 2.875 | 14.217 | 101.755 | 4.945 | 1.137 | 165.86 |
| SC1 co-p 1% | 2.874 | 14.209 | 101.623 | 4.945 | 1.012 | 189.71 |
| SC1 co-p 2% | 2.874 | 14.216 | 101.663 | 4.947 | 1.042 | 178.44 |
| SC9 | 2.872 | 14.208 | 101.511 | 4.946 | 1.007 | 179.67 |
| SC9 co-p 1% | 2.872 | 14.207 | 101.502 | 4.946 | 1.088 | 182.21 |

The parameters include the lattice constants (a and c), unit cell volume, c/a ratio, and I003/I104 peak intensity ratio, which reflects the degree of cation ordering. Samples with higher initial discharge capacities, such as PC solid 2% and SC1, tend to exhibit c/a ratios around 4.945, indicating a well-ordered layered structure. Notably, variations in the c/a ratio and I003/I104 ratio highlight differences in structural ordering and crystallinity, which are crucial for enhancing electrochemical performance.

The lattice parameter ratio (c/a) in layered oxides like NMC is a critical indicator of the degree of cationic ordering and layering perfection in the crystal structure. A higher c/a ratio typically signifies a more pronounced separation of the lithium layers from the transition metal layers, which can facilitate easier lithium-ion diffusion. (Fig. 39) This enhanced lithium mobility often correlates with improved electrochemical capacity, as the ease of lithium-ion deinsertion and insertion directly impacts the kinetics and consequently the specific capacity. [24]

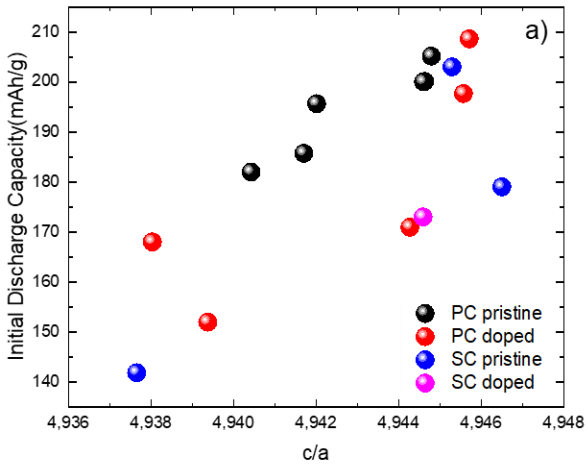


Figure 35: The relationship between the c/a ratio and electrochemical capacity is investigated. The c/a ratio is determined from the Rietveld refinement of X-ray diffraction (XRD) data, while the initial discharged capacity is measured through electrochemical testing.

### 2.5.ICP-MS

The chemical composition of the selected samples was analyzed by ICP and is shown in Table 6. It was found that the elemental proportions of nickel, cobalt, and manganese in the cathode materials are closely matched to the theoretical stoichiometric ratio of 8:1:1. This observation indicates that different preparation methods and post-treatment conditions do not influence the stoichiometric composition between lithium, nickel, cobalt, and manganese. The addition of aluminum sulfate during the co-precipitation process led to slight deviations in the elemental composition, while the addition of aluminum sulfate to the precipitated NMC precursor led to larger deviations compared to the expected stoichiometry, which is most likely due to the inhomogeneous distribution of the aluminum precursor among the NMC precursors. The results shown in Table 6 are the average values of three parallel measurements.

Table 7: ICP result of selected samples

| Sample name | Li:TM | Ni [at.%] | Co [at.%] | Mn [at.%] | Al [at.%] |
|---|---|---|---|---|---|
| PC | 1.000 | 80.890 | 9.817 | 9.293 | / |
| PC solid 2% | 1,002 | 80.859 | 9.814 | 9,327 | 3.068 |
| PC co-p 2% | 1.036 | 80.857 | 8.853 | 8.385 | 1.906 |
| SC1 | 1.044 | 80.788 | 9.928 | 9.284 | / |

### 2.6.STEM

To gain a deeper understanding of the microstructure and electronic properties of the synthesized NMC materials, Transmission Electron Microscopy (TEM) analysis was performed on selected samples: PC, PC solid 2%, PC co-p 2%, and SC1, which were chosen based on their electrochemical performance (as indicated in Figure 33). The analysis, which employed both bright-field Scanning Transmission Electron Microscopy (STEM) and high-resolution imaging techniques, provided significant insight into the crystallinity, particle size distribution, and electronic structure of these samples.

Bright-field STEM images (Figure 33) at lower and atomic resolution revealed clear differences in the microstructure of the analyzed samples. The PC and PC solid 2% samples exhibited similar crystallite sizes and maintained high crystallinity across multiple regions. The high-resolution images confirmed that aluminum doping in PC solid 2% did not drastically alter the overall crystalline structure compared to undoped PC, though subtle lattice distortions at the atomic level were observed, indicating minor structural perturbations. In contrast, the SC1 sample demonstrated significantly larger crystallites, more than twice the size of those observed

in the polycrystalline (PC) samples, consistent with the expected behavior of a single-crystalline material. This was accompanied by a high degree of crystallinity, with no amorphous phases detected.

However, the structural integrity of the PC co-p 2% sample was notably different. TEM analysis revealed the presence of an amorphous phase surrounding the crystalline regions, a feature not observed in the other samples. Furthermore, high-resolution STEM imaging of PC co-p 2% exposed a considerable degree of disorder, with alternating crystalline and amorphous regions within the same particle, suggesting that the co-precipitation method, when combined with aluminum doping, disrupts the material's structural coherence.

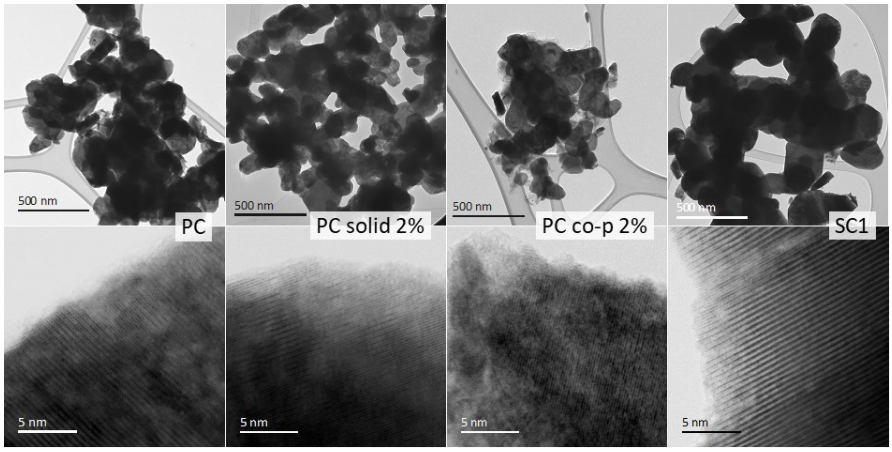


Figure 36: Bright-field STEM images at lower and atomic resolution magnifications showing variations in particle size and crystallinity for samples PC, PC-solid 2%, PC co-p 2%, and SC1. It should be noted, that the representative micron-sized particles were either not caught on the TEM grid or were non-transparent for the TEM analysis

STEM-EDS analysis showed similar atomic composition values for PC and SC1 samples with only minor deviations. However, PC solid 2% demonstrated a notable increase in Ni content, approximately 5 atomic % higher than the other samples, along with slight increases in Mn and Co concentrations. Noted that the PC co-p 2% sample showed the presence of impurities, such as sulfur (S) and silicon (Si), which were not detected in the other samples. These impurities are likely a byproduct of the co-precipitation process, and their presence may contribute to the structural disorder observed in the TEM images. (Table 7).

Table 8 Elemental content in atomic % detected by STEM-EDX. Note that in PC-co-p 2% sample small amounts of S and Si were also detected

| Sample/Element, at.% | O | Al | Ni | Mn | Co |
|---|---|---|---|---|---|
| **PC** | 56.8 | / | 35 | 4.1 | 4.6 |
| **PC solid 2%** | 49.1 | 0.2 | 40.8 | 4.7 | 5.2 |
| **PC co-p 2%** | 58.8 | 0.7 | 33 | 3.6 | 4 |
| **SC1** | 58.1 | / | 33.7 | 3.9 | 4.4 |

To assess variations in the electronic structure of the samples, scanning transmission electron microscopy-electron energy loss spectroscopy (STEM-EELS) was conducted on the thin edges of crystalline particles. The fine structures of the O K and Mn, Co, and Ni $L_{2,3}$ edges are presented in Figure 35. The O K edge spectrum, characteristic of lithium metal oxides with the R-3m layered structure, consists of two main peaks: a pre-edge peak at approximately 527–530 eV and a main peak at 538.5–540 eV. The pre-edge peak is attributed to the transition of electrons from the 1s core state to unoccupied 2p states that are hybridized with *3d* states in the transition metals (TMs) [128]. The main peak originates from electron transitions from the *1s* state to hybridized O *2p* and metal *4sp* states [129].

As depicted in Figure 35a, the shapes of the O K edge fine structure for the PC co-p 2% and PC samples are notably similar, both displaying a pronounced pre-edge peak. However, the SC1 sample shows a broadening and slight diminution of this pre-peak, with even further broadening observed in the PC-solid 2% sample. The O K pre-peak integral, calculated from the spectra (Figure 35e), reveals that the undoped PC and SC1 samples exhibit higher pre-peak intensities compared to both aluminum-doped samples (PC-solid 2% and PC co-p 2%).

In terms of the transition metal $L_{2,3}$ edges, the splitting of these edges is caused by the degeneracy of the *2p* states into $2p_{1/2}$ and $2p_{3/2}$ levels due to spin−orbit coupling [130]. Across all four samples, the fine structures of the Mn and Co $L_{2,3}$ edges appear quite similar, with no observable chemical shift (Figures 34b, 34c). However, in the case of the Ni $L_{2,3}$ edges, distinct variations are observed between the PC and PC co-p 2% samples. The $L_3$ edge in these two samples displays subtle differences in shape and an evident shift (Figure 34d). Further analysis of the original data is required to conclusively interpret the observed Ni $L_3$ edge variations.

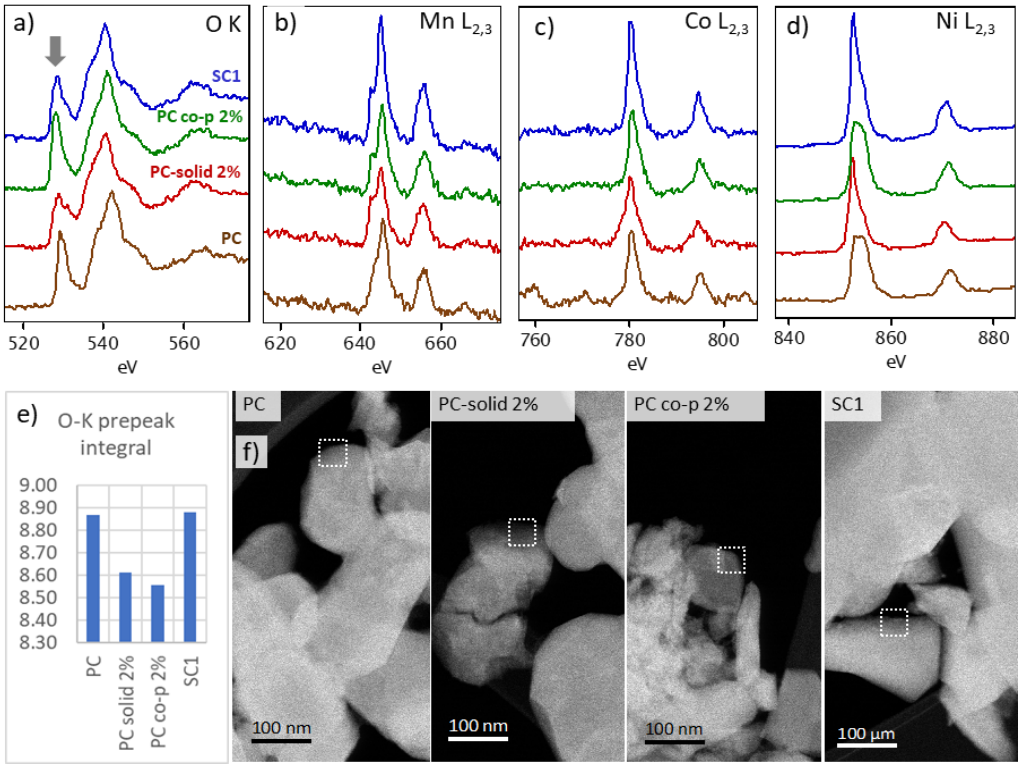


Figure 37 STEM-EELS spectra of the a) O K edge, b) Mn $L_{2,3}$, c) Co $L_{2,3}$, and d) Ni $L_{2,3}$ edges taken from the edges of PC (brown), PC-solid 2% (red), PC co-p 2% (green) and SC1 particles (blue) ca. 50 nm into particle. e) O K edge pre-peak integral calculated for all four samples from the spectra acquired from areas marked in f) STEM-HAADF images of samples.

### 2.7.Electrochemical tests

Throughout the parameter fine-tuning process for NMC811 cathode materials, several suboptimal samples (labeled PC-air 1, PC-air 2, PC-air solid Al 1%) demonstrated poor electrochemical and structural performance (Fig. 35). These samples, synthesized without an automated pH controller and in air atmosphere, exhibited initial discharge capacities below 170 mAh/g at 0.1C, significantly below the target benchmark of 200 mAh/g. These early-phase experiments, however, were crucial in identifying critical factors affecting material behavior under various synthesis conditions.

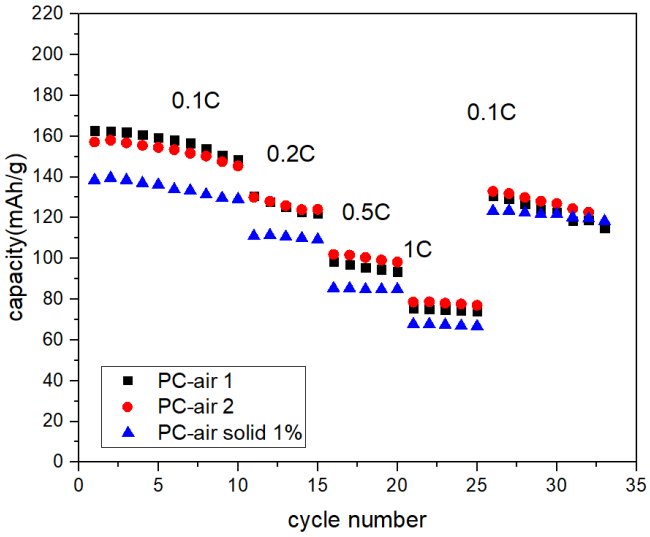


Figure 38 Electrochemical results of NMC cathodes co-precipitaed in air atmosphere.

Recognizing the limitations, the synthesis process was optimized. Here, enhanced control over synthesis parameters, particularly the introduction of a more precise pH-controlled environment and improved atmospheric conditions, as described in chapter 2 sub chapter 3-4, facilitated the production of structurally robust NMC cathodes. Electrochemical tests conducted on these refined samples demonstrated significant improvements, with initial discharge capacities exceeding 200 mAh/g at 0.1C (Figure 36a)

Variations in pH between 10 and 11 during the preparation of the NMC precursor lead to a significant difference in the capacity achieved at higher C rates, while the capacities at 0.1C are within the experimental error. Comparative evaluations between non-doped SC and PC materials show inadequate performance of sample SC9. This was synthesized with a large excess of lithium compared to SC1, where the excess stoichiometry of lithium during the calcination step was similar to the PC sample. For all three samples, we used NMC precursors precipitated at pH=10. (Figure 36b) The comparison between the SC1 and PC samples is not in agreement with the literature [51,80,131], which states that SCs with a nickel content of more than 80% and high cut-off voltages (>4.3 V vs. $Li^+/Li$) exhibit poorer cycling performance compared to their polycrystalline counterparts.

Furthermore, the process of doping by co-precipitation did not lead to an improvement in capacity or cyclability. There was a significant reduction in capacity by 16% and 24% for cathodes doped with 1% and 2% aluminum, respectively (Figure 36c). This could be due to the

altered solubility parameters introduced by adding aluminum sulfate, which required more sophisticated synthesis conditions. The introduction of Al doping by adding an Al precursor after NMC precipitation coincidentally improves the electrochemical performance of the samples. Finally, Figure 36d shows the results of different synthesis approaches and modifications applied to single-crystal (SC) NMC cathodes. The results show that the molten salt synthesis method, which requires washing after calcination, is challenging, as shown by the performance of sample SC1 compared to SC9. Furthermore, for the SC cathode, neither the introduction of dopants during the co-precipitation process nor the incorporation of dopants during solid-state calcination led to improved electrochemical performance. These results suggest that the SC-NMC cathode operates via a unique mechanism that makes it unsuitable for the modification techniques commonly used for its polycrystalline counterpart.

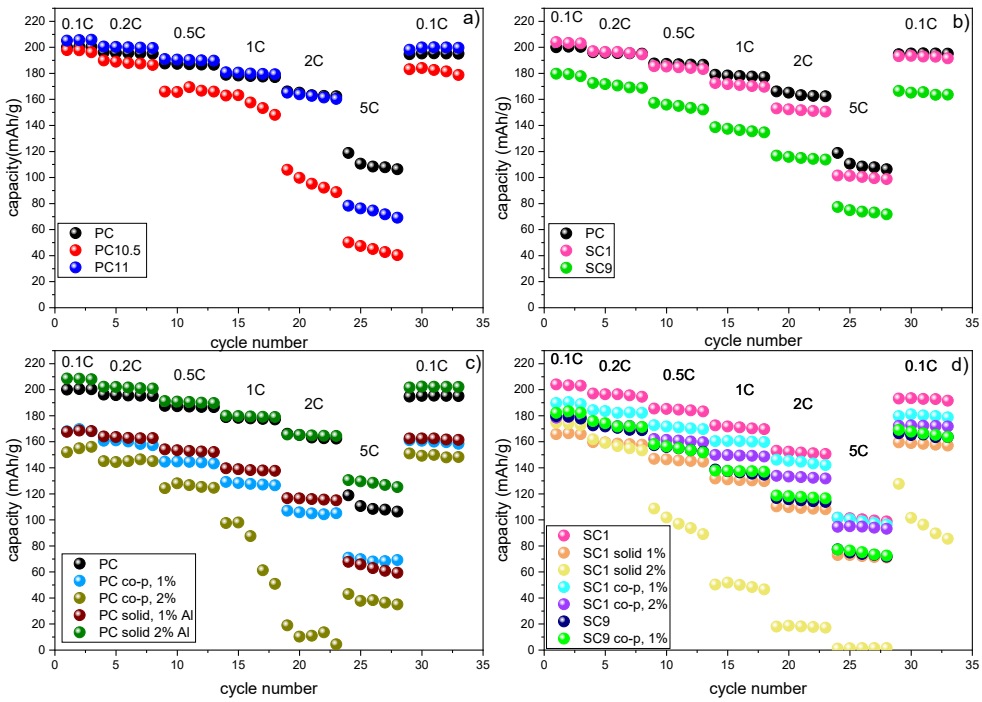


Figure 39: Electrochemical results of NMC cathodes a) comparison of samples prepared at different pH; b) comparison of different post-treatments of NMC precursor prepared at pH=10; c) comparison of polycrystalline samples prepared in this work and d) comparison of electrochemical properties for all single crystalline samples.

## 3. Conclusion

This comprehensive study explored the synthesis methodologies for both polycrystalline and single-crystalline NMC 811 cathodes, with a particular focus on the incorporation of aluminum (Al) as a dopant through co-precipitation and solid-state calcination methods. The resultant

materials underwent extensive characterizations, encompassing compositional, textural, morphological, and structural analyses through various techniques such as X-ray diffraction (XRD), inductively coupled plasma (ICP) analysis, scanning electron microscopy (SEM), transmission electron microscopy (TEM), and galvanostatic cycling testing.

The findings revealed that while aluminum doping in polycrystalline (PC) NMC cathodes led to some promising outcomes, the impact on single-crystalline (SC) NMC cathodes was contrary, indicating an adverse effect. This suggests that SC NMC cathodes operate through a mechanism distinct from that of their polycrystalline counterparts, making them incompatible with the modification methodologies employed for polycrystalline cathodes.

Galvanostatic cycling experiments demonstrated that aluminum doping positively influenced the capacity and rate performance of the polycrystalline NMC cathode, particularly at a doping level of 2% mol. This cathode showcased superior rate performance, maintaining stability at high charge-discharge rates (achieving a discharge capacity of 208.6mAh at 0.1C and 130.5mAh at 5C, within a voltage window of 3-4.3V).

The crystallographic characteristics of layered oxide materials are examined using the Rietveld refinement method. Key findings include the significance of the lattice parameter ratio (c/a), with a higher ratio indicating improved separation of lithium layers from transition metal layers, thereby enhancing lithium-ion diffusion and battery capacity. Additionally, the excessive lattice expansion of NMC cathodes might compromise structural stability and affect long-term performance.

# Chapter 4
# FUTURE STUDY

## 1. Optimization of Electrolyte Composition for further study of NMC Cathode

To further improve the electrochemical performance of the synthesized NMC811 cathode materials, the next phase of this study involves investigating the impact of various electrolyte additives. Electrolyte additives play a critical role in enhancing cycling stability, improving capacity retention, and mitigating side reactions at the electrode-electrolyte interface. In this section, the effect of different concentrations (1%, 2%, and 5%) of DTDPh (1,3,2-benzodioxathiole 2,2-dioxide) added to the commonly used LP40 electrolyte will be evaluated. The selection of DTDPh as an additive is based on its potential to form a stable solid-electrolyte interphase (SEI) and suppress the degradation of the NMC cathode material, particularly at higher operating voltages. By comparing the performance of NMC811 in LP40(1M LiPF 6 in EC/DEC 1:1 wt) electrolyte with varying amounts of DTDPH, we aim to establish an optimal additive concentration for maximizing electrochemical performance, including cycling stability and rate capability.

Noted that samples in Fig 40 were selected from the same batch from previous results from fig. 36, and the full list of samples can be found in the Table 9.

Table 9 Composition and Additive Concentrations for further study of NMC Cathode.

| Sample Name | Stoichiometric Composition of the Cathode (Ni:Co:Mn) | Morphological characteristics | Doping | Electrolyte Additive |
|---|---|---|---|---|
| NMC622 | 60:20:20 | Polycrystalline | / | / |
| NMC811 | 80:10:10 | Polycrystalline | / | / |
| NMC811_2%Al, SC | 80:10:10 | Single-Crystalline | 2% Al added during calcination | / |
| NMC622 + 1% DTDPH | 60:20:20 | Polycrystalline | / | 1% wt DTDPH |
| NMC811 + 1% DTDPH | 80:10:10 | Polycrystalline | / | 1% wt DTDPH |
| NMC811 + 2% Al, SC + 1% DTDPH | 80:10:10 | Single-Crystalline | 2% Al added during calcination | 1% wt DTDPH |
| NMC622 + 2% DTDPH | 60:20:20 | Polycrystalline | / | 2% wt DTDPH |

| | | | | |
|---|---|---|---|---|
| NMC811 + 2% DTDPH | 80:10:10 | Polycrystalline | / | 2% wt DTDPH |
| NMC811 + 2% Al, SC + 2% DTDPH | 80:10:10 | Single-Crystalline | 2% Al added during calcination | 2% wt DTDPH |
| NMC622 + 5% DTDPH | 60:20:20 | Polycrystalline | / | 5% wt DTDPH |

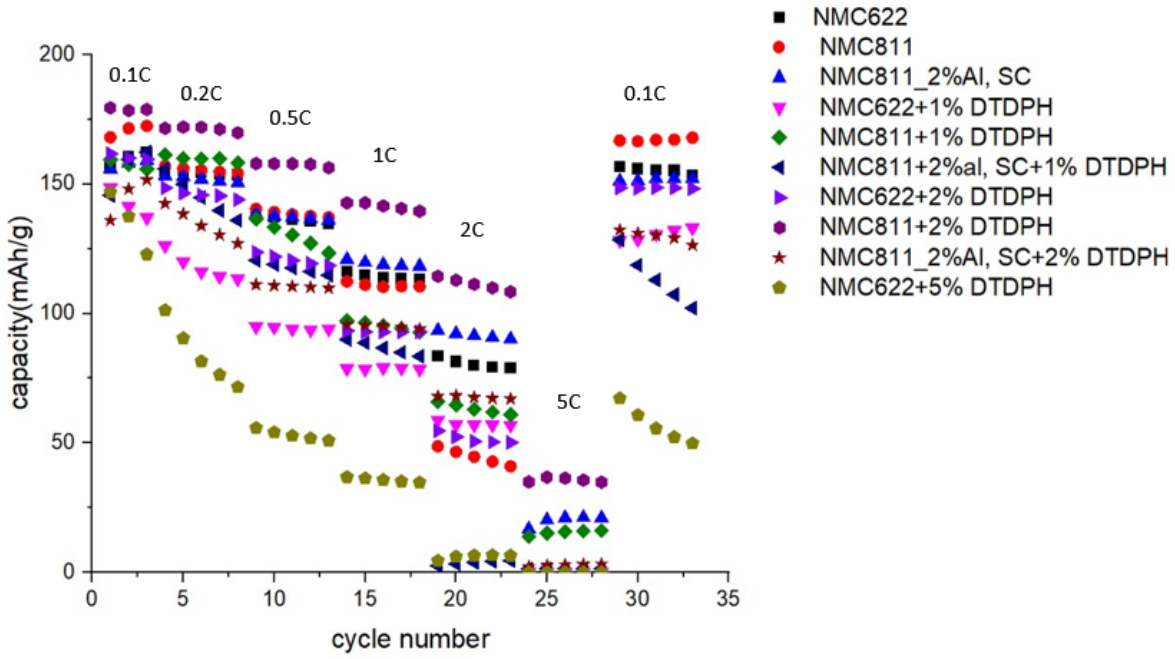


Figure 40 Cycling performance of NMC622 and NMC811 cathode materials with varying concentrations (1%, 2%, 5%) of DTDPH additive in LP40 electrolyte. The plot shows the capacity (mAh/g) as a function of cycle number for different cathode compositions and electrolyte conditions. Samples with DTDPH additive exhibit improved capacity retention compared to the baseline, though overall performance remains below the 200 mAh/g baseline at 0.1C.

The results with additives (Fig. 40) were compared against earlier tests (Fig. 36), which included baseline data without additives. Tests showed a moderate improvement in capacity retention when using DTDPH, particularly at higher concentrations (2% and 5%).

The sample with 2% DTDPH demonstrated enhanced cycling stability, with a slower decline in capacity compared to the baseline NMC811 sample without additives. This trend is similar to recently described for LNO based high voltage cathodes. [132] Nevertheless, the capacity values still fell short of the 200 mAh/g baseline, suggesting that the conditions of the performed experiment might not have been fully optimized.

This discrepancy may be attributed to variations in experimental conditions, such as synthesis parameters or cell fabrication techniques. Nonetheless, the data suggests that the DTDPH

additive has the potential to improve the long-term cycling stability of NMC cathodes, especially when used at optimal concentrations.

In particular, the improvement in capacity retention with increasing DTDPH concentrations aligns with the hypothesis that the additive forms a more robust and stable solid-electrolyte interphase (SEI), which mitigates side reactions and structural degradation of the cathode during cycling. Further investigation is required to refine the additive concentration and test its performance under different synthesis and cycling conditions.

## 2. Future Directions and Development

In future studies, further exploration of advanced cathode materials and electrolytes could lead to significant improvements in energy density, cycling stability, and overall performance of lithium-ion batteries. Beyond optimizing electrolyte additives, the focus can be expanded to include next-generation materials and designs that address the current limitations of NMC811 cathodes and broader battery technology trends.

One promising avenue is the development of solid-state batteries. By replacing the liquid electrolyte with a solid-state electrolyte, these batteries can offer enhanced safety, greater thermal stability, and the potential for increased energy density. For NMC materials, a solid electrolyte could mitigate issues like electrolyte decomposition and unwanted reactions at the cathode interface, thereby improving the cycle life and performance stability.

Single-crystal NMC materials offer several benefits for solid-state battery applications, largely due to their enhanced structural stability, reduced grain boundaries, and minimized risk of particle cracking. In conventional polycrystalline NMC cathodes, grain boundaries can become sites for lithium dendrite formation and degradation, particularly under the high stress of solid-state battery operation. Single-crystal structures, on the other hand, lack these grain boundaries, leading to a more resilient cathode that better withstands repeated cycling without mechanical failure.

In solid-state batteries, where lithium-ion diffusion relies on the solid electrolyte-cathode interface, single-crystal NMC also has an advantage due to its stable, continuous lattice structure. This promotes more uniform lithium-ion diffusion pathways, which reduces the risk of localized high resistance and improves overall ionic conductivity. Furthermore, single-crystal cathodes are less prone to forming undesirable reaction layers with the solid electrolyte, leading to a more stable interface over time. These characteristics make single-crystal NMC an ideal candidate for solid-state battery applications, potentially leading to better cycling stability,

longer battery life, and improved energy density—all critical for next-generation high-performance energy storage.

Another study direction is by integrating NMC811 or even higher-nickel-content NMC materials (such as NMC91x or NMC93x) into solid-state designs could further increase the specific capacity, although this also introduces new challenges in terms of interfacial compatibility and ionic conductivity that will require careful material and electrolyte engineering. Higher nickel content in NMCs (e.g., NMC91x and NMC93x) has the potential to achieve higher specific capacities and energy densities. However, increased nickel content can compromise structural stability, leading to faster capacity fade and increased side reactions with the electrolyte. Therefore, future work will need to focus on stabilization techniques, such as dopants, surface coatings, or grain boundary engineering, to offset these limitations while maintaining the desired electrochemical properties.

Moreover, exploring alternative dopants and novel surface coatings could enhance the structural and electrochemical stability of high-nickel NMC cathodes. Aluminum doping, for example, has shown promise in improving structural stability, but other elements such as magnesium, titanium, and boron may provide additional benefits by modifying the electronic structure or improving thermal stability. Surface coatings, like $LiNbO_3$ or $Al_2O_3$, may also protect the cathode material from direct contact with the electrolyte, thereby minimizing undesired reactions and enhancing long-term cycling performance.

In summary, the future directions for improving NMC-based cathodes involve not only optimizing electrolyte additives but also advancing solid-state battery technology, increasing nickel content while maintaining stability, and exploring new dopants and coatings. These research efforts aim to push the boundaries of energy density, cycle life, and safety, ultimately supporting the development of more powerful and reliable lithium-ion batteries.

**References**

[1] K. Mizushima, P. C. Jones, P. J. Wiseman et al., “LixCoO2 (0<x<-1): A new cathode material for batteries of high energy density,” *Materials Research Bulletin*, vol. 15, no. 6, pp. 783–789, 1980.

[2] Z. Chen, Z. Lu, and J. R. Dahn, “Staging Phase Transitions in Li[sub x]CoO[sub 2],” *Journal of The Electrochemical Society*, vol. 149, no. 12, A1604, 2002.

[3] 2025, “Global EV Outlook 2025: Licence: CC BY 4.0,” https://www.iea.org/reports/global-ev-outlook-2025.

[4] 2025, “Global EV Outlook 2025,” https://www.iea.org/reports/global-ev-outlook-2025.

[5] Colin McKerracher, “China Already Makes as Many Batteries as the Entire World Wants,” BloombergNEF.

[6] M. S. Whittingham, “The Role of Ternary Phases in Cathode Reactions,” *Journal of The Electrochemical Society*, vol. 123, no. 3, pp. 315–320, 1976.

[7] A. Manthiram, “A reflection on lithium-ion battery cathode chemistry,” *Nature communications*, vol. 11, no. 1, p. 1550, 2020.

[8] Q. Fang, “NCM/NCA vs. LFP: the Competitive Edge of LFP (in Chinese),” March 2019.

[9] C. M. Julien and A. Mauger, “NCA, NCM811, and the Route to Ni-Richer Lithium-Ion Batteries,” *Energies*, vol. 13, no. 23, p. 6363, 2020.

[10] D. Aurbach, O. Srur-Lavi, C. Ghanty et al., “Studies of Aluminum-Doped LiNi 0.5 Co 0.2 Mn 0.3 O 2 : Electrochemical Behavior, Aging, Structural Transformations, and Thermal Characteristics,” *Journal of The Electrochemical Society*, vol. 162, no. 6, A1014-A1027, 2015.

[11] L. Wang, B. Chen, J. Ma et al., “Reviving lithium cobalt oxide-based lithium secondary batteries-toward a higher energy density,” *Chemical Society reviews*, vol. 47, no. 17, pp. 6505–6602, 2018.

[12] C. A. Heck, M.-W. von Horstig, F. Huttner et al., “Review—Knowledge-Based Process Design for High Quality Production of NCM811 Cathodes,” *Journal of The Electrochemical Society*, vol. 167, no. 16, p. 160521, 2020.

[13] P. Hou, J. Yin, M. Ding et al., “Surface/Interfacial Structure and Chemistry of High-Energy Nickel-Rich Layered Oxide Cathodes: Advances and Perspectives,” *Small (Weinheim an der Bergstrasse, Germany)*, vol. 13, no. 45, 2017.

[14] J. Langdon and A. Manthiram, “A perspective on single-crystal layered oxide cathodes for lithium-ion batteries,” *Energy Storage Materials*, vol. 37, pp. 143–160, 2021.

[15] X. Liu, B. Zheng, J. Zhao et al., "Electrochemo-Mechanical Effects on Structural Integrity of Ni-Rich Cathodes with Different Microstructures in All Solid-State Batteries," *Advanced Energy Materials*, vol. 11, no. 8, 2021.

[16] C. Doerrer, I. Capone, S. Narayanan et al., "High Energy Density Single-Crystal NMC/Li6PS5Cl Cathodes for All-Solid-State Lithium-Metal Batteries," *ACS applied materials & interfaces*, vol. 13, no. 31, pp. 37809–37815, 2021.

[17] E. Trevisanello, R. Ruess, G. Conforto et al., "Polycrystalline and Single Crystalline NCM Cathode Materials—Quantifying Particle Cracking, Active Surface Area, and Lithium Diffusion," *Advanced Energy Materials*, vol. 11, no. 18, 2021.

[18] W. Zeng, F. Xia, W. Tian et al., "Single-crystal high-nickel layered cathodes for lithium-ion batteries: advantages, mechanism, challenges and approaches," *Current Opinion in Electrochemistry*, vol. 31, p. 100831, 2022.

[19] R. Chu, Y. Zou, P. Zhu et al., "Progress of Single-Crystal Nickel-Cobalt-Manganese Cathode Research," *Energies*, vol. 15, no. 23, p. 9235, 2022.

[20] G. Conforto, R. Ruess, D. Schröder et al., "Editors' Choice—Quantification of the Impact of Chemo-Mechanical Degradation on the Performance and Cycling Stability of NCM-Based Cathodes in Solid-State Li-Ion Batteries," *Journal of The Electrochemical Society*, vol. 168, no. 7, p. 70546, 2021.

[21] H. Park, H. Park, K. Song et al., "In situ multiscale probing of the synthesis of a Ni-rich layered oxide cathode reveals reaction heterogeneity driven by competing kinetic pathways," *Nature chemistry*, vol. 14, no. 6, pp. 614–622, 2022.

[22] X. Han, Q. Meng, T. Sun et al., "Preparation and electrochemical characterization of single-crystalline spherical LiNi1/3Co1/3Mn1/3O2 powders cathode material for Li-ion batteries," *Journal of Power Sources*, vol. 195, no. 10, pp. 3047–3052, 2010.

[23] W. Song, J. Harlow, E. Logan et al., "A Systematic Study of Electrolyte Additives in Single Crystal and Bimodal LiNi 0.8 Mn 0.1 Co 0.1 O 2 /Graphite Pouch Cells," *Journal of The Electrochemical Society*, vol. 168, no. 9, p. 90503, 2021.

[24] J. Li, A. R. Cameron, H. Li et al., "Comparison of Single Crystal and Polycrystalline LiNi 0.5 Mn 0.3 Co 0.2 O 2 Positive Electrode Materials for High Voltage Li-Ion Cells," *Journal of The Electrochemical Society*, vol. 164, no. 7, A1534-A1544, 2017.

[25] X. Ma, R. S. Young, L. D. Ellis et al., "1,2,6-Oxadithiane 2,2,6,6-tetraoxide as an Advanced Electrolyte Additive for Li[Ni 0.5 Mn 0.3 Co 0.2 ]O 2 /Graphite Pouch Cells," *Journal of The Electrochemical Society*, vol. 166, no. 12, A2665-A2672, 2019.

[26] J. Li, H. Li, W. Stone et al., "Development of Electrolytes for Single Crystal NMC532/Artificial Graphite Cells with Long Lifetime," *Journal of The Electrochemical Society*, vol. 165, no. 3, A626-A635, 2018.
[27] Guo Q, Huang J, Zhou M et al., "Synthesis and electrochemical performance of single crystal LiNi0.83Co0.1Mn0.07O2 cathode material," 11: 23–8., 2020.
[28] C. Yang, Z. Zhu, W. Wei et al., "Superior Cycle Stability of Single Crystal Nickel-Rich Layered Oxides with Micron-Scale Grain Size as Cathode Material for Lithium Ion Batteries," *International Journal of Electrochemical Science*, vol. 15, no. 6, pp. 5031–5041, 2020.
[29] J. Hu, H. Wang, B. Xiao et al., "Challenges and approaches of single-crystal Ni-rich layered cathodes in lithium batteries," *National Science Review*, vol. 10, no. 12, nwad252, 2023.
[30] F. Lin, I. M. Markus, D. Nordlund et al., "Surface reconstruction and chemical evolution of stoichiometric layered cathode materials for lithium-ion batteries," *Nature communications*, vol. 5, p. 3529, 2014.
[31] J. Wandt, A. T.S. Freiberg, A. Ogrodnik et al., "Singlet oxygen evolution from layered transition metal oxide cathode materials and its implications for lithium-ion batteries," *Materials Today*, vol. 21, no. 8, pp. 825–833, 2018.
[32] James A. Gilbert, Ilya A. Shkrob, and Daniel P. Abraham, "Transition Metal Dissolution, Ion Migration, Electrocatalytic Reduction and Capacity Loss in Lithium-Ion Full Cells," *Journal of The Electrochemical Society*, vol. 164, no. 2, A389-A399, 2017.
[33] W. Li, H. Y. Asl, Q. Xie et al., "Collapse of LiNi1- x- yCo xMn yO2 Lattice at Deep Charge Irrespective of Nickel Content in Lithium-Ion Batteries," *Journal of the American Chemical Society*, vol. 141, no. 13, pp. 5097–5101, 2019.
[34] W. Lee, S. Muhammad, C. Sergey et al., "Advances in the Cathode Materials for Lithium Rechargeable Batteries," *Angewandte Chemie (International ed. in English)*, vol. 59, no. 7, pp. 2578–2605, 2020.
[35] M. Bianchini, M. Roca-Ayats, P. Hartmann et al., "There and Back Again-The Journey of LiNiO2 as a Cathode Active Material," *Angewandte Chemie (International ed. in English)*, vol. 58, no. 31, pp. 10434–10458, 2019.
[36] F. Wu, J. Tian, Y. Su et al., "Effect of Ni(2+) content on lithium/nickel disorder for Ni-rich cathode materials," *ACS applied materials & interfaces*, vol. 7, no. 14, pp. 7702–7708, 2015.
[37] S. Hwang, S. M. Kim, S.-M. Bak et al., "Using Real-Time Electron Microscopy To Explore the Effects of Transition-Metal Composition on the Local Thermal Stability in Charged

Li x Ni y Mn z Co 1– y – z O 2 Cathode Materials," *Chemistry of Materials*, vol. 27, no. 11, pp. 3927–3935, 2015.
[38] H.-J. Noh, S. Youn, C. S. Yoon et al., "Comparison of the structural and electrochemical properties of layered Li[NixCoyMnz]O2 (x = 1/3, 0.5, 0.6, 0.7, 0.8 and 0.85) cathode material for lithium-ion batteries," *Journal of Power Sources*, vol. 233, pp. 121–130, 2013.
[39] H. Kobayashi, M. Shikano, S. Koike et al., "Investigation of positive electrodes after cycle testing of high-power Li-ion battery cells," *Journal of Power Sources*, vol. 174, no. 2, pp. 380–386, 2007.
[40] M. Shikano, H. Kobayashi, S. Koike et al., "Investigation of positive electrodes after cycle testing of high-power Li-ion battery cells II," *Journal of Power Sources*, vol. 174, no. 2, pp. 795–799, 2007.
[41] S. Li, Z. Yao, J. Zheng et al., "Direct Observation of Defect-Aided Structural Evolution in a Nickel-Rich Layered Cathode," *Angewandte Chemie (International ed. in English)*, vol. 59, no. 49, pp. 22092–22099, 2020.
[42] H.-H. Ryu, G.-T. Park, C. S. Yoon et al., "Microstructural Degradation of Ni-Rich LiNix Coy Mn1-x-y O2 Cathodes During Accelerated Calendar Aging," *Small (Weinheim an der Bergstrasse, Germany)*, vol. 14, no. 45, e1803179, 2018.
[43] J. P. Pender, G. Jha, D. H. Youn et al., "Electrode Degradation in Lithium-Ion Batteries," *ACS nano*, vol. 14, no. 2, pp. 1243–1295, 2020.
[44] S. G. Booth, A. J. Nedoma, N. N. Anthonisamy et al., "Perspectives for next generation lithium-ion battery cathode materials," *APL Materials*, vol. 9, no. 10, p. 109201, 2021.
[45] J. Hu, L. Li, E. Hu et al., "Mesoscale-architecture-based crack evolution dictating cycling stability of advanced lithium ion batteries," *Nano Energy*, vol. 79, p. 105420, 2021.
[46] Z. Lei, Z. Maotao, X. Xiaoming et al., "Thermal runaway characteristics on NCM lithium-ion batteries triggered by local heating under different heat dissipation conditions," *Applied Thermal Engineering*, vol. 159, p. 113847, 2019.
[47] Y. Chen, S. Song, X. Zhang et al., "The challenges, solutions and development of high energy Ni-rich NCM/NCA LiB cathode materials," *Journal of Physics: Conference Series*, vol. 1347, no. 1, p. 12012, 2019.
[48] Y. Bi, J. Tao, Y. Wu et al., "Reversible planar gliding and microcracking in a single-crystalline Ni-rich cathode," *Science (New York, N.Y.)*, vol. 370, no. 6522, pp. 1313–1317, 2020.
[49] X. Chen, Y. Tang, C. Fan et al., "A highly stabilized single crystalline nickel-rich LiNi0.8Co0.1Mn0.1O2 cathode through a novel surface spinel-phase modification," *Electrochimica Acta*, vol. 341, p. 136075, 2020.

[50] G. Qian, Y. Zhang, L. Li et al., "Single-crystal nickel-rich layered-oxide battery cathode materials: synthesis, electrochemistry, and intra-granular fracture," *Energy Storage Materials*, vol. 27, pp. 140–149, 2020.
[51] H.-H. Ryu, B. Namkoong, J.-H. Kim et al., "Capacity Fading Mechanisms in Ni-Rich Single-Crystal NCM Cathodes," *ACS Energy Letters*, vol. 6, no. 8, pp. 2726–2734, 2021.
[52] J. Zhang, P.-F. Wang, P. Bai et al., "Interfacial Design for a 4.6 V High-Voltage Single-Crystalline LiCoO2 Cathode," *Advanced materials (Deerfield Beach, Fla.)*, vol. 34, no. 8, e2108353, 2022.
[53] Q. Lin, W. Guan, J. Zhou et al., "Ni–Li anti-site defect induced intragranular cracking in Ni-rich layer-structured cathode," *Nano Energy*, vol. 76, p. 105021, 2020.
[54] S. Lee, W. Jin, S. H. Kim et al., "Oxygen Vacancy Diffusion and Condensation in Lithium-Ion Battery Cathode Materials," *Angewandte Chemie*, vol. 131, no. 31, pp. 10588–10595, 2019.
[55] P. Yan, J. Zheng, M. Gu et al., "Intragranular cracking as a critical barrier for high-voltage usage of layer-structured cathode for lithium-ion batteries," *Nature communications*, vol. 8, p. 14101, 2017.
[56] G. Azimi, T. Ouchi, K. Forsberg, et al., eds., *Rare Metal Technology 2021*, Springer International Publishing, Cham, 2021.
[57] Agus Purwanto, Cornelius Satria Yudha, U Ubaidillah et al., "NCA cathode material: synthesis methods and performance enhancement efforts," *Materials Research Express*, vol. 5, no. 12, p. 122001, 2018.
[58] X.-J. Zhu, H.-X. Liu, X.-Y. Gan et al., "Preparation and characterization of LiNi0.80Co0.20– x Al x O2 as cathode materials for lithium ion batteries," *Journal of Electroceramics*, vol. 17, 2-4, pp. 645–649, 2006.
[59] W. M. Liu, G. R. Hu, Z. D. Peng et al., "Synthesis of spherical LiNi0.8Co0.15Al0.05O2 cathode materials for lithium-ion batteries by a co-oxidation-controlled crystallization method," *Chinese Chemical Letters*, vol. 22, no. 9, pp. 1099–1102, 2011.
[60] S. H. Ju, J. H. Kim, and Y. C. Kang, "Electrochemical properties of LiNi0.8Co0.2−xAlxO2 ($0 \leq x \leq 0.1$) cathode particles prepared by spray pyrolysis from the spray solutions with and without organic additives," *Metals and Materials International*, vol. 16, no. 2, pp. 299–303, 2010.
[61] M. Malik, K. H. Chan, and G. Azimi, "Effect of Synthesis Method on the Electrochemical Performance of LiNixMnCo1-x-yO2 (NMC) Cathode for Li-Ion Batteries: A Review," in *Rare Metal Technology 2021,* G. Azimi, T. Ouchi, K. Forsberg et al., Eds., pp. 37–46, Springer International Publishing, Cham, 2021.

[62] H. Dong and G. M. Koenig, “A review on synthesis and engineering of crystal precursors produced via coprecipitation for multicomponent lithium-ion battery cathode materials,” *CrystEngComm*, vol. 22, no. 9, pp. 1514–1530, 2020.

[63] D. Wang, I. Belharouak, L. H. Ortega et al., “Synthesis of high capacity cathodes for lithium-ion batteries by morphology-tailored hydroxide co-precipitation,” *Journal of Power Sources*, vol. 274, pp. 451–457, 2015.

[64] B. Huang, L. Cheng, X. Li et al., “Layered Cathode Materials: Precursors, Synthesis, Microstructure, Electrochemical Properties, and Battery Performance,” *Small (Weinheim an der Bergstrasse, Germany)*, vol. 18, no. 20, e2107697, 2022.

[65] J. Cho, “LiNi 0.74 Co 0.26-x Mg x O 2 Cathode Material for a Li-Ion Cell,” *Chemistry of Materials*, vol. 12, no. 10, pp. 3089–3094, 2000.

[66] M.-H. Lee, Y.-J. Kang, S.-T. Myung et al., “Synthetic optimization of Li[Ni1/3Co1/3Mn1/3]O2 via co-precipitation,” *Electrochimica Acta*, vol. 50, no. 4, pp. 939–948, 2004.

[67] J. Ying, C. Wan, C. Jiang et al., “Preparation and characterization of high-density spherical LiNi0.8Co0.2O2 cathode material for lithium secondary batteries,” *Journal of Power Sources*, vol. 99, 1-2, pp. 78–84, 2001.

[68] P. Lehmann, D. G. Kurth, G. Brezesinski et al., “Structural Analysis of a Metallosupramolecular Polyelectrolyte-Amphiphile Complex at the Air/Water Interface,” *Chemistry*, vol. 7, no. 8, pp. 1646–1651, 2001.

[69] P. Barai, Z. Feng, H. Kondo et al., “Multiscale Computational Model for Particle Size Evolution during Coprecipitation of Li-Ion Battery Cathode Precursors,” *The journal of physical chemistry. B*, vol. 123, no. 15, pp. 3291–3303, 2019.

[70] Y. Ding, D. Mu, B. Wu et al., “Controllable synthesis of spherical precursor Ni0.8Co0.1Mn0.1(OH)2 for nickel-rich cathode material in Li-ion batteries,” *Ceramics International*, vol. 46, no. 7, pp. 9436–9445, 2020.

[71] W. Li, E. M. Erickson, and A. Manthiram, “High-nickel layered oxide cathodes for lithium-based automotive batteries,” *Nature Energy*, vol. 5, no. 1, pp. 26–34, 2020.

[72] Toya, H. N. et al., *Nickel-cobalt-manganese complex hydroxide particles and method for producing same, positive electrode active material for nonaqueous electrolyte secondary battery and method for producing same, and nonaqueous electrolyte secondary battery.*, 2012.

[73] H. Arai, “Characterization and cathode performance of Li1 − xNi1 + xO2 prepared with the excess lithium method,” *Solid State Ionics*, vol. 80, 3-4, pp. 261–269, 1995.

[74] *US5264201, 1993; b) J. Kim, YS Hong, KS Ryu, MG Kim, J. Cho*, 2006.

[75] R. Moshtev, P. Zlatilova, S. Vasilev et al., “Synthesis, XRD characterization and electrochemical performance of overlithiated LiNiO2,” *Journal of Power Sources*, 81-82, pp. 434–441, 1999.

[76] Z.-D. Huang, X.-M. Liu, S.-W. Oh et al., “Microscopically porous, interconnected single crystal LiNi1/3Co1/3Mn1/3O2 cathode material for Lithium ion batteries,” *Journal of Materials Chemistry*, vol. 21, no. 29, p. 10777, 2011.

[77] J. Leng, J. Wang, W. Peng et al., “Highly-Dispersed Submicrometer Single-Crystal Nickel-Rich Layered Cathode: Spray Synthesis and Accelerated Lithium-Ion Transport,” *Small (Weinheim an der Bergstrasse, Germany)*, vol. 17, no. 14, e2006869, 2021.

[78] X. Fan, G. Hu, B. Zhang et al., “Crack-free single-crystalline Ni-rich layered NCM cathode enable superior cycling performance of lithium-ion batteries,” *Nano Energy*, vol. 70, p. 104450, 2020.

[79] F. Li, L. Kong, Y. Sun et al., “Micron-sized monocrystalline LiNi 1/3 Co 1/3 Mn 1/3 O 2 as high-volumetric-energy-density cathode for lithium-ion batteries,” *Journal of Materials Chemistry A*, vol. 6, no. 26, pp. 12344–12352, 2018.

[80] J. Hu, L. Li, Y. Bi et al., “Locking oxygen in lattice: A quantifiable comparison of gas generation in polycrystalline and single crystal Ni-rich cathodes,” *Energy Storage Materials*, vol. 47, pp. 195–202, 2022.

[81] J. Duan, R. Zhang, Q. Zhu et al., “The Effect of Controlling Strategies of pH and Ammonia Concentration on Preparing Full Concentration Gradient Ni 0.8 Co 0.1 Mn 0.1 (OH) 2 via Coprecipitation in a Pilot-Scale Reactor,” *Energy Technology*, vol. 8, no. 5, p. 523, 2020.

[82] X. Fan, Y. Liu, X. Ou et al., “Unravelling the influence of quasi single-crystalline architecture on high-voltage and thermal stability of LiNi0.5Co0.2Mn0.3O2 cathode for lithium-ion batteries,” *Chemical Engineering Journal*, vol. 393, p. 124709, 2020.

[83] J. Li, H. Li, W. Stone et al., “Synthesis of Single Crystal LiNi 0.5 Mn 0.3 Co 0.2 O 2 for Lithium Ion Batteries,” *Journal of The Electrochemical Society*, vol. 164, no. 14, A3529-A3537, 2017.

[84] S.-j. Lu, L.-b. Tang, H.-x. Wei et al., “Single-Crystal Nickel-Based Cathodes: Fundamentals and Recent Advances,” *Electrochemical Energy Reviews*, vol. 5, no. 4, p. 783, 2022.

[85] R. Jung, R. Morasch, P. Karayaylali et al., “Effect of Ambient Storage on the Degradation of Ni-Rich Positive Electrode Materials (NMC811) for Li-Ion Batteries,” *Journal of The Electrochemical Society*, vol. 165, no. 2, A132-A141, 2018.

[86] J. Sicklinger, M. Metzger, H. Beyer et al., “Ambient Storage Derived Surface Contamination of NCM811 and NCM111: Performance Implications and Mitigation Strategies,” *Journal of The Electrochemical Society*, vol. 166, no. 12, A2322-A2335, 2019.

[87] N. V. Faenza, L. Bruce, Z. W. Lebens-Higgins et al., “Editors' Choice—Growth of Ambient Induced Surface Impurity Species on Layered Positive Electrode Materials and Impact on Electrochemical Performance,” *Journal of The Electrochemical Society*, vol. 164, no. 14, A3727-A3741, 2017.

[88] D. Larcher, M. R. Palacín, G. G. Amatucci et al., “Electrochemically Active LiCoO2 and LiNiO2 Made by Cationic Exchange under Hydrothermal Conditions,” *Journal of The Electrochemical Society*, vol. 144, no. 2, pp. 408–417, 1997.

[89] S.-T. Myung, F. Maglia, K.-J. Park et al., “Nickel-Rich Layered Cathode Materials for Automotive Lithium-Ion Batteries: Achievements and Perspectives,” *ACS Energy Letters*, vol. 2, no. 1, pp. 196–223, 2017.

[90] D. Wang, W. Liu, X. Zhang et al., “Review of Modified Nickel-Cobalt Lithium Aluminate Cathode Materials for Lithium-Ion Batteries,” *International Journal of Photoenergy*, vol. 2019, pp. 1–13, 2019.

[91] J. Kim, H. Lee, H. Cha et al., “Prospect and Reality of Ni-Rich Cathode for Commercialization,” *Advanced Energy Materials*, vol. 8, no. 6, p. 1702028, 2018.

[92] Q. Li, G. Li, C. Fu et al., “K(+)-doped Li(1.2)Mn(0.54)Co(0.13)Ni(0.13)O2: a novel cathode material with an enhanced cycling stability for lithium-ion batteries,” *ACS applied materials & interfaces*, vol. 6, no. 13, pp. 10330–10341, 2014.

[93] Mehmet Nurullah Ates, Qingying Jia, Ankita Shah et al., “Mitigation of Layered to Spinel Conversion of a Li-Rich Layered Metal Oxide Cathode Material for Li-Ion Batteries,” *Journal of The Electrochemical Society*, vol. 161, no. 3, A290-A301, 2013.

[94] J.-M. Kim, X. Zhang, J.-G. Zhang et al., “A review on the stability and surface modification of layered transition-metal oxide cathodes,” *Materials Today*, vol. 46, pp. 155–182, 2021.

[95] X. Yao, Q. Dong, Q. Cheng et al., “Why Do Lithium-Oxygen Batteries Fail: Parasitic Chemical Reactions and Their Synergistic Effect,” *Angewandte Chemie (International ed. in English)*, vol. 55, no. 38, pp. 11344–11353, 2016.

[96] I. H. Son, J. H. Park, S. Kwon et al., “Self-Terminated Artificial SEI Layer for Nickel-Rich Layered Cathode Material via Mixed Gas Chemical Vapor Deposition,” *Chemistry of Materials*, vol. 27, no. 21, pp. 7370–7379, 2015.

[97] P. S. Maydannik, T. O. Kaariainen, and D. C. Cameron, “Continuous atomic layer deposition: Explanation for anomalous growth rate effects,” *Journal of Vacuum Science & Technology A: Vacuum, Surfaces, and Films*, vol. 30, no. 1, 01A122, 2012.

[98] P. Yan, J. Zheng, J. Liu et al., “Tailoring grain boundary structures and chemistry of Ni-rich layered cathodes for enhanced cycle stability of lithium-ion batteries,” *Nature Energy*, vol. 3, no. 7, pp. 600–605, 2018.

[99] S.-T. Myung, K. Izumi, S. Komaba et al., “Role of Alumina Coating on Li−Ni−Co−Mn−O Particles as Positive Electrode Material for Lithium-Ion Batteries,” *Chemistry of Materials*, vol. 17, no. 14, pp. 3695–3704, 2005.

[100] M. Chen, E. Zhao, D. Chen et al., “Decreasing Li/Ni Disorder and Improving the Electrochemical Performances of Ni-Rich LiNi0.8Co0.1Mn0.1O2 by Ca Doping,” *Inorganic chemistry*, vol. 56, no. 14, pp. 8355–8362, 2017.

[101] J. E. Harlow, X. Ma, J. Li et al., “A Wide Range of Testing Results on an Excellent Lithium-Ion Cell Chemistry to be used as Benchmarks for New Battery Technologies,” *Journal of The Electrochemical Society*, vol. 166, no. 13, A3031-A3044, 2019.

[102] U.-H. Kim, S.-T. Myung, C. S. Yoon et al., “Extending the Battery Life Using an Al-Doped Li[Ni 0.76 Co 0.09 Mn 0.15 ]O 2 Cathode with Concentration Gradients for Lithium Ion Batteries,” *ACS Energy Letters*, vol. 2, no. 8, pp. 1848–1854, 2017.

[103] H. Kondo, Y. Takeuchi, T. Sasaki et al., “Effects of Mg-substitution in Li(Ni,Co,Al)O2 positive electrode materials on the crystal structure and battery performance,” *Journal of Power Sources*, vol. 174, no. 2, pp. 1131–1136, 2007.

[104] H. Li, P. Zhou, F. Liu et al., “Stabilizing nickel-rich layered oxide cathodes by magnesium doping for rechargeable lithium-ion batteries,” *Chemical science*, vol. 10, no. 5, pp. 1374–1379, 2019.

[105] Y.-C. Li, W. Xiang, Z.-G. Wu et al., “Construction of homogeneously Al3+ doped Ni rich Ni-Co-Mn cathode with high stable cycling performance and storage stability via scalable continuous precipitation,” *Electrochimica Acta*, vol. 291, pp. 84–94, 2018.

[106] Q. Liu, X. Su, D. Lei et al., “Approaching the capacity limit of lithium cobalt oxide in lithium ion batteries via lanthanum and aluminium doping,” *Nature Energy*, vol. 3, no. 11, pp. 936–943, 2018.

[107] S. Muto, K. Tatsumi, Y. Kojima et al., “Effect of Mg-doping on the degradation of LiNiO2-based cathode materials by combined spectroscopic methods,” *Journal of Power Sources*, vol. 205, Suppl. 1, pp. 449–455, 2012.

[108] S.-W. Woo, S.-T. Myung, H. Bang et al., “Improvement of electrochemical and thermal properties of Li[Ni0.8Co0.1Mn0.1]O2 positive electrode materials by multiple metal (Al, Mg) substitution,” *Electrochimica Acta*, vol. 54, no. 15, pp. 3851–3856, 2009.

[109] L. Zou, J. Li, Z. Liu et al., “Lattice doping regulated interfacial reactions in cathode for enhanced cycling stability,” *Nature communications*, vol. 10, no. 1, p. 3447, 2019.

[110] Y. Chen, Y. Zhang, B. Chen et al., “An approach to application for LiNi0.6Co0.2Mn0.2O2 cathode material at high cutoff voltage by TiO2 coating,” *Journal of Power Sources*, vol. 256, pp. 20–27, 2014.

[111] Z. Chen, G.-T. Kim, Y. Guang et al., “Manganese phosphate coated Li[Ni0.6Co0.2Mn0.2]O2 cathode material: Towards superior cycling stability at elevated temperature and high voltage,” *Journal of Power Sources*, vol. 402, no. 2, pp. 263–271, 2018.

[112] W. Cho, S.-M. Kim, J. H. Song et al., “Improved electrochemical and thermal properties of nickel rich LiNi0.6Co0.2Mn0.2O2 cathode materials by SiO2 coating,” *Journal of Power Sources*, vol. 282, no. 4, pp. 45–50, 2015.

[113] C.-H. Jo, D.-H. Cho, H.-J. Noh et al., “An effective method to reduce residual lithium compounds on Ni-rich Li[Ni0.6Co0.2Mn0.2]O2 active material using a phosphoric acid derived Li3PO4 nanolayer,” *Nano Research*, vol. 8, no. 5, pp. 1464–1479, 2015.

[114] S.-H. Lee, C. S. Yoon, K. Amine et al., “Improvement of long-term cycling performance of Li[Ni0.8Co0.15Al0.05]O2 by AlF3 coating,” *Journal of Power Sources*, vol. 234, pp. 201–207, 2013.

[115] S.-W. Lee, M.-S. Kim, J. H. Jeong et al., “Li3PO4 surface coating on Ni-rich LiNi0.6Co0.2Mn0.2O2 by a citric acid assisted sol-gel method: Improved thermal stability and high-voltage performance,” *Journal of Power Sources*, vol. 360, pp. 206–214, 2017.

[116] K. Liu, Q. Zhang, S. Dai et al., “Synergistic Effect of F- Doping and LiF Coating on Improving the High-Voltage Cycling Stability and Rate Capacity of LiNi0.5Co0.2Mn0.3O2 Cathode Materials for Lithium-Ion Batteries,” *ACS applied materials & interfaces*, vol. 10, no. 40, pp. 34153–34162, 2018.

[117] S. Neudeck, F. Strauss, G. Garcia et al., “Room temperature, liquid-phase Al2O3 surface coating approach for Ni-rich layered oxide cathode material,” *Chemical communications (Cambridge, England)*, vol. 55, no. 15, pp. 2174–2177, 2019.

[118] S.-U. Woo, C. S. Yoon, K. Amine et al., “Significant Improvement of Electrochemical Performance of AlF[sub 3]-Coated Li[Ni[sub 0.8]Co[sub 0.1]Mn[sub 0.1]]O[sub 2] Cathode Materials,” *Journal of Power Sources*, vol. 154, no. 11, A1005, 2007.

[119] J. Xie, A. D. Sendek, E. D. Cubuk et al., "Atomic Layer Deposition of Stable LiAlF4 Lithium Ion Conductive Interfacial Layer for Stable Cathode Cycling," *ACS nano*, vol. 11, no. 7, pp. 7019–7027, 2017.

[120] Z. Zhong, L. Chen, S. Huang et al., "Single-crystal LiNi0.5Co0.2Mn0.3O2: a high thermal and cycling stable cathodes for lithium-ion batteries," *Journal of Materials Science*, vol. 55, no. 7, pp. 2913–2922, 2020.

[121] W. Liu, P. Oh, X. Liu et al., "Nickel-rich layered lithium transition-metal oxide for high-energy lithium-ion batteries," *Angewandte Chemie (International ed. in English)*, vol. 54, no. 15, pp. 4440–4457, 2015.

[122] X. Ou, T. Liu, W. Zhong et al., "Enabling high energy lithium metal batteries via single-crystal Ni-rich cathode material co-doping strategy," *Nature communications*, vol. 13, no. 1, p. 2319, 2022.

[123] X. Zeng, T. Jian, Y. Lu et al., "Enhancing High-Temperature and High-Voltage Performances of Single-Crystal LiNi 0.5 Co 0.2 Mn 0.3 O 2 Cathodes through a LiBO 2 /LiAlO 2 Dual-Modification Strategy," *ACS Sustainable Chemistry & Engineering*, vol. 8, no. 16, pp. 6293–6304, 2020.

[124] X. Zeng, J. Zhu, L. Yang et al., "Electrochemical stabilities of surface aluminum-doped LiNi0.5Co0.2Mn0.3O2 single crystals under different cutoff voltages," *Journal of Electroanalytical Chemistry*, vol. 838, pp. 94–100, 2019.

[125] Z. Zhao, B. Huang, M. Wang et al., "Facile synthesis of fluorine doped single crystal Ni-rich cathode material for lithium-ion batteries," *Solid State Ionics*, vol. 342, p. 115065, 2019.

[126] M. S. Idris and A. R. West, "The Effect on Cathode Performance of Oxygen Non-Stoichiometry and Interlayer Mixing in Layered Rock Salt LiNi 0.8 Mn 0.1 Co 0.1 O 2-δ," *Journal of The Electrochemical Society*, vol. 159, no. 4, A396-A401, 2012.

[127] M. M. Thackeray, S.-H. Kang, C. S. Johnson et al., "Comments on the structural complexity of lithium-rich Li1+xM1−xO2 electrodes (M=Mn, Ni, Co) for lithium batteries," *Electrochemistry Communications*, vol. 8, no. 9, pp. 1531–1538, 2006.

[128] Q. Liu, W. Jiang, M. J. P. Munoz et al., "Stabilized Electrode/Electrolyte Interphase by a Saturated Ionic Liquid Electrolyte for High-Voltage NMC532/Si-Graphite Cells," *ACS applied materials & interfaces*, vol. 12, no. 20, pp. 23035–23045, 2020.

[129] C. Tian, Y. Xu, W. H. Kan et al., "Distinct Surface and Bulk Thermal Behaviors of LiNi0.6Mn0.2Co0.2O2 Cathode Materials as a Function of State of Charge," *ACS applied materials & interfaces*, vol. 12, no. 10, pp. 11643–11656, 2020.

[130] S. Sharifi-Asl, V. Yurkiv, A. Gutierrez et al., “Revealing Grain-Boundary-Induced Degradation Mechanisms in Li-Rich Cathode Materials,” *Nano letters*, vol. 20, no. 2, pp. 1208–1217, 2020.

[131] P. Teichert, H. Jahnke, and E. Figgemeier, “Degradation Mechanism of Monocrystalline Ni-Rich Li[Ni x Mn y Co z ]O 2 (NMC) Active Material in Lithium Ion Batteries,” *Journal of The Electrochemical Society*, vol. 168, no. 9, p. 90532, 2021.

[132] C. Wölke, A. Benayad, T.-L. Lai et al., “Single Versus Blended Electrolyte Additives: Impact of a Sulfur-Based Electrolyte Additive on Electrode Cross-Talk and Electrochemical Performance of LiNiO 2 ||Graphite Cells,” *Advanced Energy Materials*, 2025.